Epitaxial Perovskite Oxide Devices Fabricated by Lift-off Technology

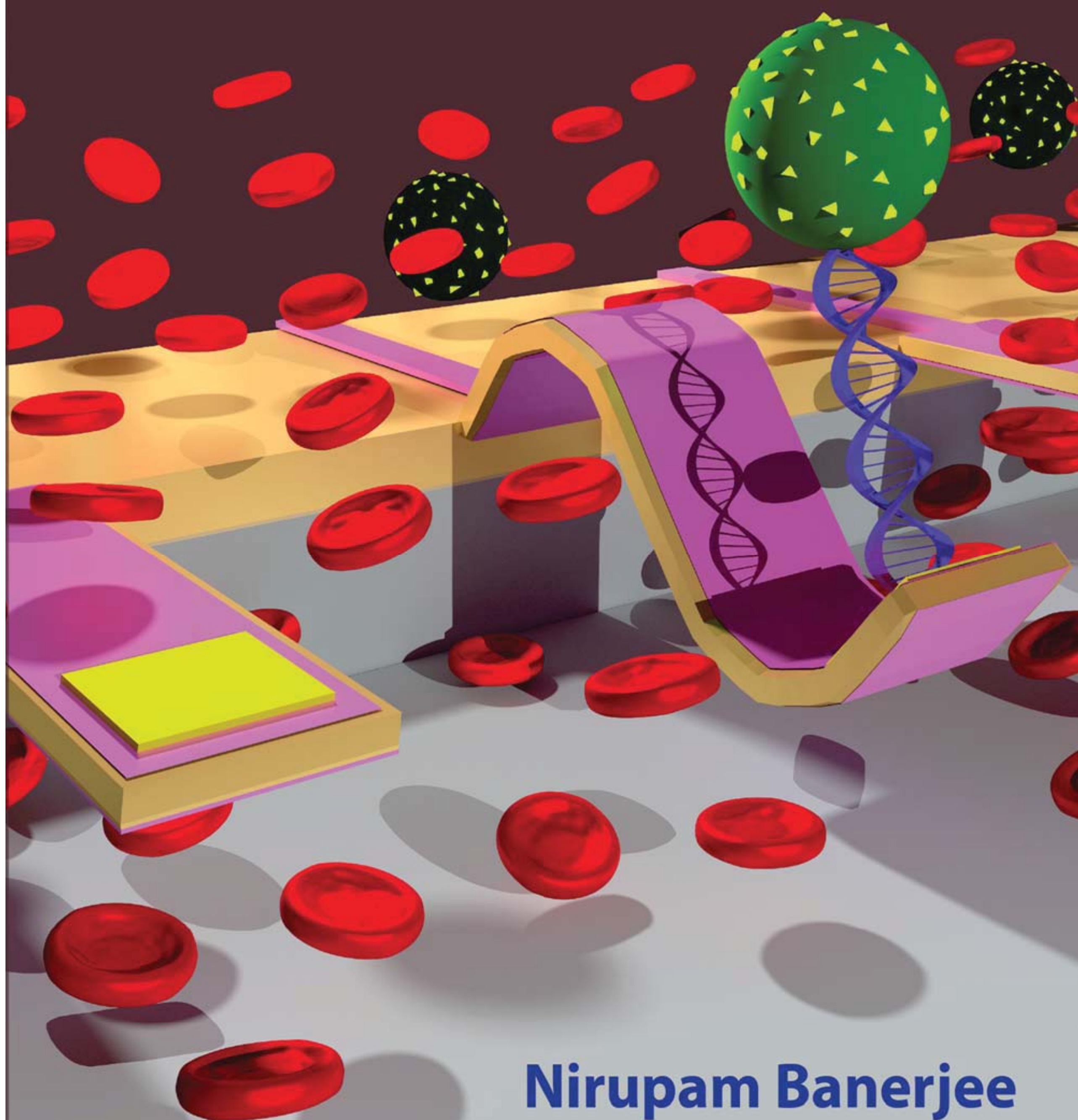

Nirupam Banerjee

Epitaxial Perovskite Oxide Devices Fabricated by Lift-off Technology

Nirupam Banerjee

Ph.D. Committee

Chairman and secretary
prof. dr. W. J. Briels (University of Twente)

Supervisor
Prof. dr. ing. A. J. H. M. Rijnders (University of Twente)

Assistant-supervisor
Dr. ir. G. Koster (University of Twente)

Members
Prof. dr. M. Alexe (University of Warwick, UK)
Prof. dr. ir. J. P. Benschop (ASML, The Netherlands)
Prof. dr. ir. S. van der Zwaag (University of Delft)
Prof. dr. ir. J. Schmitz (University of Twente)
Prof. dr. ing. D. H. A. Blank (University of Twente)

Referents
Dr. ir. M. Dekkers (SolMates BV, The Nederlands)

Cover :
Front : The cover image represents a 3D-view of the piezoelectric sensor devices triggered for the detection of biological microbes inside blood.
Back : 3D AFM of the fabricated nano-structures from this thesis overlay-ed on a model $SrTiO_3$ surface.

The research described in this thesis was performed with the Inorganic Materials Science group and the MESA+ Institute for Nanotechnology at the University of Twente, Enschede, the Netherlands. This research was carried out under project number M62.2.08SDMP21 in the framework of the Industrial Partnership Program on Size Dependent Material Properties of the Materials innovation institute (M2i) and the Foundation of Fundamental Research on Matter (FOM), which is part of the Netherlands Organization for Scientific Research. The authors gratefully acknowledge supports from the industrial partners Oće and SolMates.

Ph.D. thesis University of Twente, Enschede, the Netherlands.
ISBN 978-90-365-3743-8 ; DOI 10.3990./1.9789036537438
Printed by Wöhrmann Print Services, Zutphen, the Netherlands
Copyright © 2014 by Nirupam Banerjee

EPITAXIAL PEROVSKITE OXIDE DEVICES FABRICATED BY LIFT-OFF TECHNOLOGY

PROEFSCHRIFT

ter verkrijging van
de graad van doctor aan de Universiteit Twente,
op gezag van de rector magnificus,
prof. dr. H. Brinksma,
volgens besluit van het College voor Promoties
in het openbaar te verdedigen
op Woensdag 17 September 2014 om 16:45 uur

door

Nirupam Banerjee

geboren op 17 September 1986
te Bagnan, Howrah, India

Dit proefschrift is goedgekeurd door de promotoren
Prof. dr. ing. A. J. H. M. Rijnders

en de assistent-promotor
Dr. ir. G. Koster

To my parents

Mr. RAMANI MOHAN BANERJEE

&

Mrs. ANIMA BANERJEE

Contents

1 Lift-off Fabrication for Oxide Electronics 1

1.1 Introduction . . . 1

1.2 Outline of the thesis . . . 4

Bibliography . . . 6

2 Direct Patterning of Functional $LaAlO_3$-$SrTiO_3$ Heterointerfaces 7

2.1 Introduction . . . 9

2.1.1 $LaAlO_3$-$SrTiO_3$: Multifunctional perovskite interface . . . 9

2.1.2 Patterning of LAO-STO interface into functional device structures . . . 9

2.2 Experimental Methods . . . 10

2.2.1 Termination of $SrTiO_3$ (001) substrates . . . 10

2.2.2 Deposition and patterning of AlO_x mask . . . 12

2.2.3 High temperature deposition of $LaAlO_3$ and lift-off structuring to the final device . . . 12

2.3 Electrotransport Properties . . . 14

2.4 Magnetotransport at the Structured Interface . . . 17

2.5 Conclusion . . . 18

Bibliography . . . 19

3 Patterning of Multilayer Epitaxial $PbZr_{0.52}Ti_{0.48}O_3$ Heterostructures 23

3.1 Introduction . . . 25

3.1.1 Lead Zirconate Titanate (PZT) as the piezoelectric material 25

3.1.2 Etching technologies for PZT : dry & wet etching . . . 25

3.1.3 Patterning of multilayer heterostructures . . . 27

3.1.4 Lift-off patterning of multilayer PZT . . . 27

3.2 Experimental Methods . . . 29

3.2.1 Preparation of sacrificial template mask . . . 29

3.2.2 High temperature multilayer deposition and lift-off . . . 30

3.3 Characterization Methods . . . 30

3.4 Results and Discussions 32
3.4.1 X-ray diffraction studies after lift-off 32
3.4.2 Ferroelectric properties of the lift-off fabricated $PbZr_{0.52}Ti_{0.48}O_3$ heterostructures 32
3.4.3 Detailed investigation on the lift-off process : fabrication of PZT lines 34
3.4.4 Difference between wet-etching and lift-off approaches . . . 36
3.4.5 PFM investigation of PZT micro-lines 37
3.5 Conclusion 39
Bibliography 40

4 Submicron and Nano Patterning of Epitaxial PZT by Lift-off Strategy 45
4.1 Introduction 47
4.1.1 Nanostructures of Ferroelectric Materials 47
4.1.2 Different fabrication strategies for nano-ferroelectrics 47
4.1.3 PZT nano structures by Epitaxial Lift-off Patterning 48
4.2 Experimental- I 49
4.2.1 Fabrication of PZT nano-structures : Modification of the sacrificial mask 49
4.2.2 Ferroelectric response of PZT nano-structures by PFM . . . 50
4.3 Experimental- II 50
4.3.1 Fabrication of epitaxial $PbZr_{0.2}Ti_{0.8}O_3$ nano-structures avoiding physical ion-etching 50
4.3.2 Microscopic Characterization of Ferroelectric Nano-structures 54
4.3.3 Writing using PFM 55
4.3.4 Ferroelectric domains in lift-off fabricated epitaxial $PbZr_{0.2}Ti_{0.8}O_3$ nanostructures 56
4.4 Conclusion 59
Bibliography 60

5 Fabrication of Free-standing, all-Oxide Epitaxial Piezodriven Cantilevers Integrated on Silicon 63
5.1 Introduction 65
5.1.1 MEMS with piezoelectric actuation 65
5.1.2 Ferroelectrics for piezo-MEMS 66
5.1.3 Free-standing Epitaxial MEMS 67
5.1.4 Lift-off fabrication of free-standing epitaxial PZT MEMS devices 68
5.2 Experimental Method 70
5.2.1 Fabrication of free standing PZT MEMS devices 70
5.3 Results and Discussions 72

5.3.1 Influence of device orientation on rate of their release from substrate . . . 72
5.3.2 Structural Characterizations . . . 75
5.3.3 Initial bending of the cantilevers . . . 76
5.4 Conclusion . . . 79
Bibliography . . . 80

6 Electromechanical Properties and Vibrational Damping in Free-standing Epitaxial PZT Cantilevers 87
6.1 Introduction . . . 89
6.1.1 Mass sensors with resonating cantilevers . . . 89
6.1.2 Damping in electromechanical cantilevers . . . 89
6.1.3 Free-standing piezo-driven cantilevers for high - sensitivity mass sensors . . . 90
6.2 Methodes . . . 91
6.3 Experimental . . . 92
6.4 Results and Discussion . . . 94
6.4.1 Electromechanical response of the freestanding PZT cantilevers 94
6.4.2 Theoretical models to explain damping mechanisms . . . 96
6.5 Conclusion . . . 101
Bibliography . . . 102

7 Future Possibilities of Lift-off Patterning for Oxide-Electronics 105
7.1 Introduction . . . 107
7.2 Patterned High Mobility $SrCuO_2$-$LaAlO_3$-$SrTiO_3$(001) Hetero-Interfaces . . . 109
7.3 Epitaxial freestanding Piezo-MEMS Devices as quantitative Mass-sensor and Bio-detectors . . . 112
7.4 Conclusion . . . 114
Bibliography . . . 115

Summary 117

Samenvatting 121

Acknowledgments 125

CHAPTER 1

Lift-off Fabrication for Oxide Electronics

1.1 Introduction

The word *lithography* originates from the Greek '*lithos*', meaning stone and '*graphein*' meaning to write. It was used to describe a technique to write or draw on a smooth lithographic limestone plate using wax [1]. The process starts with drawing a piece of art using wax on a flat limestone surface with a fine hand. In the next step, the uncovered areas of the limestone surface are decayed by applying an aqueous acidic solution. This step is conventionally termed as *etching* and yields a positive mimic of the wax or oil based drawing on the more robust surface of limestone, which is much resistant to decay. Etched stones can also be used as hard stamps, for transferring the pattern (mirror image of the intended drawing) to a piece of paper by applying an oil-based ink, which sticks only to the wax and is repelled from the water covered etched trenches. This simple principle established the early foundation of printing. However, in modern times, the use of lithography is much more entangled with micro/nano-scale patterning of an organic polymer by means of a variety of techniques, for example utilizing light for micro-patterning and focused electron beam for nano-scale structures. Highly precise micro/nano-lithography is one among the most important parameters which has enabled the remarkable advancement of the present day electronic technology.

Especially in the current era of electronic miniaturization, nano-structuring of various functional materials has became an essential fabrication step yielding an extremely high device density. It has to be emphasized that both the patterning of the resist and the selective etching of the underlying material are crucial to achieve accurate patterns.

Alongside with processing technology, the invention and development of functional materials also play a prominent role to achieve compact, faster, multifunctional electronic devices. The employment of these materials in the traditional Si/SiO_2 based semiconductor technology is essential for future electronic advancement [2, 3]. Next to the integration of functional materials with the Si-technology there is the possibility to achieve novel utilities, unattainable with the traditional semiconductor technology alone. Among the different classes of functional materials, the perovskite oxides are extremely promising for their manifestation of diverse functional properties with similar crystal structures. The breadth of perovskite oxide extends from insulating (for example, $DyScO_3$) to superconducting (YBCO), from non-magnetic ($LaAlO_3$) to ferromagnetic($LaSr_{(1-x)}Mn_xO_3$), from dielectric ($SrTiO_3$) to ferroelectric ($BaTiO_3$, $Pb(Zr,Ti)O_3$). Moreover, the similarity in the underlying crystal structure gives us the additional possibilities of enhancing and manipulating their functional behavior by tuning the lattice, orbital and/or spin degrees of freedom, for example by means of epitaxial strain [4, 5]. Owing to these interesting prospects perovskite oxides were intensively investigated in the preceding decades, both from fundamental and applicative perspective. In this thesis we aim to utilize PZT, one of the most prominently applied perovskites, which shows very high quality piezo and ferroelectric behavior, to improve the performance of micro electro mechanical systems (MEMS) devices.

$PbZr_{(1-x)}Ti_xO_3$ ($0 < x < 1$) is utilized in a wide range of commercial devices due to its exceptionally high electromechanical coupling coefficients and large ferroelectric polarization values. In modern electronic technology, PZT films play an essential role in numerous devices, ranging from electromechanical systems [8] to non-volatile memory device components [9]. The majority of these functional devices require precise PZT patterns, defined by the corresponding devices geometries. The present trend of electronic miniaturization to achieve extremely high device density also demands the size of these functional PZT devices to be at the nano-scale, as can be seen in Fig. 1.1(a) showing the cross sectional SEM image of a non-volatile ferroelectric random access memory (FRAM) devices with PZT as the active ferroelectric component [6]. However, the complex solid solution PZT is a compound which is stable with respect to the different physical and chemical etching processes commonly employed in traditional semiconductor technology [10]. This fosters the need for the development of new fabrication processes, capable of fabricating nano-scale patterns of high temperature grown functional perovskite oxide PZT, which can be combined with conventional Si-based very large scale integration

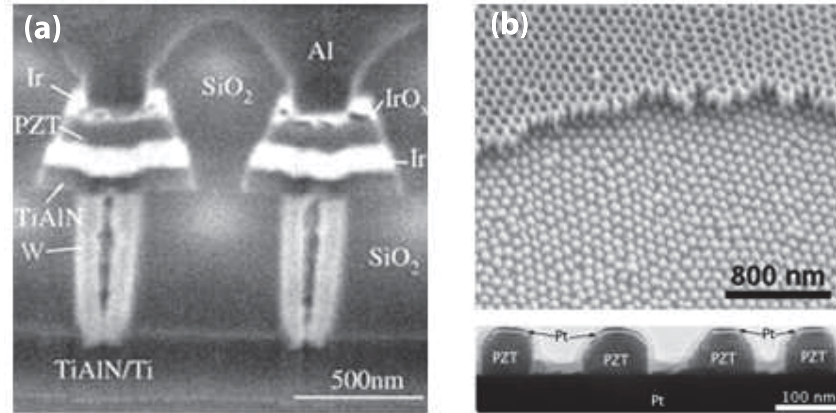

Figure 1.1: (a) Cross sectional scanning electron microscopic (SEM) image of a ferroelectric random access memory (FRAM) device (reprinted with permission from [6]), copyright 2001, American Institute of Physics. Electron microscopic images of very high density ferroelectric nano-capacitors fabricated using pulsed laser deposition (reprinted with permission from [7]), copyright 2008, Nature Publishing Group.

(VLSI) technology. Although research efforts were devoted in order to develop such fabrication techniques [7] capable of generating high density ferroelectric nano-structures as shown in Fig. 1.1(b), the developed techniques lack the design-flexibility and size control of the generated nano-structures as can be attainable with traditional nano-lithographic techniques like electron beam lithography. An additional advantage of going to the nano-scale is to demonstrate the possibility of achieving a higher functional response [11], which scales up inversely with the device dimension and to investigate the underlying physical reason.

The functionality of piezo and ferroelectric materials is typically determined utilizing electrodes. It has been shown that epitaxial perovskite electrodes are better for durable performance of the piezo/ferroelectric devices as compared to metal electrodes [12]. In such a high performance all-oxide device, the oxide electrodes need to be patterned together with the functional piezo/ferroelectric perovskite oxide. Moreover, ferroelectric superlattices with considerably enhanced polarization values [5] exist and if these epitaxial multilayers and superlattices with their enhanced properties are to be employed in multifunctional devices, a suitable patterning technology must be developed in order to pattern the functional material into device structures without damaging any pre-existing device component. The physical and chemical nature of different perovskite oxides can differ from each other. Hence, in the fabrication of all-oxide devices, incorporating multilayer perovskite systems, individual perovskite oxide layer would normally

require separate patterning processes, making the overall fabrication difficult. The development of a combined structuring strategy which is capable of simultaneously patterning all high-temperature grown perovskite layers, will therefore be useful for the fabrication of epitaxial all-oxide devices.

In this thesis, we describe the development of such a fabrication strategy for both micro and nano-scale patterning of epitaxial interfaces and multilayers. We also show that the fabrication pathway does not affect the functional behavior of the materials down to the nano-scale. Employing the new patterning pathway we have structured conducting oxide interfaces with 2DEG, fabricated heteroepitaxial micro and nano devices, prepared all-oxide free-standing piezo-MEMS devices and investigated their functional behavior; as is briefly outlined in the following chapters.

1.2 Outline of the thesis

Chapter2 describes the development of the patterning pathway termed as 'epitaxial lift-off' and its use in structuring the epitaxial interface between $LaAlO_3$ and $SrTiO_3$(001), without performing any physical ion-beam etching. The lift-off strategy involves the employment of a structured sacrificial mask of AlO_x on the substrate surface in order to pattern the epitaxial perovskite *in situ* during the deposition at high temperature. After a controlled annealing step and cool down to room temperature, the mask was lifted off, generating precise pattern of the epitaxial interface. A detailed investigation of the temperature dependent magnetotransport properties was performed with the patterned interfacial heterostructures with variable thickness of the $LaAlO_3$ layer and compared with that of the unstructured thin film analogues. The obtained results demonstrate the preservation of the high-quality interface properties in the patterned structures, showing high mobility conductivity as well as interface magnetism.

In *Chapter 3* we have extended the epitaxial lift-off pathway from structuring a single layer towards patterning heteroepitaxial multilayers. $PbZr_{0.52}Ti_{0.48}O_3$ films incorporating heteroepitaxial $SrRuO_3$ electrode layers were patterned utilizing the lift-off strategy. The fabrication process is investigated in detail and compared with the top-down wet-etching process, which is traditionally employed for patterning PZT. The ferroelectric and piezo-electric properties of the lift-off fabricated epitaxial PZT heterostructures were investigated and compared with similar structures fabricated by conventional etching schemes.

The epitaxial lift-off strategy was further modified in order to allow the integration with electron beam lithography (eBL) for the fabrication of epitaxial nano-structures, as is discussed in *Chapter 4*. Two different modified fabrication strategies have been presented which are compatible with eBL process. Similar to the previous chapter the details of the patterning process is discussed and

investigated at different fabrication steps. Epitaxial PZT nano-structures were fabricated with minimum feature size of $\sim$ 100 nm. It was observed that the ferroelectric domain configuration of low-dimensional epitaxial PZT nano-structures (with feature size $\leq$ 200 nm) was different from their unstructured counterparts.

In *Chapter 5* we have demonstrated the fabrication of all-oxide heteroepitaxial piezo-driven MEMS devices. The fabrication was enabled via epitaxial lift-off patterning of multilayer hetero-structures, followed by substrate etching. The process is investigated in detail and the impact of the orientation of the device layers with respect to the substrate surface on the final geometry and the rate of substrate release is illustrated.

Unlike traditional SOI-based epitaxial piezo-cantilevers, the fabricated devices were free standing and hence had a considerable lower mass. This is an important step towards improvement of piezo-based cantilever mass-sensor devices, as is discussed in *Chapter 6*. In order to achieve very high mass-sensitivity it is also very important to attain higher resonance quality factors in devices. By investigating the dependence of the quality factor both in ambient and in vacuum, on the length of the cantilever devices, we have identified the contribution to the vibration damping of the operational medium as well as of the internal friction in the cantilever. A viscous air damping model taking into account the internal friction inside the cantilever oxides was adopted in order to explain the electromechanical behavior.

In *Chapter 7*, the final chapter of this thesis, we have highlighted some future directions that are enabled by the epitaxial lift-off patterning strategy. We have shown some preliminary results achieved utilizing the fabrication technique such as the patterning of the $SrCuO_2$-$LaAlO_3$-$SrTiO_3$(001) interface containing high mobility carriers. While preserving the high quality interfacial transport characteristics, few interesting novel properties were observed in these structured interface-devices, including carrier mobilities up to $\sim$ 70,000 $cm^2V^{-1}s^{-1}$ and positive magnetoresistance values up to $\sim$ 800% at 2 K, possibly originating from the structural confinement. We have also demonstrated that the epitaxial freestanding piezo-MEMS cantilever devices can function as very high-sensitivity mass sensors by incorporating a patterned top layer of gold to the devices. Therefore, they can also be utilized for quantitative sensing and detection of biological molecules and microbes via gold-thiol binder coordination. These preliminary results promote the future research on lift-off fabricated epitaxial perovskite oxide devices both from fundamental and from applicative perspectives.

Bibliography

[1] W. Weber, *A history of lithography.* Thames and Hudson, 1966.

[2] D. H. Blank and G. Rijnders, “Nanoelectronics: Oxides offer the write stuff,” *Nature Nanotechnology*, vol. 4, no. 5, pp. 279–280, 2009.

[3] M. Schulz, “The end of the road for silicon?,” *Nature*, vol. 399, no. 6738, pp. 729–730, 1999.

[4] R. Ramesh and D. Schlom, “Orienting ferroelectric films,” *Science*, vol. 296, no. 5575, pp. 1975–1976, 2002.

[5] H. N. Lee, H. M. Christen, M. F. Chisholm, C. M. Rouleau, and D. H. Lowndes, “Strong polarization enhancement in asymmetric three-component ferroelectric superlattices,” *Nature*, vol. 433, no. 7024, pp. 395–399, 2005.

[6] S. Summerfelt, T. Moise, G. Xing, L. Colombo, T. Sakoda, S. Gilbert, A. Loke, S. Ma, L. Wills, R. Kavari, *et al.*, “Demonstration of scaled ($\geq$ 0.12 μm^2) $Pb(Zr,Ti)O_3$ capacitors on W plugs with Al interconnect,” *Applied Physics Letters*, vol. 79, no. 24, pp. 4004–4006, 2001.

[7] W. Lee, H. Han, A. Lotnyk, M. A. Schubert, S. Senz, M. Alexe, D. Hesse, S. Baik, and U. Gösele, “Individually addressable epitaxial ferroelectric nanocapacitor arrays with near Tb inch^{-2} density,” *Nature Nanotechnology*, vol. 3, no. 7, pp. 402–407, 2008.

[8] P. Muralt, “PZT thin films for microsensors and actuators: Where do we stand?,” *IEEE Transactions on Ultrasonics, Ferroelectrics and Frequency Control*, vol. 47, no. 4, pp. 903–915, 2000.

[9] J. Scott, “Applications of modern ferroelectrics,” *Science*, vol. 315, no. 5814, pp. 954–959, 2007.

[10] J. Baborowski, “Microfabrication of piezoelectric MEMS,” *Journal of Electroceramics*, vol. 12, no. 1-2, pp. 33–51, 2004.

[11] S. Bühlmann, B. Dwir, J. Baborowski, and P. Muralt, “Size effect in mesoscopic epitaxial ferroelectric structures: Increase of piezoelectric response with decreasing feature size,” *Applied Physics Letters*, vol. 80, no. 17, pp. 3195–3197, 2002.

[12] C. Eom, R. Van Dover, J. M. Phillips, D. Werder, J. Marshall, C. Chen, R. Cava, R. Fleming, and D. Fork, “Fabrication and properties of epitaxial ferroelectric heterostructures with $SrRuO_3$ isotropic metallic oxide electrodes,” *Applied Physics Letters*, vol. 63, no. 18, pp. 2570–2572, 1993.

CHAPTER 2

Direct Patterning of Functional $LaAlO_3$-$SrTiO_3$ Heterointerfaces

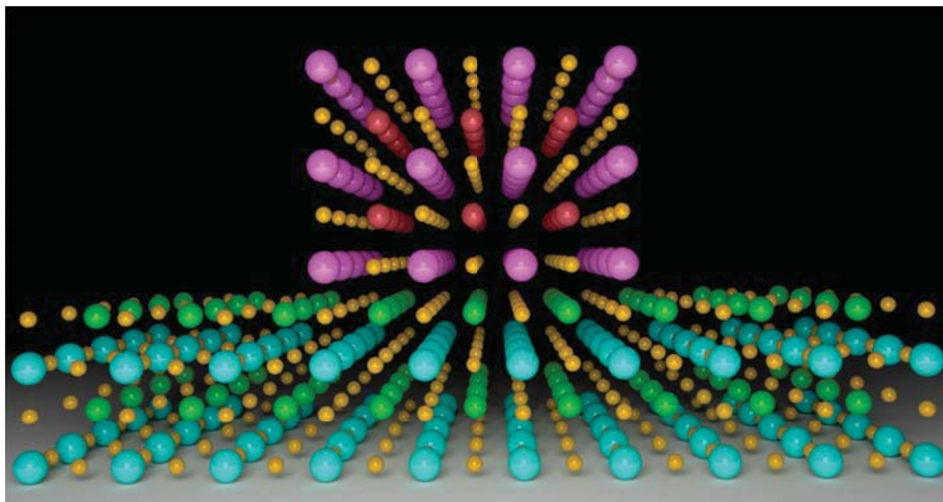

Part of the work discussed in this chapter is published in:
N. Banerjee, M. Huijben, G. Koster, G. Rijnders, "*Direct Patterning of Functional Interfaces in Oxide Heterostructures*", *Applied Physics Letters* 100, 041601 (2012).

ABSTRACT

In this chapter, the fabrication of high-quality device structures incorporating the heteroepitaxial metallic interface between $LaAlO_3$ and $SrTiO_3$ by an epitaxial lift-off technique is discussed. The patterning strategy avoids any reactive ion beam etching and utilizes a sacrificial resist mask of high temperature stable amorphous aluminum oxide (AlO_x). The oxide mask can be lithographycally developed in device patterns and lifted off after deposition of epitaxial perovskite layer at higher temperatures. Detailed studies of temperature dependent magnetotransport properties were performed on the patterned heterostructures with variable thickness of the $LaAlO_3$ layer and compared to analogous unstructured thin film samples. The results obtained from temperature dependent magnetotransport measurements demonstrate conservation of the high-quality interface-properties in the patterned structures, very similar to their unstructured analogues. This development of lift-off patterning strategy for the preparation of high-quality interfacial devices, will help enabling future studies of low-dimensional confinement on high mobility interface conductivity as well as interface magnetism.

2.1 Introduction

2.1.1 $LaAlO_3$-$SrTiO_3$: Multifunctional perovskite interface

In the year 2004, Ohtomo and Hwang reported the remarkable observation of the existence of a high-mobility electron gas at the interface between two wide-band gap perovskite insulators $SrTiO_3$ (STO) and $LaAlO_3$ (LAO) [1]. This has since initiated extensive research activities into the exceptional properties of this two dimensional heteroepitaxial system. One of the used models in order to explain this occurrence of highly conducting interface in between otherwise insulating perovskites, emphasizes the electronic reconstruction arising from polarization discontinuity at the interface [2]. (001) LAO crystal composed of alternating planes of LaO and AlO_2 with net charge of ± 1 (at the ionic limit), whereas similar constituent planes for $SrTiO_3$(001) are charge neutral SrO and TiO_2. According to the polar-catastrophe model this discontinuity of polarization at the hetrointerface ultimately leads to electronic reconstruction resulting interfacial conductivity beyond certain critical thickness of epitaxial $LaAlO_3$ layer [3]. In addition to interface conduction, several studies have demonstrated existence of a range of interesting properties such as interfacial superconductivity [4], magnetism [5], metal-insulator (M-I) transition [3], modulated electric transport [6], piezoelectricity [7], persistent photoconducticity [8]. These observations of a wide range of properties at this unique heteroepitaxial oxide interface opens up the possibility of its application in future electronic devices [9–11].

2.1.2 Patterning of LAO-STO interface into functional device structures

Although fascinating properties were observed at the epitaxial $LaAlO_3$-$SrTiO_3$ hetero-interfaces, to develop these unique interfaces into useful technologies taking advantages of their multifunctional behavior, high-quality devices have to be fabricated from thin films by reproducible patterning techniques. In the traditional patterning strategy, reactive Ar-ion etching has been extensively used to produce controlled structures in various materials [12]. However, the implementation of this technique for LAO-STO interfaces is hampered due to the formation of oxygen vacancies, which would result in a conducting surface layer at the STO substrate [13]. Very recently etching-introduced oxygen vacancies were found to induce surface-magnetic effects in otherwise non-magnetic $SrTiO_3$ single crystal [14], jeopardizing even the possibility of exploiting magnetic orders in dry-etching fabricated LAO-STO devices. Alternatively, previous studies have used UV lithography to create measurement structures by combining a hard mask of amorphous $LaAlO_3$ [15] or

AlO_x [16] and pulsed laser deposition. Researchers have also reported patterning of the epitaxial interface by locally destroying interfacial conductivity, utilizing energetic ion-beam irradiation at selective areas of pre-fabricated homogeneous interface [17, 18]. The disadvantage of these techniques is the presence of the hard mask material on the surface of the final devices. In addition, scanning probe microscopy has been applied to form structures down to the nano-scale [3, 19]. However, the created patterns were found to degrade in ambient conditions making the technique unsuitable for any practical applications. Before the research work described in this chapter, there had not been a demonstration of a reproducible technique to fabricate well-controlled structures without any of the above mentioned disadvantages.

Here, we present the direct patterning of high-quality structures incorporating the epitaxial $LaAlO_3$ - $SrTiO_3$ (LAO-STO) interface by an epitaxial lift-off technique without performing any reactive ion beam etching. In order to pattern the delicate heterointerface, we have utilized a high temperature stable sacrificial oxide template mask of amorphous aluminum oxide (AlO_x). AlO_x was chosen as the mask layer because of its ability to withstand very high temperatures [20, 21] together with the possibility of development and lift-off using basic solutions. We emphasize here that most of the perovskites are chemically inert toward basic solutions while they react strongly with acids [22]. The patterned structures incorporating the LAO-STO interface exhibited high quality interfacial properties which have previously been measured only in thin film samples. Detailed studies of temperature dependent magnetotransport properties were performed on the patterned heterostructures with variable thickness of the LAO layer and compared to their unstructured thin film analogues.

2.2 Experimental Methods

2.2.1 Termination of $SrTiO_3$ (001) substrates

Achieving B-site (TiO_2) surface termination of the $SrTiO_3$ (001) substrate is crucial to obtain a conducting heterointerface [1]. A standard termination procedure [23,24] was followed for selective B-site (TiO_2 plane) termination of commercially purchased (Crystec, GmBH) $SrTiO_3$ (001) single crystals. The termination process includes water treatment of the mixed terminated (both A and B site) substrate crystals to hydrolyze SrO unit cell planes, followed by an acid treatment with buffered hydrofluoric acid (BHF) to dissolve the hydrolyzed part. The terminated substrates were annealed in oxygen environment (with a flow-rate of 150 L/hour) at 950°C for 2 hours to achieve straight terrace edges suitable for layer by layer growth. Fig. 2.1(a) shows an AFM image of a prepared B-site terminated $SrTiO_3$ single crystal substrate after annealing, which was used to fabricate high quality LAO-

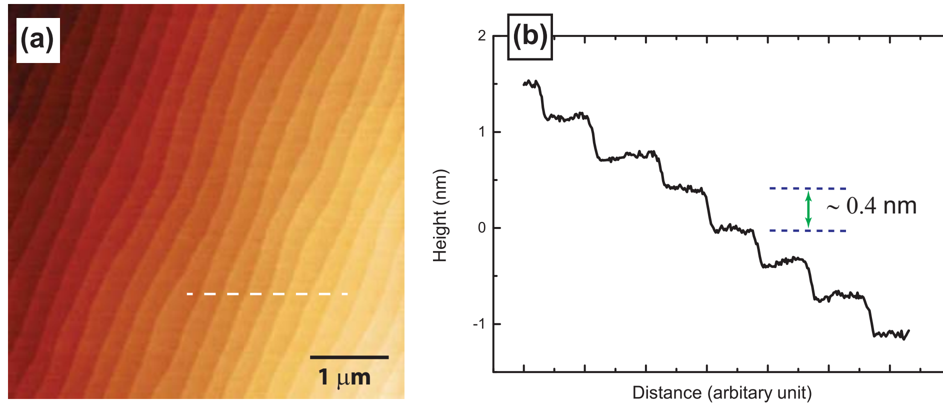

Figure 2.1: (a) AFM image of a representative TiO_2-terminated $SrTiO_3$ (001) single crystal substrate, used for the device fabrication. (b) Height profile as probed by the AFM tip corresponding to the indicated line in (a).

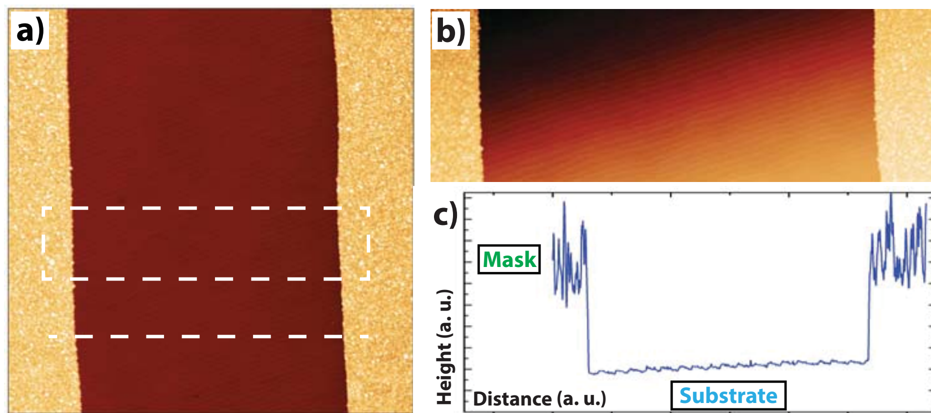

Figure 2.2: (a) AFM image of the AlO_x mask with developed area displaying substrate area underneath. (b) zoomed-in image of selected area in image (a) displaying substrate steps. (c) AFM height profile corresponding to the indicated region in the image, showing clean substrate surface with visible terraces.

STO heterointerfacial devices. It can be noticed that the substrate had average terrace width ∼ 350 nm. A height profile probed by the AFM tip (corresponding to the dotted line in the AFM image) is given in Fig. 2.1(b). Observation of clear vicinal steps of the bare $SrTiO_3$ with height difference of ∼ 0.4 nm confirms the single termination.

2.2.2 Deposition and patterning of AlO_x mask

To fabricate the mask on the substrate crystal, initially a thin (∼ 30 nm) layer of amorphous aluminum oxide (AlO_x) was deposited on a TiO_2-terminated STO (001) single crystal substrate [24] by pulsed laser deposition (PLD). A KrF excimer laser was applied to ablate a single crystalline AlO_x target at a repetition rate of 2 Hz and a laser fluence of ∼ 1.5 J cm^{-2}. During growth, the substrate was held at room temperature in an oxygen environment of 0.15 mbar.

In order to pattern the AlO_x mask layer, substrate covered with mask was subjected to conventional photolithographic process in which a negative mask with hall-bar structures was UV illuminated. The used photolithographic developer solution (OPD 4262) for the positive resist is a basic solution and hence it reacts also with exposed aluminum oxide to form water-soluble alkali-metal aluminates. All photoresist was removed subsequently using organic solvents. This simple process creates a negative mimic of the mask into amorphous AlO_x layer, which yields a TiO_2-terminated STO substrate covered with amorphous aluminum oxide with structured openings. Fig. 2.2 shows AFM images of a representative mask in (a) low and (b) high magnification displaying clean substrate substrate after development of the AlO_x mask. Fig. 2.2(c) presents height-profile along the indicated line in (a). In both Fig. 2.2(b) and (c) clear substrate steps can be noticed, suggesting lithographic processes for development and patterning of the lift-off AlO_x mask does not affect substrate surface and it's termination.

2.2.3 High temperature deposition of $LaAlO_3$ and lift-off structuring to the final device

Thin LAO films of different thicknesses were grown by PLD on these pre-patterned substrates at 800°C and 10^{-3} mbar O_2 from a single crystalline LAO target at a repetition rate of 1 Hz and a laser fluence of ∼ 1.3 Jcm^{-2}, similar to previous studies [5, 25]. After growth, the samples were slowly cooled down to room temperature at deposition pressure without any extra annealing step. In the final step the lift-off process was performed using a 4M aqueous NaOH solution in which the aluminum oxide dissolves as water soluble sodium aluminate removing the LAO layer on top as well. The final result is a well-defined structure incorporating a LAO/STO interface without any surface contamination of the original mask. The fabrication process is schematically represented step by step in Fig. 3.1 from

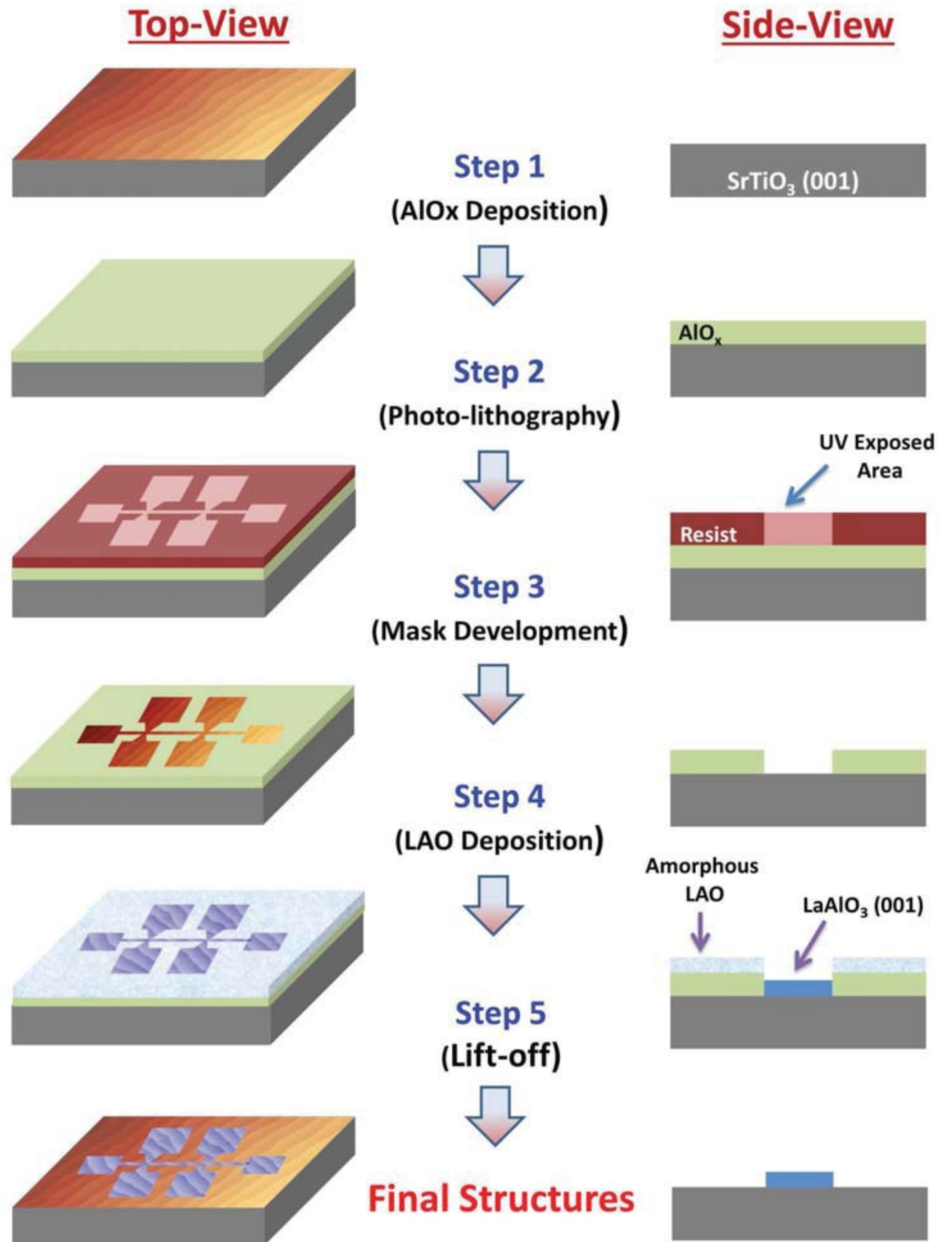

Figure 2.3: Schematic representation from both the top and side-view perspectives of the epitaxial lift-off patterning process to create well-defined structures incorporating LAO/STO(001) heterointerface.

both top and side view perpectives. Scanning electron microscopic (SEM) image of a lift-off fabricated hall-bar device, incorporating LAO-STO hetero-interface, is presented in Fig. 2.4(a). Figure 2.4(b) shows 3D representation of an atomic force micrograph at the edge of the fabricated device structures, proving the edge-smoothness.

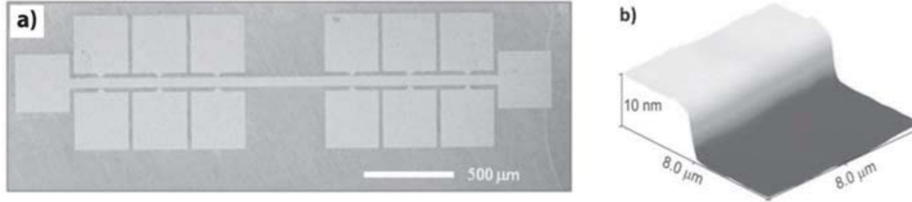

Figure 2.4: (a) Scanning electron micrograph displaying the final Hall bars incorporating a LAO/STO interface. (b) 3D representation of an atomic force micrograph at an edge of the structure.

2.3 Electrotransport Properties

To compare the electrical transport properties of patterned structures to their unstructured thin film analogues, samples with identical deposition condition were grown on TiO_2-terminated STO substrates. The patterned Hall bars in the structured samples, as well as the thin films, were ultrasonically wire-bonded with Al wire to form Ohmic contacts for electrical transport measurement.

The temperature dependence of the sheet resistance for both thin [$\sim$ 10 unit cell (u.c.)] and thick ($\sim$ 26 u.c.) LAO layers is shown in Figure 2.5, in which can be clearly observed that LAO/STO interfaces in thin films and Hall bars provide very similar transport properties. It is evident that thick LAO layers in both Hall bars and thin films show an upturn in sheet resistance at low temperatures, which is in good agreement with previous reports [5, 26]. An explanation given for the observed logarithmic temperature dependence of the sheet resistance upturn was the Kondo effect, which describes the interplay between localized magnetic moments and mobile charge carriers [5]. The sheet resistance can be described in this temperature range ($\sim$ 5 - 50 K) by

$$R_S = aln(T/T_{eff}) + bT^2 + cT^5 \tag{2.1}$$

where T_{eff} is an effective crossover temperature scale, and where the T^2 and T^5 terms are suggestive of electron-electron and electron-phonon scattering, relevant at higher temperatures. Saturation of the logarithmic term is observed below $\sim$ 5 K. Although similar transport properties are observed for thin films and Hall

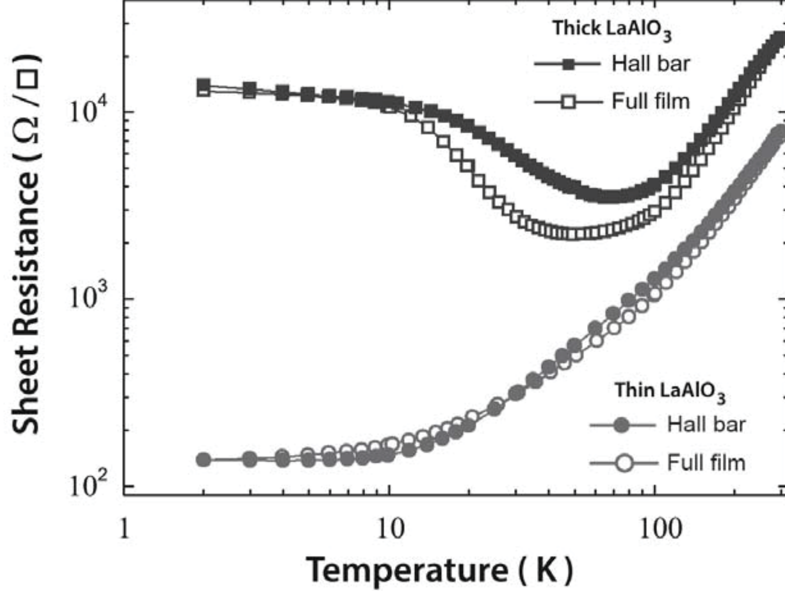

Figure 2.5: Temperature dependent sheet resistance of the conducting $LaAlO_3$-$SrTiO_3$ interface for different $LaAlO_3$ layer thicknesses (thin: $\sim$ 10 u.c., thick: $\sim$ 26 u.c.) situated in thin films and Hall bars.

bars, fitting of the measurement results demonstrates the small variations in T_{eff} of $\sim$ 50 K and $\sim$ 70 K, for respectively thin films and Hall bars. The presumable reason for this observed difference in T_{eff} is structural confinement, although detailed experimental proof of this claim is subject of further study. For thin LAO layers metallic behavior down to 2 K is observed in agreement with previous reports [26, 27].

The temperature dependencies of the corresponding sheet carrier density n_S and carrier mobility μ are shown in Figure 2.6, which were deduced from measurements of the Hall coefficient R_H, using n_S=-1/R_He. Also here, the structurization technique induced no measurable effect on the transport properties as similar results are observed for thin films and Hall bars. All samples exhibited thermally activated carriers comparable to previous observations [28] with the room temperature sheet carrier density decreasing with increasing LAO thickness [26]. At low temperatures the thick samples show an enhancement in sheet carrier density together with a decrease in carrier mobility similar to previous reports for thin films [25, 26]. Thin samples display a carrier density of $\sim 1 \times 10^{13}$ cm^{-2} and a high carrier mobility of $\sim$ 4000 cm^{2}V^{-1}s^{-1}. These observations of high carrier mobilities in structured Hall bars are comparable to reports on thin films [29], but these Hall bars enable future detailed studies on the physics of these interfaces in low-dimensional structures.

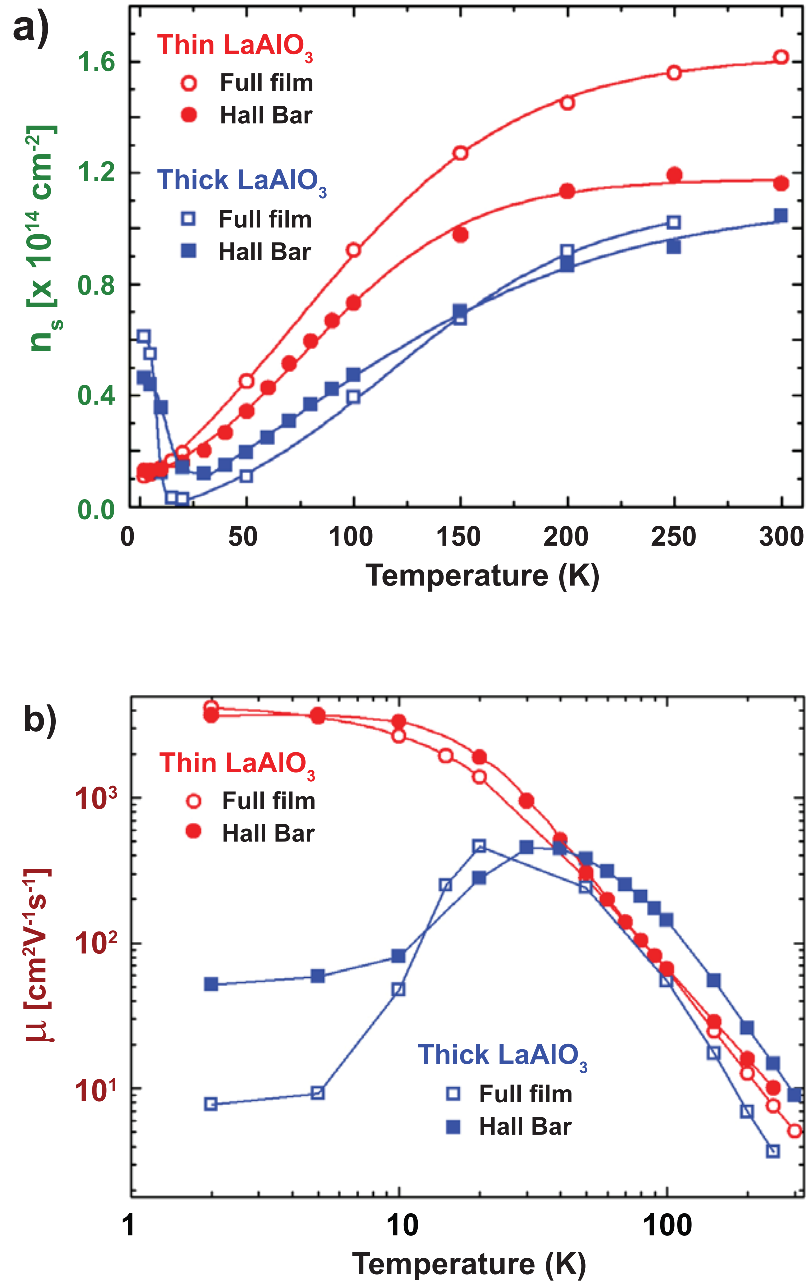

Figure 2.6: Temperature dependent carrier density, n_S (a) and carrier mobility, μ (b) of the conducting $LaAlO_3$-$SrTiO_3$ interface for different $LaAlO_3$ layer thicknesses (thin: $\sim$ 10 u.c., thick: $\sim$ 26 u.c.) situated in thin films and Hall bars.

2.4 Magnetotransport at the Structured Interface

In addition to the interface induced conductivity, magnetic effects at low temperatures with large negative magnetoresistance values have been reported for the LAO-STO interface [5]. Subsequent study of the LAO thickness dependence demonstrated the manifestation of this effect only for thick ($\sim$ 25 u.c.) LAO layers [26]. In good agreement to those previous reports our thick samples show large negative magnetoresistance at 2 K in both thin films and Hall bars, see Fig. 2.7, while thin samples only display positive magnetoresistance. The magnetoresistance was defined as the change in the sheet resistance with respect to the zero field resistance [Rs(H) = Rs(H)/Rs(0)]. Figure 2.7 clearly shows the occurrence of large negative magnetoresistance at 2 K for both thin films and Hall bars of $\sim$ 2%. Strikingly, the sample with structured Hall bars shows hysteresis behavior at 2 K, while for thin films this has only been observed [5] at much lower temperatures of 0.3 K. Magnetoresistance hysteresis is usually indicative of ferromagnetic domain formation in which domains change polarity above a certain coercive field. Domain formation typically creates a remanence in the signal when crossing zero-field, providing a butterfly shape of the magnetoresistance curve. An additional suppression around zero-field seems to occur, which could suggest additional spin/domain reorientation effects, such as observed in granular and spin-valve giant magnetoresistance systems and the Kondo effect in quantum dots in the presence of ferromagnetism [30].

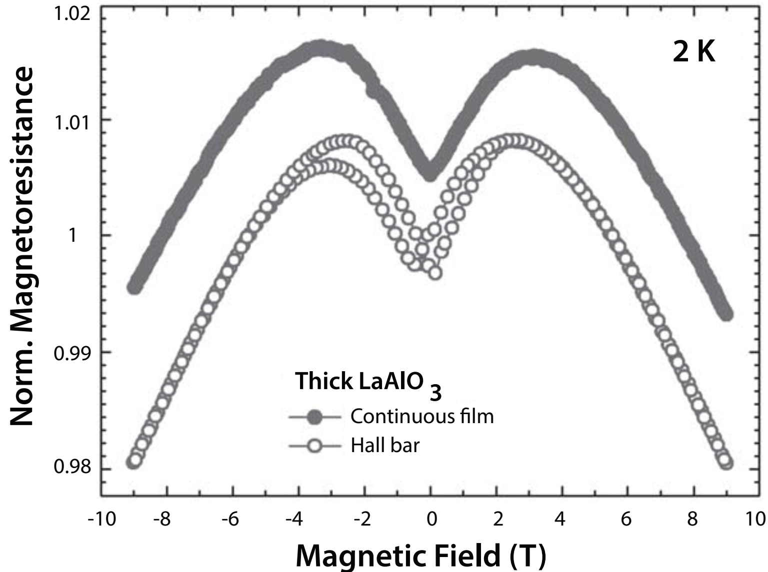

Figure 2.7: Magnetoresistance of the conducting $LaAlO_3$-$SrTiO_3$ interface for thick ($\sim$ 26 u.c.) LAO layer. Data for the thin film are shifted upwards for clarity.

2.5 Conclusion

In conclusion, we have studied the electrical transport properties of LAO-STO interfaces in patterned structures and compared them to their unstructured thin film analogues. This study was enabled by the development of a direct patterning technique, consisting of a lift-off process avoiding reactive ion etching, to create structures containing functional interfaces. The disadvantages of previous fabrication techniques have been prevented and the resulting structures exhibit interface phenomena previously observed in unstructured thin film samples. Electrotransport measurements demonstrated the conservation of the high-quality interface conductivity in the patterned $LaAlO_3$-$SrTiO_3$ structures with carrier mobility as high as ~ 4000 $cm^2V^{-1}s^{-1}$ at low temperatures (2 K). At the same time we have observed large negative magnetoresistance at 2 K. Although different effective crossover temperature and hysteresis behavior in magnetoresistance were observed for structured devices, which were absent in continuous films, our results demonstrate the conservation of the high-quality interface properties in the patterned structures. Hence, the development of this patterning method provides a first step in integrating high quality oxide interfaces exhibiting unique two-dimensional properties with other essential components on the same substrate crystal for innovative device applications. Our direct patterning method is capable of enabling the detailed future study of low-dimensional confinement on high mobility interface conductivity in heterostructures with thin LAO layers as well as interface magnetism in heterostructures with thick LAO layers.

Bibliography

[1] A. Ohtomo and H. Hwang, “A high-mobility electron gas at the $LaAlO_3/SrTiO_3$ heterointerface,” *Nature*, vol. 427, no. 6973, pp. 423–426, 2004.

[2] N. Nakagawa, H. Y. Hwang, and D. A. Muller, “Why some interfaces cannot be sharp,” *Nature Materials*, vol. 5, no. 3, pp. 204–209, 2006.

[3] C. Cen, S. Thiel, G. Hammerl, C. Schneider, K. Andersen, C. Hellberg, J. Mannhart, and J. Levy, “Nanoscale control of an interfacial metal-insulator transition at room temperature,” *Nature Materials*, vol. 7, no. 4, pp. 298–302, 2008.

[4] N. Reyren, S. Thiel, A. Caviglia, L. F. Kourkoutis, G. Hammerl, C. Richter, C. Schneider, T. Kopp, A.-S. Rüetschi, D. Jaccard, *et al.*, “Superconducting interfaces between insulating oxides,” *Science*, vol. 317, no. 5842, pp. 1196–1199, 2007.

[5] A. Brinkman, M. Huijben, M. Van Zalk, J. Huijben, U. Zeitler, J. Maan, W. Van der Wiel, G. Rijnders, D. Blank, and H. Hilgenkamp, “Magnetic effects at the interface between non-magnetic oxides,” *Nature Materials*, vol. 6, no. 7, pp. 493–496, 2007.

[6] A. Caviglia, S. Gariglio, N. Reyren, D. Jaccard, T. Schneider, M. Gabay, S. Thiel, G. Hammerl, J. Mannhart, and J.-M. Triscone, “Electric field control of the $LaAlO_3/SrTiO_3$ interface ground state,” *Nature*, vol. 456, no. 7222, pp. 624–627, 2008.

[7] C. Bark, P. Sharma, Y. Wang, S. H. Baek, S. Lee, S. Ryu, C. Folkman, T. R. Paudel, A. Kumar, S. V. Kalinin, *et al.*, “Switchable induced polarization in $LaAlO_3/SrTiO_3$ heterostructures,” *Nano Letters*, vol. 12, no. 4, pp. 1765–1771, 2012.

[8] P. Irvin, Y. Ma, D. F. Bogorin, C. Cen, C. W. Bark, C. M. Folkman, C.-B. Eom, and J. Levy, “Rewritable nanoscale oxide photodetector,” *Nature Photonics*, vol. 4, no. 12, pp. 849–852, 2010.

[9] J. Mannhart and D. Schlom, “Oxide interfaces - an opportunity for electronics,” *Science*, vol. 327, no. 5973, pp. 1607–1611, 2010.

[10] D. G. Schlom and J. Mannhart, “Oxide electronics: Interface takes charge over Si,” *Nature Materials*, vol. 10, no. 3, pp. 168–169, 2011.

[11] J. Mannhart, D. Blank, H. Hwang, A. Millis, and J.-M. Triscone, "Two-dimensional electron gases at oxide interfaces," *MRS Bulletin*, vol. 33, no. 11, pp. 1027–1034, 2008.

[12] S. J. Pearton and D. P. Norton, "Dry etching of electronic oxides, polymers, and semiconductors," *Plasma Processes and Polymers*, vol. 2, no. 1, pp. 16–37, 2005.

[13] D. W. Reagor and V. Y. Butko, "Highly conductive nanolayers on strontium titanate produced by preferential ion-beam etching," *Nature Materials*, vol. 4, no. 8, pp. 593–596, 2005.

[14] W. Rice, P. Ambwani, M. Bombeck, J. Thompson, G. Haugstad, C. Leighton, and S. Crooker, "Persistent optically induced magnetism in oxygen-deficient strontium titanate," *Nature materials*, 2014.

[15] C. Schneider, S. Thiel, G. Hammerl, C. Richter, and J. Mannhart, "Microlithography of electron gases formed at interfaces in oxide heterostructures," *Applied Physics Letters*, vol. 89, no. 12, pp. 122101–122101, 2006.

[16] C. Bell, S. Harashima, Y. Kozuka, M. Kim, B. Kim, Y. Hikita, and H. Hwang, "Dominant mobility modulation by the electric field effect at the $LaAlO_3/SrTiO_3$ interface," *Physical Review Letters*, vol. 103, no. 22, p. 226802, 2009.

[17] P. P. Aurino, A. Kalabukhov, N. Tuzla, E. Olsson, T. Claeson, and D. Winkler, "Nano-patterning of the electron gas at the $LaAlO_3/SrTiO_3$ interface using low-energy ion beam irradiation," *Applied Physics Letters*, vol. 102, no. 20, p. 201610, 2013.

[18] S. Mathew, A. Annadi, T. K. Chan, T. C. Asmara, D. Zhan, X. R. Wang, S. Azimi, Z. Shen, A. Rusydi, M. B. Breese, *et al.*, "Tuning the interface conductivity of $LaAlO_3/SrTiO_3$ using ion beams: Implications for patterning," *ACS Nano*, vol. 7, no. 12, pp. 10572–10581, 2013.

[19] C. Cen, S. Thiel, J. Mannhart, and J. Levy, "Oxide nanoelectronics on demand," *Science*, vol. 323, no. 5917, pp. 1026–1030, 2009.

[20] D. C. Suh, Y. D. Cho, S. W. Kim, D.-H. Ko, Y. Lee, M.-H. Cho, and J. Oh, "Improved thermal stability of $Al_2O_3/HfO_2/Al_2O_3$ high-k gate dielectric stack on gaas," *Applied Physics Letters*, vol. 96, no. 14, pp. 142112–142112, 2010.

[21] H. S. Chang, S. Jeon, H. Hwang, and D. W. Moon, "Excellent thermal stability of $Al_2O_3/ZrO_2/Al_2O_3$ stack structure for metal–oxide–semiconductor gate dielectrics application," *Applied physics letters*, vol. 80, no. 18, pp. 3385–3387, 2002.

[22] H.-J. Zhao, T.-L. Ren, L.-T. Zhang, J.-S. Liu, L.-T. Liu, and Z.-J. Li, "Preparation and etching of silicon-based piezoelectric thin films for integrated devices," *Integrated Ferroelectrics*, vol. 48, no. 1, pp. 271–279, 2002.

[23] M. Kawasaki, K. Takahashi, T. Maeda, R. Tsuchiya, M. Shinohara, O. Ishiyama, T. Yonezawa, M. Yoshimoto, and H. Koinuma, "Atomic control of the $SrTiO_3$ crystal surface," *Science*, vol. 266, no. 5190, pp. 1540–1542, 1994.

[24] G. Koster, B. L. Kropman, G. J. Rijnders, D. H. Blank, and H. Rogalla, "Quasi-ideal strontium titanate crystal surfaces through formation of strontium hydroxide," *Applied Physics Letters*, vol. 73, no. 20, pp. 2920–2922, 1998.

[25] M. Huijben, A. Brinkman, G. Koster, G. Rijnders, H. Hilgenkamp, and D. H. Blank, "Structure-property relation of $LaAlO_3/SrTiO_3$ interfaces," *Advanced Materials*, vol. 21, no. 17, pp. 1665–1677, 2009.

[26] C. Bell, S. Harashima, Y. Hikita, and H. Hwang, "Thickness dependence of the mobility at the $LaAlO_3/SrTiO_3$ interface," *Applied Physics Letters*, vol. 94, no. 22, pp. 222111–222111, 2009.

[27] R. Pentcheva, M. Huijben, K. Otte, W. Pickett, J. Kleibeuker, J. Huijben, H. Boschker, D. Kockmann, W. Siemons, G. Koster, *et al.*, "Parallel electron-hole bilayer conductivity from electronic interface reconstruction," *Physical Review Letters*, vol. 104, no. 16, p. 166804, 2010.

[28] M. Huijben, G. Rijnders, D. H. Blank, S. Bals, S. Van Aert, J. Verbeeck, G. Van Tendeloo, A. Brinkman, and H. Hilgenkamp, "Electronically coupled complementary interfaces between perovskite band insulators," *Nature Materials*, vol. 5, no. 7, pp. 556–560, 2006.

[29] A. Caviglia, S. Gariglio, C. Cancellieri, B. Sacépé, A. Fete, N. Reyren, M. Gabay, A. Morpurgo, and J.-M. Triscone, "Two-dimensional quantum oscillations of the conductance at $LaAlO_3/SrTiO_3$ interfaces," *Physical Review Letters*, vol. 105, no. 23, p. 236802, 2010.

[30] A. N. Pasupathy, R. C. Bialczak, J. Martinek, J. E. Grose, L. A. Donev, P. L. McEuen, and D. C. Ralph, "The kondo effect in the presence of ferromagnetism," *Science*, vol. 306, no. 5693, pp. 86–89, 2004.

Chapter 3

Patterning of Multilayer Epitaxial $PbZr_{0.52}Ti_{0.48}O_3$ Heterostructures

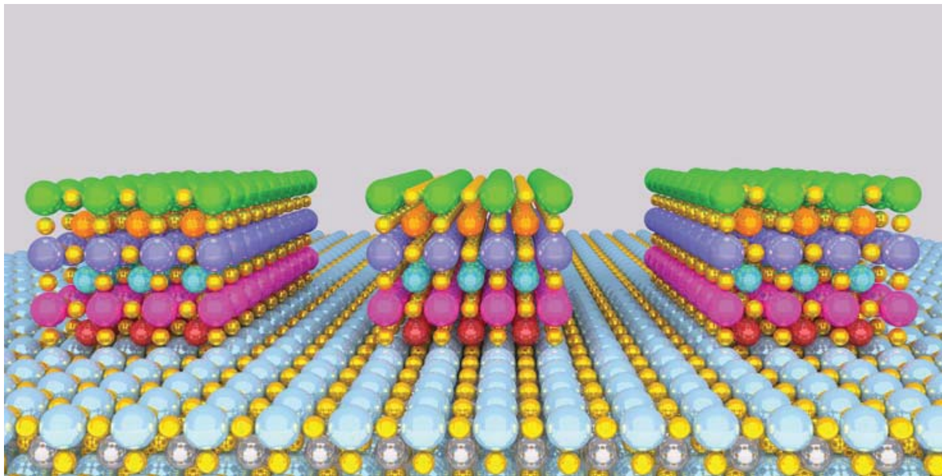

Part of the work discussed in this chapter is published in:
N. Banerjee, G. Koster, G. Rijnders, "*Submicron Patterning of Epitaxial $PbZr_{0.52}Ti_{0.48}O_3$ Heterostructures*", *Applied Physics Letters* 102, 142909 (2013).

ABSTRACT

Epitaxial multilayer and superlattices are highly valued as electronic materials because of their often exhibited superior functional properties in comparison to the individual constituents. In order to utilize these functional multilayer oxides for practical electronic devices, precise structures have to be fabricated, which can be integrated with other device components. For perovskite oxide superlattices this is often hampered because of the different physical and chemical nature of the individual layers. The development of a fabrication strategy, which is capable of simultaneously patterning the high temperature grown epitaxial multilayer, is therefore highly desirable. In this chapter, we demonstrate that the epitaxial lift-off technique is suitable for structuring the epitaxial multilayers of $PbZr_{0.52}Ti_{0.48}O_3$ *incorporating* $SrRuO_3$ *(SRO) electrodes. The added advantage of the patterning strategy is that it does not require any corrosive acids (like HF, HCl) which are conventionally used for PZT-etching. Our procedure involves the use of a pre-patterned* AlO_x *mask, which acts as a high temperature resistant sacrificial template, as described in the previous chapter and enables the patterning of the perovskite multilayer via a single lift-off step. We have investigated the ferroelectric properties of the lift-off patterned epitaxial PZT heterostructures, grown on* $SrTiO_3$*(001) as well as on commercial platinized Si substrates. Piezoresponse force microscopy was employed to investigate the ferroelectric behavior of the* $\sim 2\ \mu m$ *structures. The lift-off fabricated structures displayed well-behaved ferroelectric and piezoelecctric response analogous to the similar structures prepared through conventional wet-etching process.*

3.1 Introduction

3.1.1 Lead Zirconate Titanate (PZT) as the piezoelectric material

Since its discovery in $\sim$ 1880 by the brothers Jacques and Pierre Curie [1], piezoelectricity has been a focus point in crystal physics research, from both the perspectives of fundamental understanding and technological implementations. In the piezoelectric crystals, application of an external elastic stress (in suitable crystal orientations) develops a proportional change in the electrical polarization as well as suitably oriented external electric field generates a proportional elastic stress, making them an ideal material for combined sensing and actuation purposes. Although the range of piezoelectric material covers a wide variety of naturally occurring substances, for simple piezoeletrics (like topaz or bone) the effect is too small to be employed for any practical purposes. The solid solution lead zirconate titanate, $\mathrm{PbZr}_x\mathrm{Ti}_{1-x}\mathrm{O}_3$ (PZT) displays a much stronger piezoelectric effect and is one of the most industrially used piezoelectric material [2, 3]. Owing to its superior piezo-electric properties, PZT has been traditionally utilized as the key functional material in numerous electromechanical devices such as - sensors and actuators [4–6], energy harvesters [7–9], transducers [10–12], accelometers [13,14] etc. At the 'morphotropic phase boundary' (MPB) with the composition $\mathrm{PbZr}_{0.52}\mathrm{Ti}_{0.48}\mathrm{O}_3$, PZT shows very high electromechanical coupling coefficients and stable polarization response with respect to external mechanical and/or electrical perturbations [15–18]. At the MPB the ferroelectric phase boundary is crossed from Ti-rich tetragonal side to Zr-rich rhombohedral side, directing the polar domain vectors to change their orientation spontaneously. This makes it very easy for an external electric field to tilt the polar domain vectors, leading to stronger electromechanical activity. In this chapter we have performed all experimental research work with MPB-PZT, but our conclusions can be extended to other compositions as well.

3.1.2 Etching technologies for PZT : dry & wet etching

Owing to its potential piezo/ferroelectric properties PZT has been extensively used in numerous electromechanical devices covering wide range of applications. Following the recent trend of electronic miniaturization the size of such functional piezo devices must be in the few μm - submicron range to achieve very high device densities. Miniaturization of piezo/ferro electric electromechanical devices in micro/nano electro mechanical systems (MEMS/NEMS) processing technology, requires precise patterning of the PZT-film down to the few micro - submicron scale. This is one of the few key challenging issue in integrating PZT with silicon-based very large scale integration (VLSI) technology and has attracted considerable

research attention over the past decades. PZT is a stable perovskite oxide and it possess substantial inertness towards chemical and physical etching processes. Traditional etching of PZT involves "top-down" approaches through dry and wet etching procedures employing highly energetic ions or extremely reactive chemicals.

Acidic wet chemical etching is one of the most widely used processing methodologies for structuring PZT, which uses a buffered solution of corrosive hydrofluoric acid (HF) together with hydrochloric acid (HCl) and nitric acid (HNO_3) [19–26]. The HF solution is generally buffered by mixing with NH_4F (in 1:10 wt%) in order to make it photo-lithography compatible and to stabilize the etching rate by controlling the depletion rate of F^-. In PZT, the zirconium component can be etched using HF or HNO_3, the titanium component by HCl, HF, H_2SO_4 and the lead-component can be dissolved in HNO_3, HCl or in acetic acid solution [22, 23]. Existence of multiple elements in PZT makes one-step chemical etching difficult. Although some acids like HF can dissolve more than one component, differences in reaction rates between different components hamper the simultaneous etching process. HF reacts with PZT as follows :

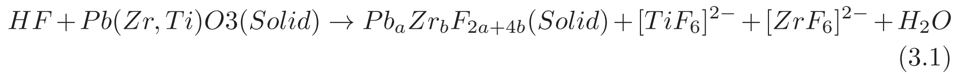

$$HF + Pb(Zr, Ti)O3(Solid) \rightarrow Pb_aZr_bF_{2a+4b}(Solid) + [TiF_6]^{2-} + [ZrF_6]^{2-} + H_2O \quad (3.1)$$

The reaction rate of the Ti-component with HF is much faster than the analogous reaction with the Zr-component, leading to easy formation of Pb-rich residues which need a second acidic solution (HNO_3 or HCl) to dissolve [23]. Etching residues with the composition $Pb_{0.85}Zr_{0.15}F_{2.3}$ and Pb_5ZrF_{14} has been experimentally identified after HF based etching of PZT [19, 21]. Apart from the production of lead-rich residues [19, 23], several other major problems were encountered as well, while etching PZT films with strongly acidic solutions through photoresist masks. This includes heavy undercut and brim damage [20,24] attack of HF to pre-existing device components underneath PZT and the degradation of the ferroelectric properties in etched films [22]. Although intensive research was performed to improve the wet-etching procedure using multiple chemical treatments [19, 22, 23] of etched films, the enhanced possibility of contamination in successive steps and chemical attack of these reactive acids to any pre-existing device components (other than PZT) still remains a concern.

Several dry ion etching procedures, both reactive and non-reactive dry etching technologies have also been investigated to pattern PZT-based thin films [27–35]. The key challenges faced in order to incorporate dry-etched PZT in VLSI technology were achieving a high etch rate, a vertical etch-profile and a very high etch-selectivity with respect to the electrode materials. Halogen gases (mainly fluorine and chlorine) have been popular for the investigation of reactive ion etching (RIE) of PZT. However the difference between vapor pressures of etch-byproduct metal-halogen compounds causes stoichiometric deviation of individual metal components in post-etched PZT [35]. Also very low vapor pressures of these metal-halogen compounds

make the etch rate very slow. In order to obtain better results several improvements were suggested to the simple RIE etching. These include magnetically enhanced reactive ion etching (MERIE) [36], helicon plasma etching [37] and inductively coupled plasma (ICP) etching [29, 31]. However, very slow etching rates, even with higher density plasma-assisted techniques like electron cyclotron resonance (ECR) [32] make these processes less suitable for commercial use. Also the poor etch selectivity of PZT as compared to the photoresist mask, differences in sputter yields between the atomic components of PZT and metallic electrodes, degradation of the film properties due to the bombardment produced local stress and redeposition at the side walls [38] pose challenges for producing reliable PZT patterns.

3.1.3 Patterning of multilayer heterostructures

Many applications of ferroelectric films (e.g. memory devices, piezo-MEMS devices) require electrodes on one or both sides of the film. Together with the ferroelectric (for example PZT) these electrode layers also need to be patterned in functional devices for applying an electric field in selective areas. It was established that the conducting oxide electrodes are superior to their metallic counterparts for stable performance of the ferroelectric with respect to multiple switching cycles, known as *ferroelectric fatigue* [39, 40]. Most of these perovskite oxide materials are high temperature grown phases and unlike metals they cannot be patterned through photolithography assisted lift-off at room temperature. Generally all-oxide multilayer electrode/PZT/electrode capacitors are patterned through multiple etching steps incorporating both dry ion and wet chemical etching procedures, depending on the nature of the particular oxide layer [41–43]. The multiple-step etching strategy is time-consuming, possesses enhanced possibility of contamination from individual steps, delicate to perform (since one has to stop the etching precisely at the desired layer). Hence the development of a single step fabrication pathway to pattern the high temperature grown all-oxide multilayer capacitors would be a key achievement in oxide fabrication technology.

3.1.4 Lift-off patterning of multilayer PZT

In the previous chapter (*Chapter 2*) we have discussed a lift-off patterning procedure for structuring high temperature grown perovskite oxides, utilizing an amorphous AlO_x layer as the high temperature resistant sacrificial oxide hard mask. It was shown that the epitaxial lift-off pathway is capable of patterning the delicate epitaxial interface between $LaAlO_3$ and $SrTiO_3$, while preserving the high quality interfacial metallic properties [44]. In this chapter we investigate the application of the developed lift-off strategy to pattern thin film $PbZr_{0.52}Ti_{0.48}O_3$ heterostructures incorporating epitaxial oxide electrode layers ($SrRuO_3$). If successful, this direct 'bottom up' fabrication technique can lead to an one-step lift-off patterning of

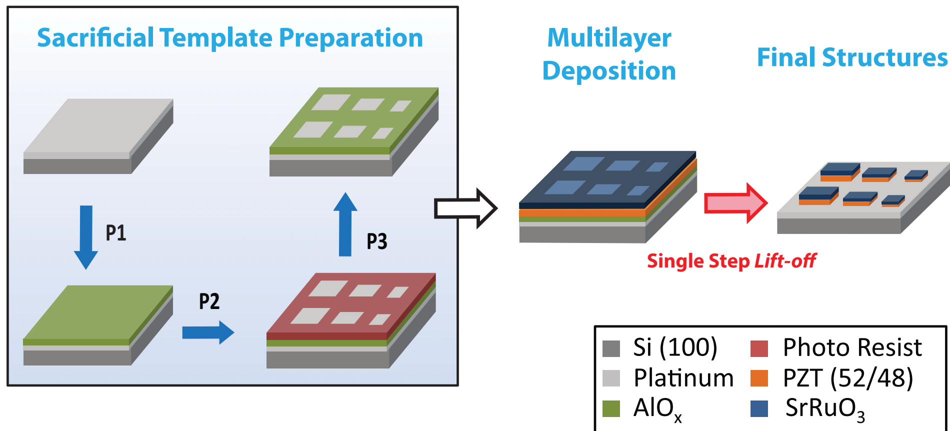

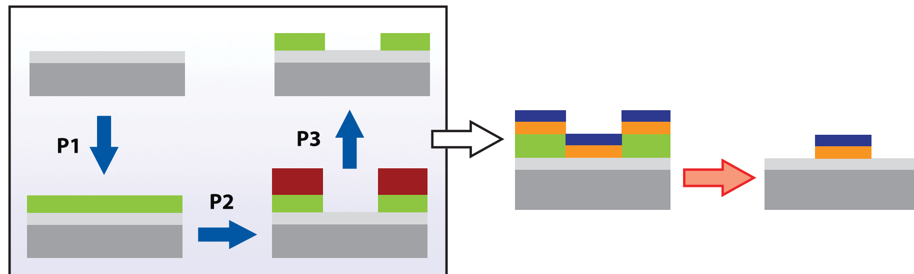

Figure 3.1: Schematic representation of the patterning process of $PbZr_{0.52}Ti_{0.48}O_3$ films together with epitaxially grown top $SrRuO_3$ perovskite electrode on a platinized Si substrate. Step P1- P3 describe the preparation of a sacrificial amorphous aluminum oxide (AlO_x) template. Step P1 : the deposition of the AlO_x layer on a platinized-Si substrate. Step P2 and P3 : photolithographic patterning of the template AlO_x layer. Next, PZT and SRO multilayers were deposited at elevated temperatures by PLD. Finally, the template layer was lifted off together with the amorphous layers deposited on top.

entire high temperature grown heteroepitaxial oxide stack. An added advantage is that the amorphous AlO_x layer, utilized as high temperature resist material was patterned through traditional photolithography, without performing any additional fabrication step. We also investigate the influence of the patterning procedure on the functional ferroelectric properties of MPB-PZT thin films on different substrates. This is done by fabricating lift-off patterned structures on different substrates and comparing their functional properties with traditional wet-etch fabricated analogues. Epitaxial $SrRuO_3$-$SrTiO_3$ substrates as well as commercial Pt/Si wafers were used for PZT growth and lift-off patterning to verify their compatibility with the fabrication process and to investigate the ferroelectric properties lift-off PZT on different substrates. To provide a detailed insight in the patterning procedure and its influence on the fabricated structures we demonstrate a detailed investigation on the fabrication of ~ 2 μm wide PZT lines. As discussed in the previous sections heavy undercut and associated brim damage are among the most important concerns in the wet-etching technology. We show that lift-off patterned heterostructures have minimal undercut. It is well established that the ferro/piezo electric properties of PZT are very sensitive to the processing conditions and low dimensionality [45–47]. Therefore we investigated the functional behavior of PZT lines with a width of a few μm by employing piezo response force microscopy (PFM). The results obtained in this chapter are useful to establish the *epitaxial lift-off* fabrication strategy as an alternative pathway for patterning a heteroepitaxial PZT multilayer, which can be of fundamental and industrial importance in fabricating MEMS/NEMS devices with good ferro/piezoelectric properties.

3.2 Experimental Methods

3.2.1 Preparation of sacrificial template mask

$PbZr_{0.52}Ti_{0.48}O_3$ heterostructures were patterned on silicon as well as on single crystalline substrates using a structured amorphous aluminum oxide (AlO_x) layer as sacrificial template mask, which is capable of withstanding high temperatures. First, a thin layer of AlO_x was deposited on the desired substrate using pulsed laser ablation. A single crystalline Al_2O_3 target was ablated at room temperature using a high energy KrF excimer laser of 248 nm wavelength with a typical pulse length of 20 - 30 ns. The deposition was achieved with 2.5 mm^2 spot size, 1.5 J/cm^2 laser fluency and in 0.2 mbar of oxygen pressure. The deposition time and repetition rate was adjusted in order to obtain the required thickness. In the next step a positive photoresist (OLIN 17) layer was spin coated ($\sim$ 1.2 μm thick) and patterned with a conventional photolithographic process. The standard photoresist-developer solution is a basic solution and reacts with the AlO_x mask layer forming water soluble alkali-metal aluminates. Hence, while developing the photoresist pattern

(after ultra-violate light exposure) the underlying alumina layer also develops and dissolves in the water. This mimics the photoresist pattern in the AlO_x layer and opens up selective areas on the substrate, where the perovskite materials can be deposited at high temperatures. The remaining photoresist was removed using organic solvents leaving substrates with a patterned amorphous alumina layer. The whole lithographic procedure was performed in a clean-room environment to minimize any contamination.

3.2.2 High temperature multilayer deposition and lift-off

Substrates covered with patterned amorphous aluminum oxide layers were subjected to deposition of multilayer perovskite heterostructures at high temperatures by pulsed laser deposition (PLD), resulting in epitaxial growth in uncovered areas. Growth details to achieve optimum growth of different perovskites with the PLD process can be found elsewhere [48]. After high temperature deposition of oxide multilayers and subsequent controlled cooling down to room temperature the samples were treated with a 4M NaOH solution, which dissolved the sacrificial AlO_x template as alkali metal aluminate in the solution with simultaneous removal of the amorphous oxides deposited on top of it [44]. This leads to a one step removal of all unwanted oxide layers and produces the desired pattern directly. Finally the samples with perovskite patterns were cleaned with deionized water several times in order to remove any surface contamination. For the specific case of the fabrication of heterostructure capacitors on top of a $SrRuO_3$ conducting bottom electrode, the $SrRuO_3$ film was deposited via PLD before the AlO_x mask layer deposition and patterning. The fabrication process is presented schematically in both top and side views in Figure 3.1.

3.3 Characterization Methods

Heterostructures, incorporating $PbZr_{0.52}Ti_{0.48}O_3$, were patterned in different sizes, from larger area capacitors of $\sim 10^4$ μm^2 area (in order to measure ferroelectric properties) down to lines of ~ 2 μm width, which is close to the conventional contact printing photo-lithographic limit. Patterned sacrificial AlO_x template mask and fabricated PZT micro structures were characterized using high resolution scanning electron microscopy (SEM) (Zeiss) and atomic force microscope (AFM) (Veeco) for detailed study of the patterning process. To gain insight on crystal structure and phase purity, patterned PZT heterostructures were subjected to X-ray diffraction (XRD, X'pert^{TM} Philips). In order to measure the ferroelectric properties, heteroteroepitaxial capacitors with metal-insulator-metal (M-I-M) configuration were fabricated by growing and patterning SRO/PZT on commercial $Pt/Ti/SiO_2/Si$ (100) substrate, as well as on single crystalline $SrTiO_3$ (001) substrates with the

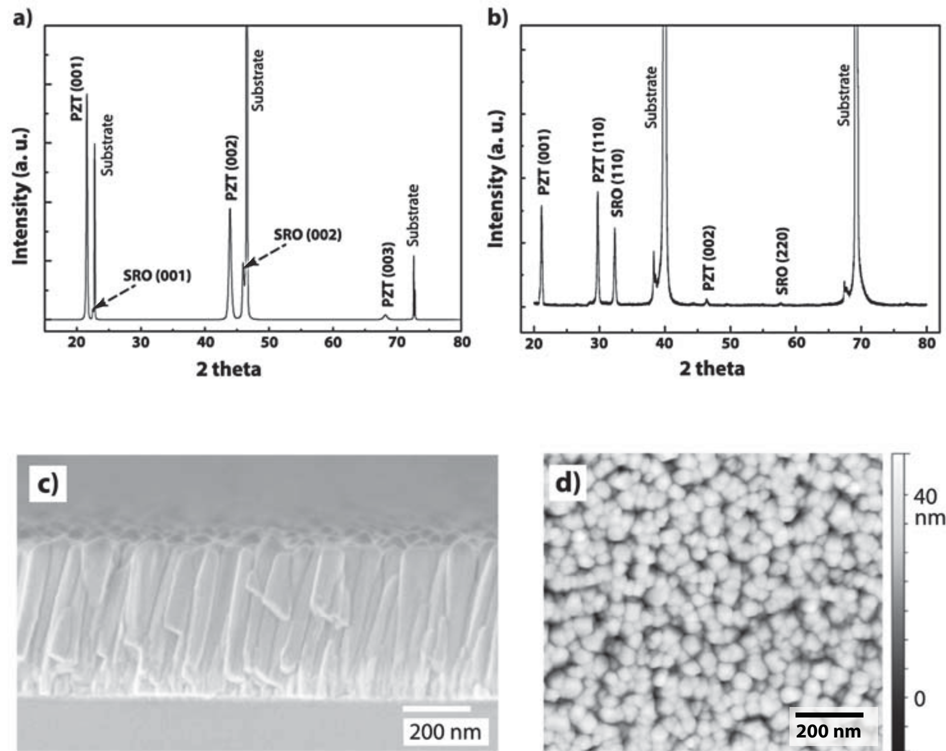

Figure 3.2: X-ray diffraction spectrum of the lift-off fabricated epitaxial PZT capacitors on (a) STO (001) and on (b) Pt/Si(001). SEM image of the PZT layer on Pt/Si substrate in cross-sectional view is shown in (c) and the corresponding topographic AFM image is presented in (d), revealing the columnar growth of PZT.

film of a conducting perovskite, $SrRuO_3$ as the bottom electrode. The ferroelectric behavior, i.e. the out of plane polarization hysteresis loop (P-E), and the multiple cycle fatigue response of the structured morphotropic PZT capacitors in M-I-M configuration were measured using a modified Sawyer-Tower circuit (aixACCT TFAnalyzer 2000). During the measurement, the films were subjected to bipolar triangular switching cycles at a frequency of 2 kHz and with 250 kV/cm amplitude.

3.4 Results and Discussions

3.4.1 X-ray diffraction studies after lift-off

Fig. 3.2 shows representative XRD spectra of patterned morphotropic PZT samples on $SrTiO_3$ as well as on Pt/Si substrates. All the oxide layers after the lift off step were found to be crystalline. While the growth on STO substrate was (001) epitaxial, on platinized Si (100) PZT show two domain orientations, corresponding to (110) and (100) growth [41]. No reflections corresponding to AlO_x were observed with post-etched samples indicating complete removal of the sacrificial mask by the lift off process. For the (001) epitaxial PZT/STO sample the (103) reflection in a reciprocal space map (RSM) appeared as a single reflection within the resolution of the diffraction (not shown) implying no mixed a- and c- domain formation. This is in accordance with the nearly cubic unit-cell structure of PZT at/near the morphotropic phase boundary [43].

3.4.2 Ferroelectric properties of the lift-off fabricated $PbZr_{0.52}Ti_{0.48}O_3$ heterostructures

Fig. 3.3 (a) and (b) represent the out of plane polarization hysteresis loops (P-E) measured from $\sim$ 500 nm thick capacitors with 50 $\times$ 50 μm^2 size, fabricated on (001) STO and platinized Si (001) substrate respectively. Remnant polarization and coercive field values obtained from 500 nm PZT 52/48 films on (001) STO substrate were $\sim$ 50 $\mu C/cm^2$ and 85 kV/cm, and on platinized Si (001) substrate were $\sim$ 22 $\mu C/cm^2$ and 40 kV/cm as is given in Fig. 3.3(a) and (c) respectively with corresponding current-voltage behavior shown in Fig. 3.3(b) and (d) respectively. The observed ferroelectric properties from lift-off fabricated hetero-epitaxial capacitors are in good agreement with the analogous measurements on samples based on wet-etched PZT [41, 43, 48]. It was shown that the nature of the P-E loop for ferroelectric thin films, especially the values of remnant polarization and coercive field are crucially dependent on the crystal orientation [16] and nature of the strain induced by the substrate [43, 49, 50] which explains the different shape of the P-E loop obtained on different substrates. While sharp switching peaks were observed for the (001)epitaxial sample on $SrTiO_3$, splitting of the switching peak can be noticed for the other, which can be ascribed to the asymmetries between the top ($SrRuO_3$) and the bottom (Pt) electrode. Ferroelectric fatigue behavior of structured PZT capacitors were measured up to 10^8 switching cycles, which is presented in Fig. 3.4(b) and Fig. 3.4(d). While films grown epitaxially on a STO substrate had a very stable ferroelectric response during repetitive switching, films on platinized Si manifested larger fatigue with 15 % loss in remnant polarization after 10^8 switching cycles. Similar results have been observed on the PZT

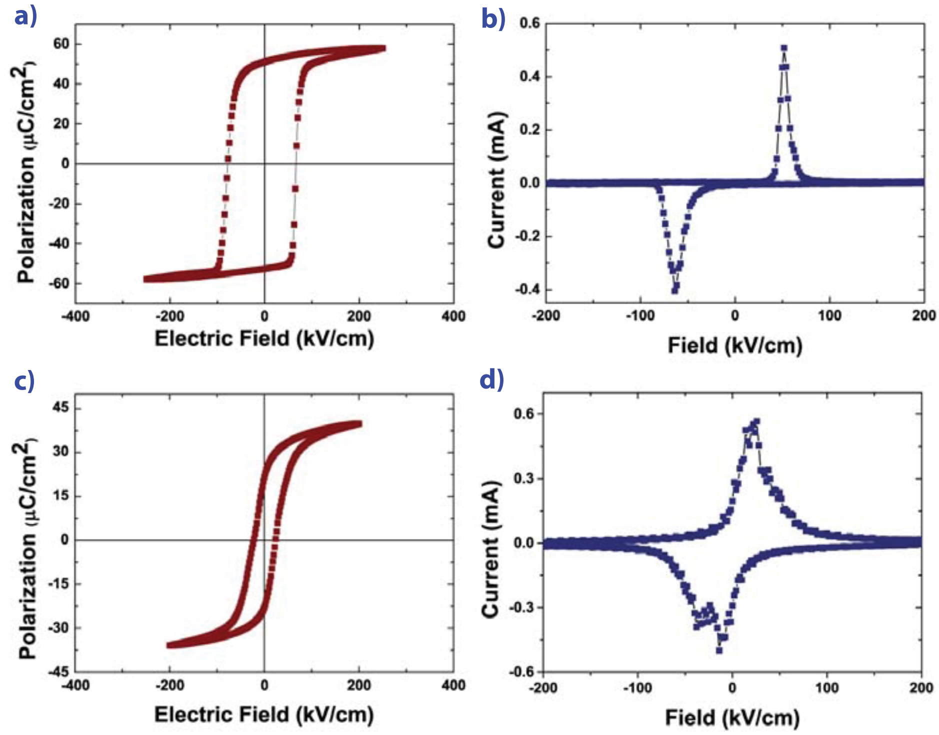

Figure 3.3: Polarization - Electric field (P-E) hysteresis loops of patterned $PbZr_{0.52}Ti_{0.48}O_3$ thin film capacitors in M-I-M configuration, grown - (a) epitaxially on single crystalline $SrTiO_3$ (001) substrate and (c) on Pt/Ti/SiO_2/Si (100) substrate. (b) and (d) shows the current-voltage (I-V) behavior corresponding to the P-E loops shown respectively.

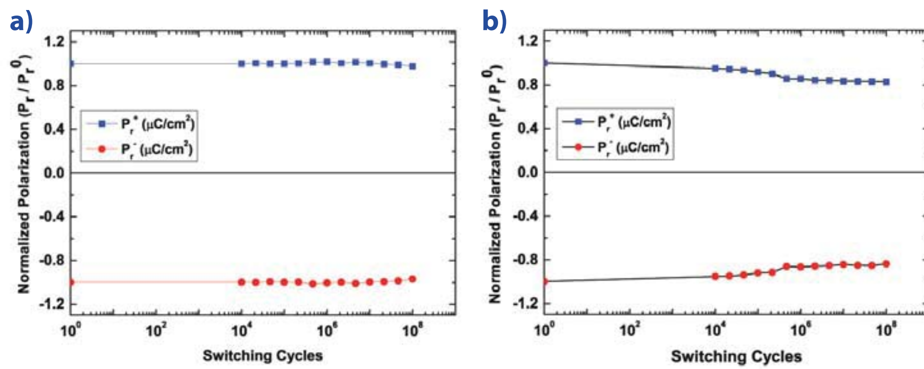

Figure 3.4: Normalized polarization fatigue behavior up to 10^8 switching cycles, measured with the lift-off fabricated epitaxial PZT capacitors on (a) SRO/STO (001) and on (b) Pt/Si(001).

capacitors fabricated by the traditional wet-etching method [41]. Hence our results demonstrate that the lift-off structuring procedure does not affect the functional ferroelectric behavior of PZT hetero-structures and is able to produce high quality ferroelectric properties, previously observed in heteroepitaxial devices with multiple etching steps.

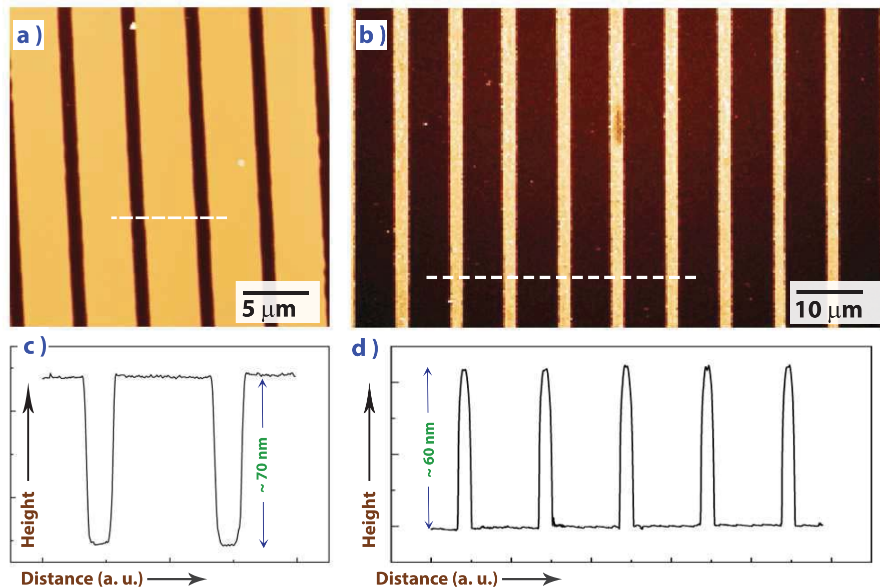

Figure 3.5: AFM image of (a) the patterned AlO_x mask before the high temperature perovskite deposition and of (b) $PbZr_{0.52}Ti_{0.48}O_3$ micro-lines after the lift-off of the mask. Height profiles measured by the AFM tip corresponding to the broken lines indicated in the AFM images, is shown in (c) and (d).

3.4.3 Detailed investigation on the lift-off process : fabrication of PZT lines

To analyze the selective area growth process using the high temperature resistant, sacrificial AlO_x template we have fabricated PZT (52/48) lines on platinized Si substrates with a width of ~ 2 μm, separated by the distance of ~ 6 μm from each other. With conventional contact printing photo-lithographic patterning, the ~ 2 μm feature size is near the resolution limit, unless advanced exposure techniques are used. Fig. 3.5(a) shows an atomic force microscopic (AFM) image of the structured AlO_x mask, obtained after lithographic development with basic (TMAH) solution and subsequent resist removal. Height profile corresponding to the indicated broken line in the AFM image is shown in Fig. 3.5(c). It shows

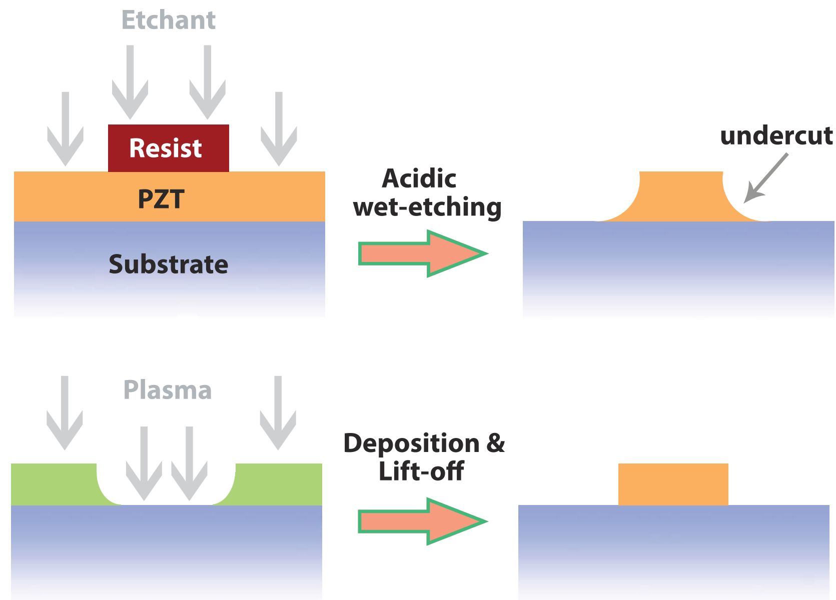

Figure 3.6: Schematics of the different fabrication approaches from the side view, traditional wet-etching mediated *top-down* patterning (top) and *bottom-up* lift-off patterning (bottom). For the details of the lift-off fabrication scheme, see Fig. 3.1.

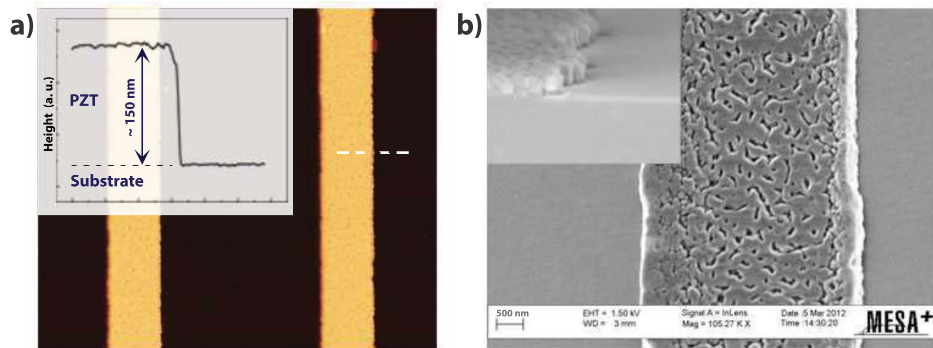

Figure 3.7: (a) AFM image of the PZT lines on Pt/Si(001) substrates with average width of $\sim 2\ \mu$m. The inset shows the height profile corresponding to the indicated broken line in the image. (b) SEM image of a single PZT line with the cross sectional view in the inset.

a near perpendicular edge and has a well defined profile. The thickness of the AlO_x mask was in this case $\sim$ 70 nm, employed to obtain $\sim$ 1:1, mask : PZT thick microstructures. Morphotropic PZT of $\sim$ 60 nm thickness was grown at high temperature (600°C). After deposition, subsequent annealing and cool down to room temperature, the mask together with the top grown amorphous PZT were lifted off using a basic solution. Fig. 3.5(b) represents the AFM morphology of the obtained PZT line-patterns with $\sim$ 2 μm line width and $\sim$ 6 μm separation from each other. The corresponding height profile is shown in Fig. 3.5(c). It can be noticed that the individual PZT (52/48) lines with $\sim$ 2 μm width were well structured, sharp edged and have a high individual aspect ratio.

From detailed morphological investigations of a single line it was found that the film surface constituted of densely packed columnar grains of $\sim$ 40 nm diameter. Thus the growth behavior was quite similar to that of unstructured analogous films of morphotropic PZT on identical substrates. It was also possible to pattern thicker heterostructures employing the lift-off fabrication. In our experiments we have structured PZT films up to the thickness of $\sim$ 1 μm by employing a thicker AlO_x sacrificial template, which makes the patterning pathway promising for MEMS/NEMS fabrication.

3.4.4 Difference between wet-etching and lift-off approaches

Fig. 3.6 shows a schematic representation of the difference between the top-down and lift-off fabrication approaches to pattern PZT. In the traditional reactive chemical-based wet etching, the chemical reacts isotropically with the PZT. In isotropic etching the chemical etches PZT also in the side-way direction, together with the desired vertical direction. This gives rise to an undercut in the patterned structure. In contrast, the lift-off technique relies on the growth of the material in pre-patterned substrate areas. The advantage of PLD mediated growth is that it is preferably unidirectional [51]. Thus although undercut exists on the mask (because of its chemical patterning), minimal undercut is expected for the final perovskite structures, nucleated uni-directionally from the plasma. Fig. 3.7(a) represents an AFM image of lift-off fabricated, $\sim$ 150 nm thick, PZT lines on a Pt/Si substrate. A representative height profile along the line edge is shown as the inset. The line edge was found to be perpendicular as probed by the AFM, revealing no visible broadening of the PZT growth in the under-etched AlO_x mask. This point is further strengthened by SEM studies of the fabricated lines from the top and cross-sectional views as given in Fig. 3.7(b). The cross-sectional view (shown in the inset) of an individual PZT line clearly shows the existence of perpendicular PZT columnar structures at the line-edges.

3.4.5 PFM investigation of PZT micro-lines

The ferroelectric response of the fabricated PZT micro-lines was probed employing piezoresponse force microscopy (PFM). This particular scaning probe technique is capable of imaging and switching ferroelectric domains through external AC and DC bias voltages, applied using a metalized AFM tip. The metallic platinum layer on the substrate functioned as the ground electrode plane, while the conducting scanning probe tip acts as the top electrode. PFM images corresponding to out of plane (OP) amplitude and phase characteristics, after consecutive switchings of selected areas with opposite DC bias voltages ($\geq$ coercive field, $\pm$ 6 V DC) are presented in Fig. 3.8(a) and (b). It can be noticed from the OP phase image (b) that the unpoled, virgin PZT was positively polarized, which is a generic feature observed for PLD made PZT-films [52–55]. The small contrast difference in the negatively switched film area was presumably arising from the tip-artifact. Fig. 3.9 (a) and (b) shows phase and amplitude switching characteristics with applied sweeping DC bias voltage obtained from a fabricated PZT micro-line. It is evident from the PFM studies that the morphotropic PZT lines patterned through the sacrificial template assisted lift-off procedure with widths down to a few micrometers display piezoelectric response, retain the induced polarization and can be switched to the opposite polarization state by application of a large enough reverse bias voltage.

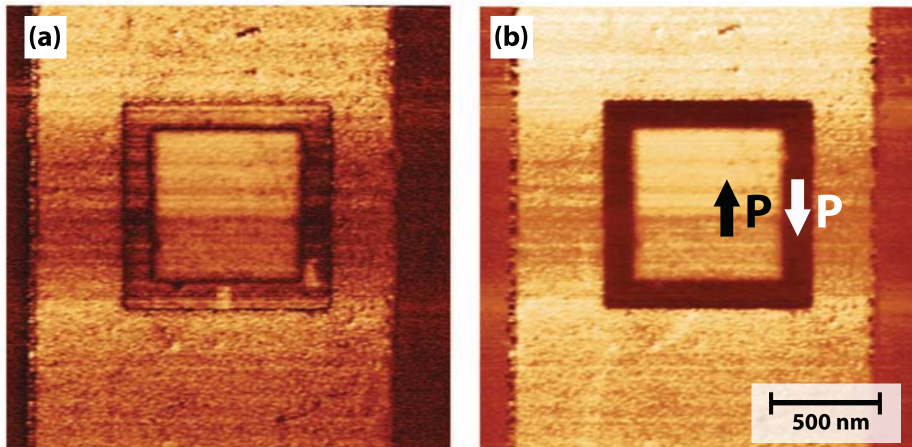

Figure 3.8: Piezo Response Force microscopic (PFM) images corresponding to out of plane (a) amplitude and (b) phase after selective area consecutive switchings on a PZT micro-line by applying opposite bias voltages through the PFM tip.

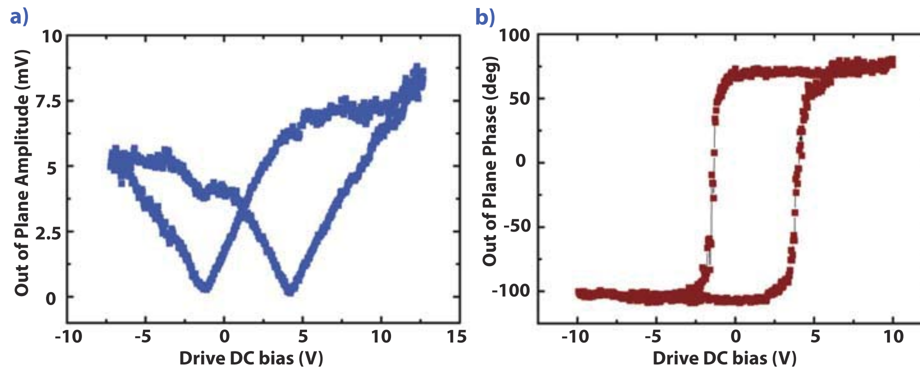

Figure 3.9: Out of plane PFM (a) amplitude and (b) Phase sweeps in response to an external DC drive bias voltage applied by the conducting PFM tip.

3.5 Conclusion

In this chapter we have demonstrated a sacrificial mask assisted fabrication procedure to achieve the single step lift-off patterning of epitaxial perovskite multilayers grown at elevated temperatures. The patterning strategy was enabled through the use of a pre-patterned amorphous AlO_x sacrificial template layer, which is capable of withstanding higher temperatures. In order to demonstrate, heteroepitaxial $SrRuO_3/PbZr_{0.52}Ti_{0.48}O_3$ multilayer devices of different micro-scale sizes were simultaneously patterned utilizing the lift-off pathway, without employing any dry-ion etching and/or wet-acidic chemical etching. The PZT heterostructures were grown and patterned on different substrates, in order to examine and compare the perovskite-growth and their ferroelectric properties with similar structures patterned via traditional dry and acidic wet etching techniques. Structural and morphological investigations proved that the growth of the perovskite layers was unaffected by the masking process and was similar to continuous film samples. No signature of the mask was observed in XRD spectrum of patterned samples, suggesting the complete removal of the mask in the lift-off step. Ferroelectric properties of the structured PZT heterolayers, grown epitaxially on (001) $SrTiO_3$ substrates as well as on commercially important platinized Si substrates were investigated in a capacitor configuration and were in good agreement with the analogous structures prepared with conventional wet-etching process. Hence, it is concluded that the patterning procedure does not harm the functional behavior of the ferroelectric heterostructures. To investigate the patterning process in detail we have also fabricated a series of narrow PZT lines with line with of $\sim 2\ \mu$m and separation of $\sim 6\ \mu$m. These fabricated unidirectional microstructures had a vertical line profile edge and did not display any visible undercut as investigated by SEM and AFM. They also manifested switchable ferroelectric response when probed by piezoresponse force microscopy, suggesting conservation of the ferroelectric properties. The demonstrated multilayer lift-off patterning method can find useful application in the fabrication of various functional devices like high-density memory device elements (discussed in *Chapter 4*), electromechanical (MEMS/NEMS) devices (discussed in *Chapter 5*) etc.

Bibliography

[1] J. Curie and P. Curie *Bull. Soc. Fr. Mineral.*, vol. 3, no. 90, 1880.

[2] E. Cross, “Materials science: Lead-free at last,” *Nature*, vol. 432, no. 7013, pp. 24–25, 2004.

[3] C.-P. De Araujo, J. Cuchiaro, L. McMillan, M. Scott, and J. Scott, “Fatigue-free ferroelectric capacitors with platinum electrodes,” *Nature*, vol. 374, no. 6523, pp. 627–629, 1995.

[4] R. E. Newnham and G. R. Ruschau, “Smart electroceramics,” *Journal of the American Ceramic Society*, vol. 74, no. 3, pp. 463–480, 1991.

[5] P. Muralt, “Ferroelectric thin films for micro-sensors and actuators: a review,” *Journal of Micromechanics and Microengineering*, vol. 10, no. 2, p. 136, 2000.

[6] F. P. Sun, Z. Chaudhry, C. Liang, and C. Rogers, “Truss structure integrity identification using PZT sensor-actuator,” *Journal of Intelligent Material Systems and Structures*, vol. 6, no. 1, pp. 134–139, 1995.

[7] W. Choi, Y. Jeon, J.-H. Jeong, R. Sood, and S.-G. Kim, “Energy harvesting MEMS device based on thin film piezoelectric cantilevers,” *Journal of Electroceramics*, vol. 17, no. 2-4, pp. 543–548, 2006.

[8] D. Shen, J.-H. Park, J. H. Noh, S.-Y. Choe, S.-H. Kim, H. C. Wikle III, and D.-J. Kim, “Micromachined PZT cantilever based on SOI structure for low frequency vibration energy harvesting,” *Sensors and actuators A: physical*, vol. 154, no. 1, pp. 103–108, 2009.

[9] S. P. Beeby, M. J. Tudor, and N. White, “Energy harvesting vibration sources for microsystems applications,” *Measurement Science and Technology*, vol. 17, no. 12, p. R175, 2006.

[10] T. Morita, M. Kurosawa, and T. Higuchi, “An ultrasonic micromotor using a bending cylindrical transducer based on PZT thin film,” *Sensors and Actuators A: Physical*, vol. 50, no. 1, pp. 75–80, 1995.

[11] Y. Yang and Y. Hu, “Electromechanical impedance modeling of PZT transducers for health monitoring of cylindrical shell structures,” *Smart Materials and Structures*, vol. 17, no. 1, p. 015005, 2008.

[12] T. Kanda, A. Makino, T. Ono, K. Suzumori, T. Morita, and M. K. Kurosawa, “A micro ultrasonic motor using a micro-machined cylindrical bulk PZT transducer,” *Sensors and Actuators A: physical*, vol. 127, no. 1, pp. 131–138, 2006.

[13] K. Kunz, P. Enoksson, and G. Stemme, "Highly sensitive triaxial silicon accelerometer with integrated PZT thin film detectors," *Sensors and Actuators A: Physical*, vol. 92, no. 1, pp. 156–160, 2001.

[14] Y. Nemirovsky, A. Nemirovsky, P. Muralt, and N. Setter, "Design of novel thin-film piezoelectric accelerometer," *Sensors and Actuators A: Physical*, vol. 56, no. 3, pp. 239–249, 1996.

[15] B. Jaffe, R. S. Roth, and S. Marzullo, "Piezoelectric properties of lead zirconate-lead titanate solid-solution ceramics," *Journal of Applied Physics*, vol. 25, no. 6, pp. 809–810, 1954.

[16] B. Jaffe, *Piezoelectric ceramics*, vol. 3. Elsevier, 2012.

[17] E. Sawaguchi, "Ferroelectricity versus antiferroelectricity in the solid solutions of $PbZrO_3$ and $PbTiO_3$," *Journal of the Physical Society of Japan*, vol. 8, no. 5, pp. 615–629, 1953.

[18] G. Shirane, K. Suzuki, and A. Takeda, "Phase transitions in solid solutions of $PbZrO_3$ and $PbTiO_3$ (*ii*) X-ray study," *Journal of the Physical Society of Japan*, vol. 7, no. 1, pp. 12–18, 1952.

[19] K. Zheng, J. Lu, and J. Chu, "A novel wet etching process of $Pb(Zr, Ti)O_3$ thin films for applications in microelectromechanical system," *Japanese Journal of Applied Physics*, vol. 43, no. 6S, p. 3934, 2004.

[20] S. Mancha, "Chemical etching of thin film PLZT," *Ferroelectrics*, vol. 135, no. 1, pp. 131–137, 1992.

[21] L. P. Wang, R. Wolf, Q. Zhou, S. Trolier-McKinstry, and R. J. Davis, "Wet-etch patterning of lead zirconate titanate (PZT) thick films for microelectromechanical systems (MEMS) applications," *Mater. Res. Soc. Symp. Proc.*, vol. 657, p. EE5391, 2001.

[22] S. Ezhilvalavan and V. D. Samper, "Ferroelectric properties of wet-chemical patterned $PbZr_{0.52}Ti_{0.48}O_3$ films," *Applied Physics Letters*, vol. 86, no. 7, p. 072901, 2005.

[23] L. Che, E. Halvorsen, and X. Chen, "An optimized one-step wet etching process of $PbZr_{0.52}Ti_{0.48}O_3$ thin films for microelectromechanical system applications," *Journal of Micromechanics and Microengineering*, vol. 21, no. 10, p. 105008, 2011.

[24] R. A. Miller and J. J. Bernstein, "A novel wet etch for patterning lead zirconate-titanate (PZT) thin-films," *Integrated Ferroelectrics*, vol. 29, no. 3-4, pp. 225–231, 2000.

[25] J. K. Lee, Y. Park, I. Chung, S. J. Oh, D. J. Jung, Y. J. Song, B. J. Koo, S. Y. Lee, K. Kim, and S. B. Desu, "Improvement in the electrical properties in Pt/$PbZr_{0.52}Ti_{0.48}O_3$/Pt ferroelectric capacitors using a wet cleaning method," *Journal of Applied Physics*, vol. 86, no. 11, pp. 6376–6381, 1999.

[26] Y. Lin, Q. Liu, T. Tang, X. Yao, and W. Huang, "Wet chemical etching of lead zirconate titanate thin film for microelectro-mechanical systems applications," *Ferroelectrics*, vol. 263, no. 1, pp. 33–38, 2001.

[27] D. Remiens, L. RuiHong, D. Troadec, D. Deresmes, C. Soyer, A. DaCosta, and R. Desfeux, "Piezoelectric response of PZT nanostructures obtained by focused ion beam," *Integrated Ferroelectrics*, vol. 100, no. 1, pp. 16–25, 2008.

[28] W. Lau, I. Bello, M. Sayer, and L. Zou, "Fluorine ion etching of lead zirconate-titanate thin films," *Applied Physics Letters*, vol. 64, no. 3, pp. 300–302, 1994.

[29] C. W. Chung and C. J. Kim, "Etching effects on ferroelectric capacitors with multilayered electrodes," *Japanese journal of applied physics*, vol. 36, no. part 1, pp. 2747–2753, 1997.

[30] C. W. Chung, "Reactive ion etching of $Pb(Zr_xTi_{1-x})O_3$ thin films in an inductively coupled plasma," *Journal of Vacuum Science and Technology B*, vol. 16, no. 4, pp. 1894–1900, 1998.

[31] J.-K. Jung and W.-J. Lee, "Dry etching characteristics of $Pb(Zr_xTi_{1-x})O_3$ films in CF_4 and Cl_2/CF_4 inductively coupled plasmas," *Japanese Journal of Applied Physics*, vol. 40, no. 3R, p. 1408, 2001.

[32] D. P. Vijay, S. B. Desu, and W. Pan, "Reactive ion etching of lead zirconate titanate (PZT) thin film capacitors," *Journal of The Electrochemical Society*, vol. 140, no. 9, pp. 2635–2639, 1993.

[33] K. Saito, J. H. Choi, T. Fukuda, and M. Ohue, "Reactive ion etching of sputtered $Pb(Zr_xTi_{1-x})O_3$ thin films," *Japanese Journal of Applied Physics*, vol. 31, no. 9A, p. L1260, 1992.

[34] C. Soyer, E. Cattan, and D. Remiens, "Reactive ion beam etching of PZT thin films," *Ferroelectrics*, vol. 288, no. 1, pp. 253–263, 2003.

[35] C. B. Fleddermann, "Plasma etching of PLZT: Review and future prospects," *Integrated Ferroelectrics*, vol. 5, no. 1, pp. 29–37, 1994.

[36] Y.-y. Lin, Q. Liu, T.-a. Tang, X. Yao, and W.-n. Huang, "Magnetically enhanced reactive ion etching of lead zirconate titanate thin film by CHF_3 plasma," *Japanese Journal of Applied Physics*, vol. 39, no. 1R, p. 320, 2000.

[37] N. Ikegami, T. Matsui, and J. Kanamori, "Dry-etching mechanism of sputtered $Pb(Zr_xTi_{1-x})O_3$ film," *Japanese Journal of Applied Physics*, vol. 35, no. 4S, p. 2505, 1996.

[38] J. Baborowski, "Microfabrication of piezoelectric MEMS," *Journal of Electroceramics*, vol. 12, no. 1-2, pp. 33–51, 2004.

[39] R. Ramesh, H. Gilchrist, T. Sands, V. Keramidas, R. Haakenaasen, and D. Fork, "Ferroelectric La-Sr-Co-O/Pb-Zr-Ti-O/La-Sr-Co-O heterostructures on silicon via template growth," *Applied Physics Letters*, vol. 63, no. 26, pp. 3592–3594, 1993.

[40] C. Eom, R. Van Dover, J. M. Phillips, D. Werder, J. Marshall, C. Chen, R. Cava, R. Fleming, and D. Fork, "Fabrication and properties of epitaxial ferroelectric heterostructures with $SrRuO_3$ isotropic metallic oxide electrodes," *Applied Physics Letters*, vol. 63, no. 18, pp. 2570–2572, 1993.

[41] M. Dekkers, M. D. Nguyen, R. Steenwelle, P. M. Te Riele, D. H. Blank, and G. Rijnders, "Ferroelectric properties of epitaxial $Pb(Zr,Ti)O_3$ thin films on silicon by control of crystal orientation," *Applied Physics Letters*, vol. 95, no. 1, p. 012902, 2009.

[42] M. D. Nguyen, H. Nazeer, K. Karakaya, S. Pham, R. Steenwelle, M. Dekkers, L. Abelmann, D. Blank, and G. Rijnders, "Characterization of epitaxial $Pb(Zr,Ti)O_3$ thin films deposited by pulsed laser deposition on silicon cantilevers," *Journal of Micromechanics and Microengineering*, vol. 20, no. 8, p. 085022, 2010.

[43] M. D. Nguyen, M. Dekkers, E. Houwman, R. Steenwelle, X. Wan, A. Roelofs, T. Schmitz-Kempen, and G. Rijnders, "Misfit strain dependence of ferroelectric and piezoelectric properties of clamped (001) epitaxial $PbZr_{0.52}Ti_{0.48}O_3$ thin films," *Applied Physics Letters*, vol. 99, no. 25, p. 252904, 2011.

[44] N. Banerjee, M. Huijben, G. Koster, and G. Rijnders, "Direct patterning of functional interfaces in oxide heterostructures," *Applied Physics Letters*, vol. 100, no. 4, p. 041601, 2012.

[45] S. Bühlmann, B. Dwir, J. Baborowski, and P. Muralt, "Size effect in mesoscopic epitaxial ferroelectric structures: Increase of piezoelectric response with decreasing feature size," *Applied Physics Letters*, vol. 80, no. 17, pp. 3195–3197, 2002.

[46] S. Buhlmann, P. Muralt, and S. Von Allmen, "Lithography-modulated self-assembly of small ferroelectric $Pb(Zr,Ti)O_3$ single crystals," *Applied Physics Letters*, vol. 84, no. 14, pp. 2614–2616, 2004.

[47] M. Alexe, C. Harnagea, D. Hesse, and U. Gosele, "Patterning and switching of nanosize ferroelectric memory cells," *Applied Physics Letters*, vol. 75, no. 12, pp. 1793–1795, 1999.

[48] P. M. Te Riele, G. Rijnders, and D. H. Blank, "Ferroelectric devices created by pressure modulated stencil deposition," *Applied Physics Letters*, vol. 93, no. 23, p. 233109, 2008.

[49] N. Pertsev, V. Kukhar, H. Kohlstedt, and R. Waser, "Phase diagrams and physical properties of single-domain epitaxial $Pb(Zr_xTi_{1-x})O_3$ thin films," *Physical Review B*, vol. 67, no. 5, p. 054107, 2003.

[50] J. Zhang, D. Schlom, L. Chen, and C. Eom, "Tuning the remanent polarization of epitaxial ferroelectric thin films with strain," *Applied Physics Letters*, vol. 95, no. 12, p. 122904, 2009.

[51] R. Eason, *Pulsed laser deposition of thin films: applications-led growth of functional materials.* John Wiley & Sons, 2007.

[52] W. Lee, H. Han, A. Lotnyk, M. A. Schubert, S. Senz, M. Alexe, D. Hesse, S. Baik, and U. Gösele, "Individually addressable epitaxial ferroelectric nanocapacitor arrays with near Tb inch^{-2} density," *Nature Nanotechnology*, vol. 3, no. 7, pp. 402–407, 2008.

[53] M. D. Nguyen, E. Houwman, M. Dekkers, H. N. Vu, and G. Rijnders, "A fast room-temperature poling process of piezoelectric $Pb(Zr_{0.45}\ Ti_{0.55})O_3$ thin films," *Science of Advanced Materials*, vol. 6, no. 2, pp. 243–251, 2014.

[54] X. Gao, B. J. Rodriguez, L. Liu, B. Birajdar, D. Pantel, M. Ziese, M. Alexe, and D. Hesse, "Microstructure and properties of well-ordered multiferroic $Pb(Zr,Ti)O_3/CoFe_2O_4$ nanocomposites," *ACS Nano*, vol. 4, no. 2, pp. 1099–1107, 2010.

[55] B. Rodriguez, X. Gao, L. Liu, W. Lee, I. Naumov, A. Bratkovsky, D. Hesse, and M. Alexe, "Vortex polarization states in nanoscale ferroelectric arrays," *Nano Letters*, vol. 9, no. 3, pp. 1127–1131, 2009.

Chapter 4

Submicron and Nano Patterning of Epitaxial PZT by Lift-off Strategy

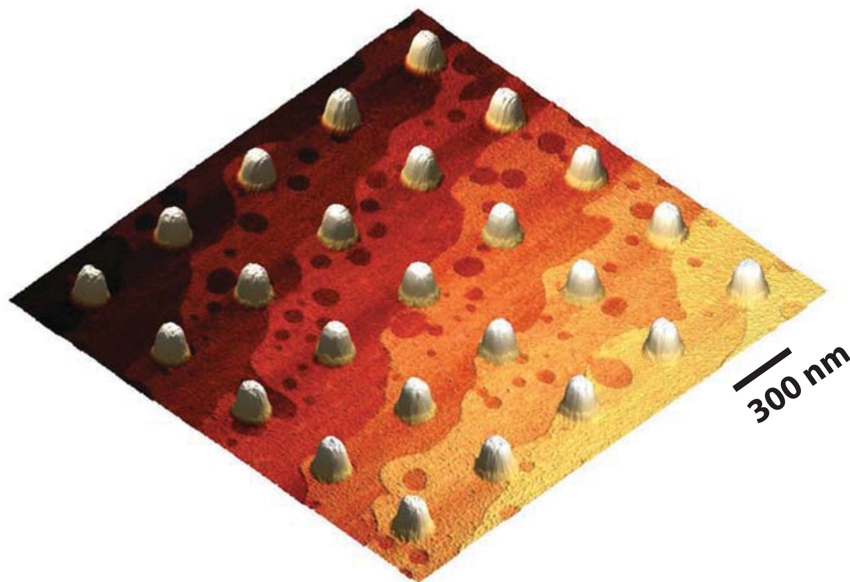

Part of the work discussed in this chapter is published in :
N. Banerjee, G. Koster, G. Rijnders, "*Submicron Patterning of Epitaxial $PbZr_{0.52}Ti_{0.48}O_3$ Heterostructures*", *Applied Physics Letters* 102, 142909 (2013).

ABSTRACT

In this chapter we address the sub-micron and nano patterning of epitaxial ferroelectric $PbZr_{(1-x)}Ti_xO_3$ (PZT) heterostructures utilizing the epitaxial lift-off patterning strategy. As described in the previous chapters, the sacrificial AlO_x mask assisted patterning pathway is able to structure oxide interfaces containing a 2DEG and hetero-epitaxial ferroelectric multilayer, while preserving their functional properties. But the fabricated structures were in micro-scale, derived from conventional photo-lithographic processing. In order to miniaturize the device sizes nano-patterning is an essential step. Thus, it is highly desirable to integrate the epitaxial lift-off fabrication with the conventional nano-lithographic techniques to fabricate sub-micron and nano-structures of epitaxial perovskite oxides and multilayers. In the current chapter, we demonstrate the integration of the lift-off fabrication with the electron beam lithography (eBL) process which is a flexible-design high resolution lithographic technique. The fabrication pathway was modified by the insertion of a thin metallic layer to prevent the charging-effect arising from the insulating sacrificial mask layer. An improvement of this modified patterning strategy is also demonstrated in which no physical-ion etching process is needed to pattern the metallic layer. PZT nano-structures down to the dimensions of $\sim$ 100 nm were fabricated utilizing this pathway. Piezoresponse force microscopic (PFM) investigations revealed that the fabricated structures were individually addressable, preserved ferroelectric response and were separately switchable without any noticeable cross-talk. Reciprocal space maps (RSM) of the fabricated structures revealed the existence of extended c-domains below dimensions of $\sim$ 200 nm, which can potentially give hints for the understanding of the ferroelectric size effect.

4.1 Introduction

4.1.1 Nanostructures of Ferroelectric Materials

The ability to store the induced polarization, artificially written by an external electric field has made ferroelectric materials a promising alternative to magnetic and dielectric materials for non-volatile data storage applications [1–7]. With the progress in electronic miniaturization, the size of ferroelectric devices has to be minimized, which requires the dimension of the data-storage elements to approach submicron sizes and eventually to the nano-scale. Fabrication of well-defined patterns comprised of ferroelectric materials with dimensions down to submicron and nanoscale is of increasing importance, not only for technological applications like ultrahigh density ferroelectric data storage [8–10] but also for gaining fundamental insights into the physics of these complicated materials [11–14]. As mentioned in the previous chapter solid solution $PbZr_{(1-x)}Ti_xO_3$ is one of the most applied ferroelectric materials because of its very high polarization response which is substantially stable towards external perturbations [15]. Complex perovskite oxides like PZT are very stable towards different physical and chemical etching strategies, which are traditionally used in very large scale integration (VLSI) processing. Hence innovative structuring pathways are required in order to integrate functional perovskite oxides, like PZT, with the conventional semiconductor technology.

4.1.2 Different fabrication strategies for nano-ferroelectrics

Fabrication of complex perovskite oxides is conventionally done via a 'top-down' approach, incorporating depositions of unpatterned films, followed by the removal of selective areas through different etching techniques. For example a 'top-down' approach using focus ion beam (FIB) was employed to fabricate nano-structured ferroelectric devices utilizing selective area etching with high energy gallium ions [16]. Although very precise, the technique suffers from contamination by the ion-source itself. Furthermore 'bottom-up' approaches such as chemical solution deposition (CSD) method were also employed to prepare ferroelectric nano-structures [17]. Although these chemical synthetic pathways allow the synthesis of nano-scale ferroelectrics with sizes down to tens of nanometers, major limitations exist in controlling the size of individual nano-structures and precisely locating them in desired patterns. Recently a new technique has been developed by Lee et. al utilizing a high temperature stable nano-porous anodic aluminum oxide (AAO) membrane as mask during deposition of ferroelectric perovskites at elevated temperatures [8]. In spite of these developments, the integration of an lift-off patterning method using a high temperature stable, sacrificial oxide mask with other design-flexible nano-lithographic techniques such as e-beam lithography remained elusive.

4.1.3 PZT nano structures by Epitaxial Lift-off Patterning

In this chapter the lift-off patterning has been integrated with conventional electron beam lithography (eBL) in order to fabricate submicron and nano-structures of high temperature grown oxide materials. As described in the previous chapters, the epitaxial lift-off patterning strategy utilizes a sacrificial mask of amorphous alumina. The AlO_x mask needs to be patterned before deposition of high temperature grown perovskite single/multi layers. In previous chapter we have utilized conventional photolithography in order to pattern the sacrificial AlO_x mask, yielding micro-scale perovskite patterns after the final lift-off. To fabricate submicron and nano-patterns, the lift-off strategy needs to be integrated with nano-lithographic techniques. We have chosen electron beam lithography (eBL) to serve this purpose owing to its very high resolution and design flexibility. One of the major problems encountered in this respect was the accumulation of electrons on the e-beam resist (PMMA) layer due to the presence of the insulating AlO_x mask layer underneath. Moreover, the instability of the resist in basic solutions, required to etch the AlO_x sacrificial template mask, posses difficulties to obtain high resolution nano-structures. Although some alternative organic resists are suggested [18–20] which are self-conducting, they often need an acid treatment posing a threat to the underlying alumina mask [21–23] and are mostly limited in their resolution to the standard resist PMMA. Here we present a modification to the epitaxial lift off patterning strategy to fabricate sub-micron and nano structures of epitaxial ferroelectic (PZT) perovskites. Two different approaches of the modification are presented here with and without using physical ion etching. Also we have investigated the structural parameters of lift-off fabricated epitaxial PZT nano-structures in order to provide insights on observed interesting phenomena with nano-scale ferroelectrics like the size-effect [14, 24–26].

4.2 Experimental- I

4.2.1 Fabrication of PZT nano-structures : Modification of the sacrificial mask

Figure 4.1 shows a schematic representation of the lift-off mediated fabrication strategy for submicron and nano patterns of perovskite oxides utilizing electron beam lithography (eBL). To integrate the lift-off patterning pathway with eBL, the fabrication process was modified and a thin metallic layer was introduced in between the sacrificial AlO_x template and the e-beam resist layer. A gold layer ($\sim$ 20 nm) was sputter deposited on a AlO_x covered Pt/Si substrate. The sample was subjected to the electron beam lithography process using poly(methyl methacrylate) (PMMA) as the resist. After the resist development, gold residing over the developed area was etched away with Ar ion-beam, which mimics the e-beam resist mask in the gold layer. In the subsequent processes the PMMA e-beam resist was dissolved and AlO_x was developed with a basic solution through the Au mask. This mask with sub-micron structures was subsequently used for high temperature deposition of morphotropic PZT and for lift-off of the material grown on top.

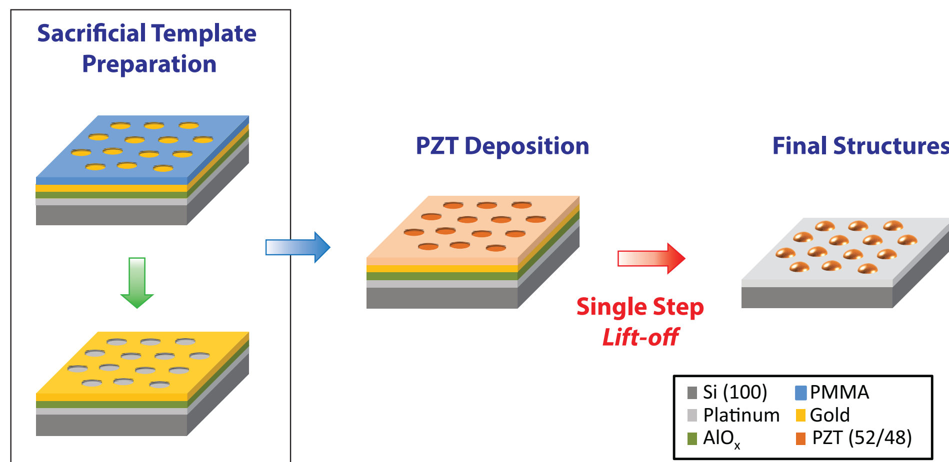

Figure 4.1: Schematic representation of the fabrication process flow for sacrificial mask (AlO_x) assisted lift-off nano-patterning strategy, compatible with the conventional electron-beam lithography.

4.2.2 Ferroelectric response of PZT nano-structures by PFM

Figure 4.2(a) presents an representative atomic force microscopic (AFM) image of an array of the fabricated submicron PZT dots on platinized Si substrate after complete removal of the sacrificial AlO_x mask. The corresponding height profile as measured by AFM is given in (b), which revealed that the obtained PZT dots were about $\sim$ 300 nm in diameter and $\sim$ 25 nm in height. The fabricated nano-dots were of uniform shape and height, had a high fabrication yield with rarely missing dots and were well separated from each other according to the design. Ferroelectric properties of the fabricated morphotropic PZT nanostructures were probed through PFM. An out-of-plane (OP) phase PFM image is presented in Fig. 4.2(c). As presented in the previous chapter and also seen in other research works [13, 27], the as-deposited film or as fabricated nanostructures via pulsed laser deposition were found to be self polarized. The contrast difference at the edges of the nano-structures presumably arises from the height-deflection of the PFM tip. The discrete PZT dot at the center (shown inside the broken rectangle) was switched to a positive polarization state by applying + 4V DC external bias via the conducting PFM tip. Out of plane PFM phase and amplitude characteristics with respect to external DC sweep-bias ($\pm$ 4.5 V), measured from a representative PZT dot are given in Fig. 4.2(d). The clear opening of the sweep-curves confirms the hysteric nature, although the reason behind the observed asymmetry of the out of plane amplitude-loop is not clear and is subject of further research. The PFM investigation confirms that the fabricated structures exhibit ferroelectric behavior and are individually addressable.

4.3 Experimental- II

4.3.1 Fabrication of epitaxial $PbZr_{0.2}Ti_{0.8}O_3$ nano-structures avoiding physical ion-etching

In the previous section we have demonstrated the achievement of submicron and nano-structuring of high temperature grown perovskite PZT by modifying the fabrication strategy. The key modification in the fabrication process was the introduction of a metallic layer (Au) in between the sacrificial mask layer (AlO_x) and the electron beam lithographic resist layer in order to avoid the building up of electrical charges during lithographic process. The metallic gold layer has to be etched afterwards, in order to mimic the eBL-generated mask into the metallic surface. Although submicron PZT structures (of diameter $\sim$ 300 nm) were achieved displaying well behaved ferroelectric response, one of the limiting factors in down-scaling the feature size was the larger number of processing steps. Moreover, care must be taken during the dry Ar-ion etching to prevent the over-etching related

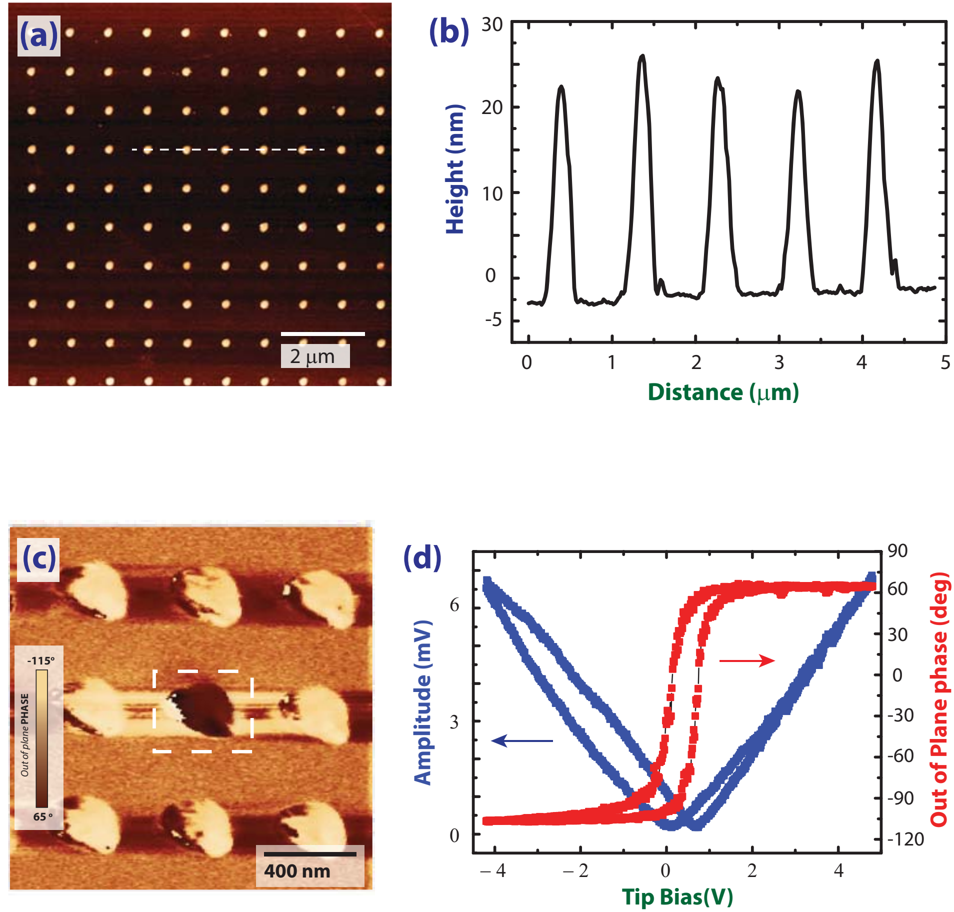

Figure 4.2: (a) Atomic force microscopic image of sub-micron $PbZr_{0.52}Ti_{0.48}O_3$ structures fabricated through e-beam lithography assisted epitaxial lift-off pathway. (b) Height profile along the marked line in (a), as probed by the AFM-tip. (c) Out-of-plane phase image of nano-structures probed by Piezoresponse Force Microscopy (PFM). The nano-dot inside the marked rectangle at the center was switched by applying +4 V DC external bias by the PFM-tip. (d) Measured phase and amplitude loops in response to the applied DC bias voltages sweeps by PFM.

damage at the substrate surface. It would therefore be beneficial to develop a fabrication strategy including combined etching of the metallic inter-layer and the sacrificial mask which avoids any possibility of damaging the underlying substrate.

In this section we demonstrate a further modification of the nano-patterning strategy to achieve the combined etching. This modification allowed us to achieve nano-structures with sizes down to ∼ 100 nm in diameter. We emphasize that one key difference between the conventional top-down nano-structuring approach and the sacrificial mask-mediated epitaxial lift-off nano-patterning is that, in the latter technique the material is directly patterned during growth, at high temperature. The ferroelectric domains are formed in the nano-structures during cooling down in the confinement of the mask, when the PZT goes to ferroelectric phase. Hence the strain conditions for lift-off fabricated nano-structures are expected to be different from their top-down fabricated analogues, leading to a different domain microstructure and population. To investigate this further we have fabricated epitaxial tetragonal PZT nano-structures of the $PbZr_{0.2}Ti_{0.8}O_3$ composition on 0.5 wt% Nb-doped $SrTiO_3$(001) substrates (Nb-STO). The substrates were single terminated using the buffered-HF treatment [28, 29] and annealed in an oxygen environment. Post-annealed substrates displayed vicinal terraces with unit-cell height differences as probed by AFM, implying single (B-site) termination. Subsequently, the amorphous AlO_x mask layer was deposited at room temperature using pulsed laser deposition(PLD). In order to achieve the combined etching of the metallic inter layer and the AlO_x mask underneath, we have used a very thin layer (∼ 5 nm) of metallic aluminum (Al), instead of gold, as described in the previous section. After the e-beam lithographic process, the mask is subjected to a basic developer solution. The metallic aluminum and the underlying AlO_x mask, both reacts with the basic developer solution forming water soluble aluminates, which enabled simultaneous patterning of both layers. The rest of the fabrication procedure is similar to the previous section, including high temperature deposition of $PbZr_{0.2}Ti_{0.8}O_3$ and subsequent lift-off, apart from an intermediate heating at 400 °C in an oxygen environment to oxidize the thin metallic layer. The fabrication procedure is schematically presented in Fig. 4.3.

Figure 4.4 shows AFM images of the patterned AlO_x mask on Nb-STO(001), after development of the sacrificial mask using basic solution and removal of PMMA resist using organic solvents. Corresponding height profiles are shown at the bottom of individual images. Fig. 4.4(a) shows the amorphous mask for fabrication of an array of lines, having individual width of ∼ 300 nm. Sharp edges were observed from the AFM height profile. To gain insight on the surface of the AlO_x-masked substrate prior to deposition, AFM image of a single line-mask (with width of ∼ 1 μm) was recorded and is presented in Fig. 4.4(b). Vicinal substrate terraces can be noticed by careful observation of the unmasked substrate surface, which is also evident from the height profile shown. This proves the existence of a clean, single

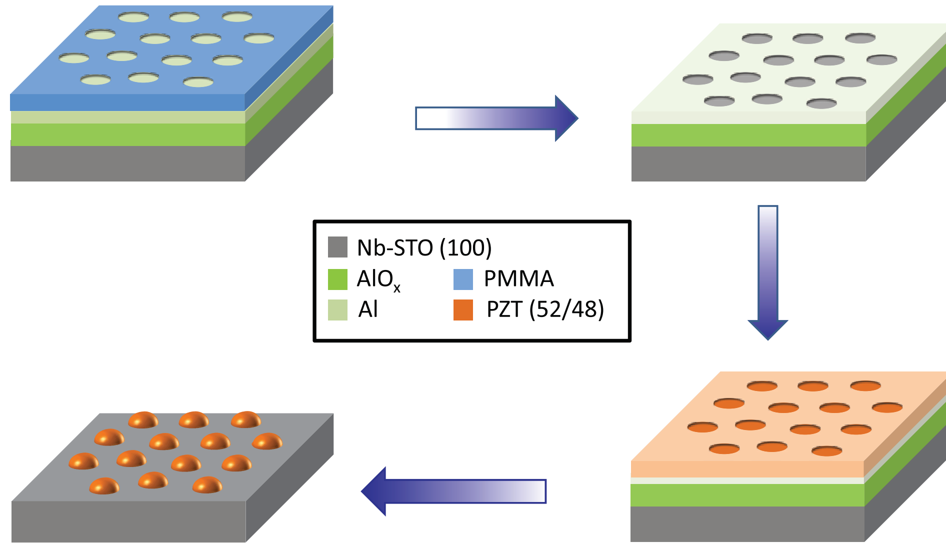

Figure 4.3: Modified process flow for the sacrificial mask assisted lift-off nano-patterning, avoiding any physical ion etching.

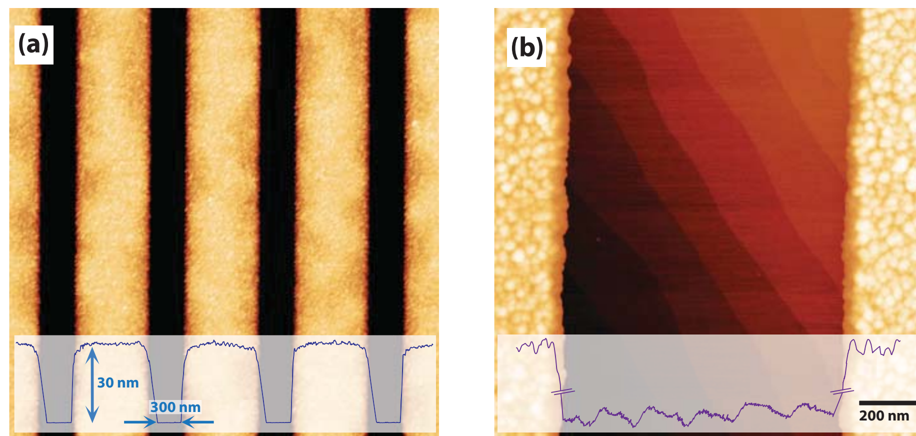

Figure 4.4: AFM image of the sacrificial AlO_x mask before PZT deposition. Height profiles along a representative horizontal line is shown at the bottom of the individual images. (a) Shows an image of the mask for an array of nano-lines with dimension of $\sim$ 300 nm while (b) represents the image of a single line-mask of 1 μm width, with clearly visible vicinal substrate steps.

terminated substrate surface for the growth of PZT, without any contamination from the sacrificial AlO_x mask or from the fabrication process.

4.3.2 Microscopic Characterization of Ferroelectric Nano-structures

Figure 4.5 shows SEM and AFM images of nano-lines of ∼ 200 nm width [Fig. (a) and (b)] and nano-dots of ∼ 100 - 150 nm diameter [Fig.(c) and (d)] after lifting off the sacrificial AlO_x mask. It can be noticed that the fabricated nano-structures were clean and well separated from each other. The AFM images reveal the presense of vicinal substrate terraces indicating complete removal of the sacrificial mask on lift-off. The recovery of the single terminated substrate can be crucial for growth of other functional materials for integration with PZT-nanostructures. Very small perovskite particles (∼ 10 - 20 nm size) are occasionally seen at the edge of the nano-structures. Although these images are for representative low dimensional

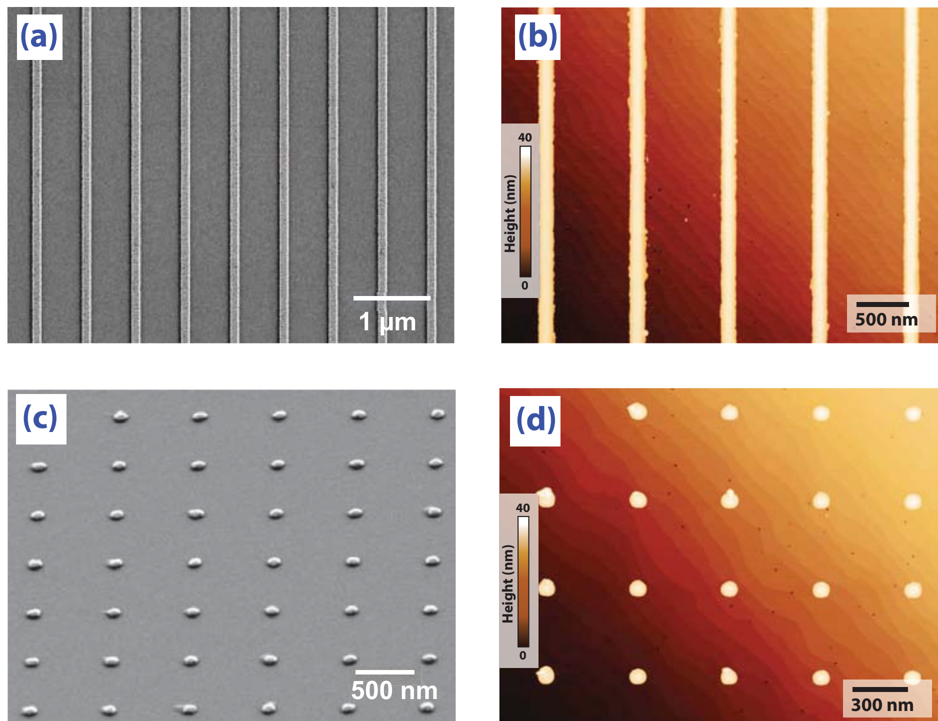

Figure 4.5: (a), (c) SEM and (b), (d) AFM images of zero and one dimensional $PbZr_{0.2}Ti_{0.8}O_3$ nano-structures fabricated utilizing modified strategy as illustrated in Fig. 4.3. In the AFM images, vicinal steps of the substrate $SrTiO_3(001)$ crystal are visible in the unpatterned areas after the mask was lifted off.

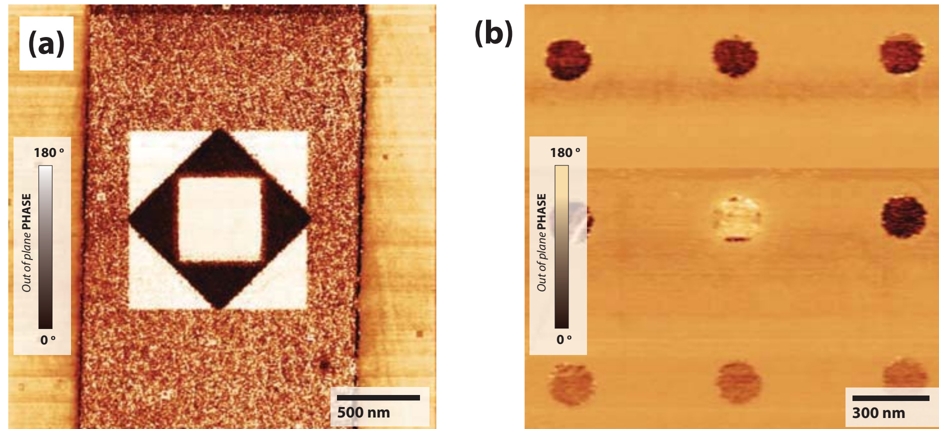

Figure 4.6: (a) Piezo-response force microscopic (PFM) images of out-of-plane phase, after writing of ferroelectric domains in lift-off fabricated PZT structures using externally applied ± DC bias voltages by the conducting PFM tip

nano-structures, several other submicron and micro $PbZr_{0.2}Ti_{0.8}O_3$ structures were also fabricated using the same fabrication strategy to investigate the ferroelectric domain population with varying shape and size.

4.3.3 Writing using PFM

The ferroelectric response of the fabricated nano-structures was probed using PFM, similar to the nano-structures of morphotropic PZT on Pt/Si as described in section 4.2.2. Nano-structures of different sizes, fabricated using epitaxial lift-off patterning were found to display ferroelectric response. The polarization of the as fabricated nano-structures was switchable by application of a bias-voltage, higher than the coercive field, through the PFM tip [30,31]. Fig. 4.6 (a) shows consecutive writing of positive and negatively polarized domains in selected areas on a PZT line of ∼ 2 μm, proving that the domains were re-writable. Selected switching of a nano-dot (∼ 100 - 150 nm diameter) was as well possible as shown in Fig. 4.6 (b). No cross talk between different nano-structures or polarized domains was observed. Although, a subtle difference in contrast between the unswitched nano-dots at top and bottom of Fig 4.6 (b) can be noticed which presumably is a tip-artifact, as the resonance frequency of the tip was changed with scanning presumably due to the decay in the metallic coating of the PFM tip. PFM investigations proved that lift-off fabricated $PbZr_{0.2}Ti_{0.8}O_3$ preserves ferroelectric behavior down to the investigated nano-dimension.

4.3.4 Ferroelectric domains in lift-off fabricated epitaxial $PbZr_{0.2}Ti_{0.8}O_3$ nanostructures

Bulk $PbZr_{0.2}Ti_{0.8}O_3$ has a tetragonal crystal structure at room temperature (P4mm space group) with lattice parameters of a = 0.39525 and c = 0.4148 nm [32–34]. The lattice parameter of the cubic Nb-doped $SrTiO_3$(001) is 0.3905nm. This gives rise to an in plane lattice mismatch of - 1.2%. At growth temperature $PbZr_{0.2}Ti_{0.8}O_3$ is paraelectric with a cubic crystal structure and has an even higher lattice mismatch with Nb-STO(001) substrate [35, 36]. Thus an epitaxial film of tetragonal PZT experiences compressive strain on Nb-STO (001) substrates directing the formation of ferroelastic a and c domains with in plane and out of plane polarization directions respectively, which is schematically represented in Fig. 4.7 (a).

Fig. 4.7 (b) shows a typical X-ray reciprocal space map (RSM) of an unpatterned 40 nm thick film $PbZr_{0.2}Ti_{0.8}O_3$ on Nb-STO(001) around the (002) Bragg reflection. The reflections of the ferroelectric a and c domains are indicated in the RSM image. The out of plane lattice parameter as determined from the maximum intensity c-domain peak is 0.4140 nm, which is close to the bulk value. To probe any change in the lattice parameter of ferroelectric domains and/or their relative population in the lift-off fabticated tetragonal PZT nano-structures, we have investigated high resolution X-ray reciprocal space maps for samples with large area covered PZT nano-structure (lines or dots) of identical size and shape. Since the nano-structured film contains substantially less PZT as compared to their unstructured analogues, the intensity of the PZT peak is weaker for nano-structures, requiring a high signal to noise ratio and longer counting time. RSM around the (002) Bragg reflection for the sample constituted of $PbZr_{0.2}Ti_{0.8}O_3$ nano-lines of $\sim$ 200 nm width is shown in Fig. 4.7 (d). It can be seen that apart from the c-domain peak analogous to unpatterned films, additional diffracted intensities appear corresponding to out of plane lattice parameters in the range of 0.4273 - 0.4347 nm. Appearance of similar peaks corresponding to domains with elongated c-axis were also observed for zero-dimensional nanostructures with diameter of $\sim$ 100 nm, as shown in Fig. 4.7 (f). For the a-domains, the Q_{in} reciprocal lattice vectors, representing in-plane tilting of the a-domains, were found to be enhanced for the nano-lines. This concludes nicely to the observed elongated c-domains, requiring higher tilting of the a-domains in order to compensate the additional compressive strain. Interestingly for nano-dots, no peaks corresponding to a-domains were observed in the RSM. This can either imply that they are tilted further and outside the scan area or are not present. A third possibility is that, owing to the very low intensity of the PZT peaks (originating from the low amount of material), the intensities of the a-domain peaks are comparable to the noise-level and therefore not detected by the instrument. Hence further research is necessary to directly visualize the a-domains in nano-dots using high resolution transmission electron microscope (TEM) or to

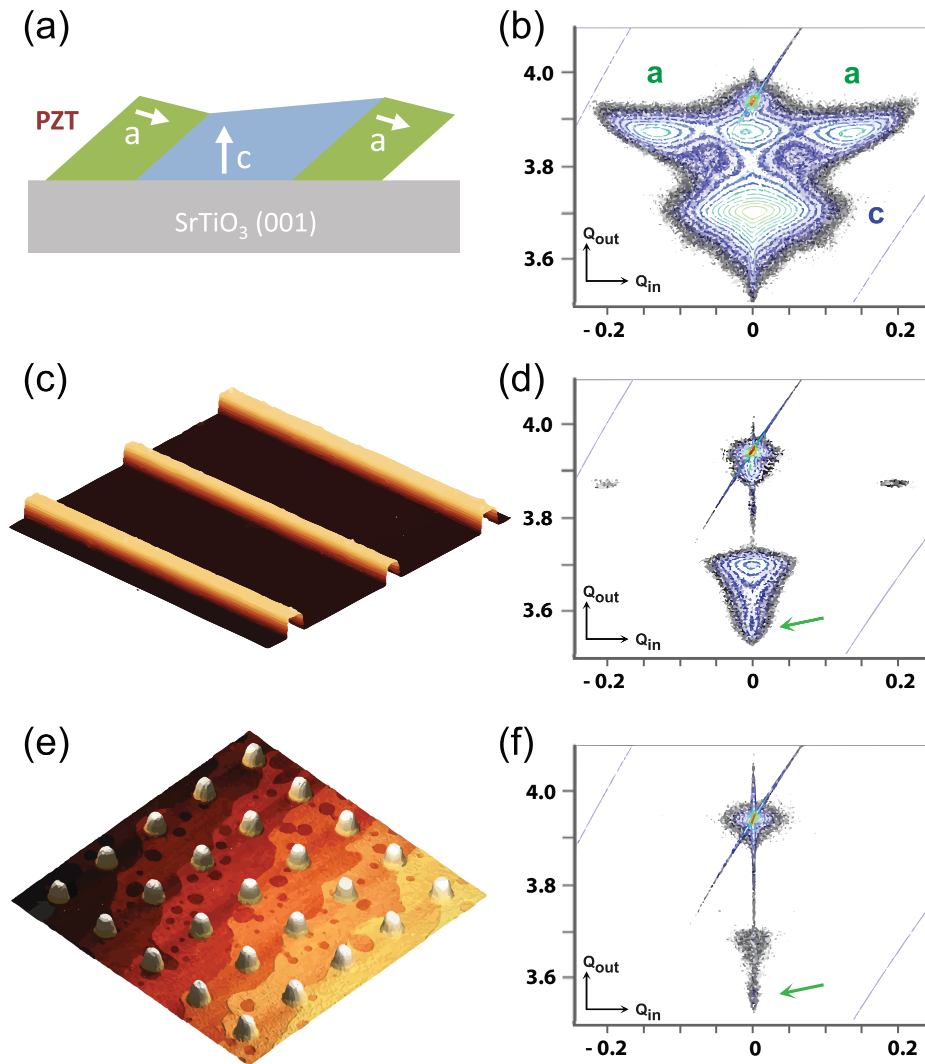

Figure 4.7: (a) Schematic representation of different domains of tetragonal PZT on compressively strained $SrTiO_3$(001) substrate. High resolution reciprocal space maps (RSM) of (b) unstructured film, (d) lines of ∼ 200 nm width and (f) dots of ∼ 100 nm diameter of tetragonal PZT on STO(001) along (002) brag reflection. a/c domains are indicated in (b) and the appearance of extended c-domain for nano-structures is indicated using arrows in both (d) and (f). (c) and (e) shows representative 3D AFM images of the respective nano-structures.

use very high intensity X-ray radiation, utilizing for example a synchrotron source. It is to be emphasized here that unlike the traditional top-down approach, the perovskite was *in situ* structured, while growing inside the nano-confined dimension by the AlO_x mask. Although lacking experimental evidence, we presume that the extended domains preferably form at the edges of the nano-structures, to compensate the higher strain gradient.

4.4 Conclusion

In conclusion, we have fabricated epitaxial submicron and nano-structures of $PbZr_{(1-x)}Ti_xO_3$ (PZT) thin films on different substrates via a sacrificial mask assisted lift-off pathway without using any acidic wet-etching. The fabrication scheme was modified in order to be integrated with electron beam lithographic processing for obtaining nano-scale patterns with design flexibility. Morphorohic PZT (x = 0.48) was structured on platinized Si substrates together with a $SrRuO_3$ electrode layer. The obtained submicron structures (with minimum feature size of $\sim$ 250 nm) were investigated using piezoresponse force microscopy (PFM) and found to display a prominent ferroelectric response. In order to reduce the number of fabrication steps further, which is important for decreasing the feature size and also to avoid use of physical etching process, the fabrication scheme is further modified. Utilizing this new fabrication strategy, one dimensional nano-structures (nano-lines), with a feature size of $\sim$ 200 nm and zero-dimensional nano-structures (nano-dots) with a feature size of $\sim$ 100 nm, of epitaxial $PbZr_{0.2}Ti_{0.8}O_3$ were fabricated on Nb-$SrTiO_3$(001) substrates.

Ferroelectric response of the fabricated epitaxial nano-structures was probed using PFM. The lift-off fabricated PZT nano-structures were found to be individually addressable, self-polarized in the as-fabricated state, consecutively switchable and did not show any noticeable cross-talk. The population of ferroelastic a/c domains in the lift-off fabricated tetragonal PZT nano-structures, compressively strained on STO (001), were probed by high resolution X-ray reciprocal space mapping (RSM) and compared with their unstructured analogues. The appearance of domains with elongated c-axis was observed for nano-structures with feature sizes under $\sim$ 200 nm, accompanied by higher tilting of the a-domains as compared to identical unpatterned films. We emphasize here that, unlike traditional top-down patterning, the lift-off fabrication involves *in situ* patterning of the perovskites during their growth at elevated temperatures. Hence, the strain state of the material is expected to be different when fabricated in a nano-confined structure via epitaxial lift-off strategy, especially at the edges of the nano-structures. For $PbZr_{0.2}Ti_{0.8}O_3$ on STO, this can lead to an elongation of the c-axis and corresponding enhancement in the tilt of the a-domains in order to accommodate the compressive strain. For nano-dots with a characteristic diameter of $\sim$ 100 nm, no prominent signature of a-domains were noticed from RSM investigations. Further insight in the underlying ferroelectric domain population and orientation of the lift-off fabricated $PbZr_{0.2}Ti_{0.8}O_3$ nanostructures require TEM and/or synchrotron studies, especially for structures with very low dimensions. The observation of the appearance of elongated c-domains with decreasing nano-dimensions, can give a clue for understanding observed ferroelectric size effects [14].

Bibliography

[1] J. F. Scott and C. A. P. De Araujo, "Ferroelectric memories," *Science*, vol. 246, no. 4936, pp. 1400–1405, 1989.

[2] L. E. Cross, "Ferroelectric ceramics: tailoring properties for specific applications," in *Ferroelectric Ceramics*, pp. 1–85, Springer, 1993.

[3] J. F. Scott, *Ferroelectric memories*, vol. 3. Springer, 2000.

[4] O. Auciello, J. F. Scott, and R. Ramesh, "The physics of ferroelectric memories," *Physics Today*, vol. 51, no. 7, pp. 22–27, 2008.

[5] S.-W. Cheong and M. Mostovoy, "Multiferroics: a magnetic twist for ferroelectricity," *Nature Materials*, vol. 6, no. 1, pp. 13–20, 2007.

[6] Y. Cho, "Nanoscale ferroelectric information storage based on scanning nonlinear dielectric microscopy," *Journal of Nanoscience and Nanotechnology*, vol. 7, no. 1, pp. 105–116, 2007.

[7] P. R. Evans, X. Zhu, P. Baxter, M. McMillen, J. McPhillips, F. D. Morrison, J. F. Scott, R. J. Pollard, R. M. Bowman, and J. M. Gregg, "Toward self-assembled ferroelectric random access memories: Hard-wired switching capacitor arrays with almost Tb/in.^{2} densities," *Nano Letters*, vol. 7, no. 5, pp. 1134–1137, 2007.

[8] W. Lee, H. Han, A. Lotnyk, M. A. Schubert, S. Senz, M. Alexe, D. Hesse, S. Baik, and U. Gösele, "Individually addressable epitaxial ferroelectric nanocapacitor arrays with near Tb inch^{-2} density," *Nature Nanotechnology*, vol. 3, no. 7, pp. 402–407, 2008.

[9] Y. Cho, K. Fujimoto, Y. Hiranaga, Y. Wagatsuma, A. Onoe, K. Terabe, and K. Kitamura, "Tbit/inch^2 ferroelectric data storage based on scanning nonlinear dielectric microscopy," *Applied Physics Letters*, vol. 81, no. 23, pp. 4401–4403, 2002.

[10] J. Scott, F. Morrison, M. Miyake, and P. Zubko, "Nano-ferroelectric materials and devices," *Ferroelectrics*, vol. 336, no. 1, pp. 237–245, 2006.

[11] A. M. Ionescu, "Nanoelectronics: Ferroelectric devices show potential," *Nature Nanotechnology*, vol. 7, no. 2, pp. 83–85, 2012.

[12] I. I. Naumov, L. Bellaiche, and H. Fu, "Unusual phase transitions in ferroelectric nanodisks and nanorods," *Nature*, vol. 432, no. 7018, pp. 737–740, 2004.

[13] B. Rodriguez, X. Gao, L. Liu, W. Lee, I. Naumov, A. Bratkovsky, D. Hesse, and M. Alexe, "Vortex polarization states in nanoscale ferroelectric arrays," *Nano Letters*, vol. 9, no. 3, pp. 1127–1131, 2009.

[14] S. Bühlmann, B. Dwir, J. Baborowski, and P. Muralt, "Size effect in mesoscopic epitaxial ferroelectric structures: Increase of piezoelectric response with decreasing feature size," *Applied Physics Letters*, vol. 80, no. 17, pp. 3195–3197, 2002.

[15] E. Cross, "Materials science: Lead-free at last," *Nature*, vol. 432, no. 7013, pp. 24–25, 2004.

[16] C. Ganpule, A. Stanishevsky, Q. Su, S. Aggarwal, J. Melngailis, E. Williams, and R. Ramesh, "Scaling of ferroelectric properties in thin films," *Applied Physics Letters*, vol. 75, no. 3, pp. 409–411, 1999.

[17] A. Roelofs, T. Schneller, K. Szot, and R. Waser, "Piezoresponse force microscopy of lead titanate nanograins possibly reaching the limit of ferroelectricity," *Applied Physics Letters*, vol. 81, no. 27, pp. 5231–5233, 2002.

[18] M. Angelopoulos, J. M. Shaw, R. D. Kaplan, and S. Perreault, "Conducting polyanilines: Discharge layers for electron-beam lithography," *Journal of Vacuum Science and Technology B*, vol. 7, no. 6, pp. 1519–1523, 1989.

[19] S. Persson, P. Dyreklev, and O. Inganäs, "Patterning of poly (3-octylthiophene) conducting polymer films by electron beam exposure," *Advanced Materials*, vol. 8, no. 5, pp. 405–408, 1996.

[20] M. Angelopoulos, N. Patel, J. M. Shaw, N. C. Labianca, and S. A. Rishton, "Water soluble conducting polyanilines: applications in lithography," *Journal of Vacuum Science and Technology B*, vol. 11, no. 6, pp. 2794–2797, 1993.

[21] G. H. Posner, "Organic reactions at alumina surfaces," *Angewandte Chemie International Edition in English*, vol. 17, no. 7, pp. 487–496, 1978.

[22] R. Ramsier, P. Henriksen, and A. Gent, "Adsorption of phosphorus acids on alumina," *Surface Science*, vol. 203, no. 1, pp. 72–88, 1988.

[23] F. Li, L. Zhang, and R. M. Metzger, "On the growth of highly ordered pores in anodized aluminum oxide," *Chemistry of Materials*, vol. 10, no. 9, pp. 2470–2480, 1998.

[24] S. Buhlmann, P. Muralt, and S. Von Allmen, "Lithography-modulated self-assembly of small ferroelectric Pb(Zr, Ti)O_3 single crystals," *Applied Physics Letters*, vol. 84, no. 14, pp. 2614–2616, 2004.

[25] N. Setter and R. Waser, “Electroceramic materials,” *Acta Materialia*, vol. 48, no. 1, pp. 151–178, 2000.

[26] A. Tagantsev and I. Stolichnov, “Injection-controlled size effect on switching of ferroelectric thin films,” *Applied Physics Letters*, vol. 74, no. 9, pp. 1326–1328, 1999.

[27] X. Gao, B. J. Rodriguez, L. Liu, B. Birajdar, D. Pantel, M. Ziese, M. Alexe, and D. Hesse, “Microstructure and properties of well-ordered multiferroic Pb (Zr, Ti) $O_3/CoFe_2O_4$ nanocomposites,” *ACS Nano*, vol. 4, no. 2, pp. 1099–1107, 2010.

[28] G. Koster, B. L. Kropman, G. J. Rijnders, D. H. Blank, and H. Rogalla, “Quasi-ideal strontium titanate crystal surfaces through formation of strontium hydroxide,” *Applied Physics Letters*, vol. 73, no. 20, pp. 2920–2922, 1998.

[29] M. Kawasaki, K. Takahashi, T. Maeda, R. Tsuchiya, M. Shinohara, O. Ishiyama, T. Yonezawa, M. Yoshimoto, and H. Koinuma, “Atomic control of the $SrTiO_3$ crystal surface,” *Science*, vol. 266, no. 5190, pp. 1540–1542, 1994.

[30] C. Ahn, T. Tybell, L. Antognazza, K. Char, R. Hammond, M. Beasley, Ø. Fischer, and J.-M. Triscone, “Local, nonvolatile electronic writing of epitaxial $Pb(Zr_{0.52}Ti0_{.48})O_3/SrRuO_3$ heterostructures,” *Science*, vol. 276, no. 5315, pp. 1100–1103, 1997.

[31] C. Ahn, K. Rabe, and J.-M. Triscone, “Ferroelectricity at the nanoscale: local polarization in oxide thin films and heterostructures,” *Science*, vol. 303, no. 5657, pp. 488–491, 2004.

[32] J. Frantti, J. Lappalainen, S. Eriksson, V. Lantto, S. Nishio, M. Kakihana, S. Ivanov, and H. Rundlöf, “Neutron diffraction studies of $Pb(Zr_xTi_{(1-x)})O_3$ ceramics,” *Japanese Journal of Applied Physics*, vol. 39, p. 5697, 2000.

[33] K. Hellwege and A. Hellwege, “Ferroelectrics and related substances,” *Landolt-Bornstein, New Series, Group III*, vol. 3, 1981.

[34] L. Cao, Y. Xu, B. Zhao, L. Guo, L. Li, B. Xu, Y. Zhang, H. Chen, A. Zhu, Z. Mai, *et al.*, “A structural investigation of high-quality epitaxial thin films,” *Journal of Physics D: Applied Physics*, vol. 30, no. 10, p. 1455, 1997.

[35] J. Matthews and A. Blakeslee, “Defects in epitaxial multilayers: I. misfit dislocations,” *Journal of Crystal Growth*, vol. 27, pp. 118–125, 1974.

[36] S. Gariglio, N. Stucki, J.-M. Triscone, and G. Triscone, “Strain relaxation and critical temperature in epitaxial ferroelectric $Pb(Zr_{0.20}Ti_{0.80})O_3$ thin films,” *Applied Physics Letters*, vol. 90, no. 20, p. 202905, 2007.

CHAPTER 5

Fabrication of Free-standing, all-Oxide Epitaxial Piezodriven Cantilevers Integrated on Silicon

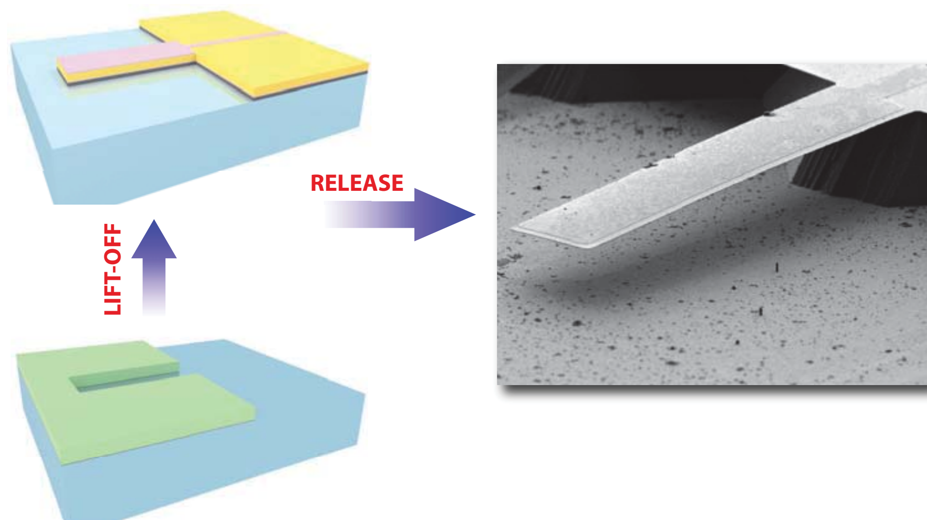

Part of the work discussed in this chapter is accepted for publication in the scientific journal **APL Materials** as : **N. Banerjee, E. P. Houwman, G. Koster, G. Rijnders**, "***Fabrication of piezodriven, free-standing, all-oxide heteroepitaxial cantilevers on silicon***"

ABSTRACT

The coupling between mechanical and electrical properties in piezoelectrical materials has been traditionally employed for both sensing and actuation purposes. One such vital application is piezo-mass sensors, with piezoelectric cantilevers as the most popular device configuration. Although free-standing epitaxial piezo-cantilever devices are promising to achieve very high sensitivity (down to zeptogram level), experimental realization of such device-systems have been hampered because of difficulties in their fabrication, specially when epitaxial oxides are key functional component materials. In this chapter we demonstrate the fabrication and mechanical properties of all-oxide free standing heteroepitaxial piezoelectric microelectromechanical systems (MEMS) on silicon, using piezoelectric $PbZr_{0.52}Ti_{0.48}O_3$ *as the key functional material. We have utilized the epitaxial lift-off strategy for in situ simultaneous patterning of multilayer oxide heterostructures grown directly on Si(001) substrate, employing a high temperature stable, sacrificial oxide template mask. The lift-off patterned heteroepitaxial multilayer oxide stack were released from the substrate using base-assisted anisotropic etching, to obtain free standing cantilever MEMS devices. The key advantages of the demonstrated MEMS fabrication process over the traditional silicon on insulator (SOI) based technology is - achievement of free-standing cantilever PZT MEMS devices without residual Si at the bottom, reduction in number of processing steps and no requirement of backside-substrate etching.*

5.1 Introduction

5.1.1 MEMS with piezoelectric actuation

Interconversion between electrical and mechanical energies is one of the most important aspect of modern electronic technology. With rapid reduction in the size of electronic gadgets such devices also need to be smaller giving rise to micro/nano electro mechanical systems (MEMS/NEMS). Majority of present day MEMS devices utilizes electrostatic actuation of flexural device structures [1–6]. These electrostatic MEMS devices solely depends on electrostatic forces for displaying actuation and are easily implementable. But to achieve large actuation amplitudes, they need very high drive voltages [7–9]. An additional disadvantage is electrostatic MEMS devices often show substantially large hysteresis while going through repeated actuation cycles [10–13]. Alternative drive-current based actuation approaches has been achieved which are mostly employed in thermal and/or magnetically operating devices. These devices need high power to operate as well and are often inherently slow [8, 14]. In this scenario MEMS devices driven by direct and/or converse piezoelectric effect are advantageous which can be utilized to obtain large actuating displacement at modest input drive voltages, low powers and with low hysteresis. In contrary to traditional sensor devices, piezoelectric sensors do not need self-power for operation (although associated electronics needs to be powered). They can as well act as low-capacity power sources [15–19]. Electrostatic MEMS resonator devices generally operate at lower resonant frequencies (f_n) [20, 21], in order to enhance f_n and achieve high quality factors the device size needs to be very smaller (nano-scale) [22–24], which makes them vulnerable to changes due to mass-loading on environmental exposure. Piezoelectric micro-resonators with comparative sizes have higher f_n (in MHz - GHz range) than analogous electrostatic devices and are extensively utilized in scanning probe instruments. Piezoelectricity is well-scalable with size, implying available energy density for actuation remains higher energy density even at smaller device sizes. Like electrostatic devices, piezo-MEMS elements are CMOS-compatible and devices need only metallic contacts for operation, thus they can be easily incorporated with integrated circuit (IC)designs. Owing to these advantages piezo-MEMS devices have been utilized for wide range of applications including filters [25–28], accelometers [29–32], micropumps [33–36] scanning force microscopy tips [37, 38], micro-sonar arrays [39–41] etc.

5.1.2 Ferroelectrics for piezo-MEMS

Piezoelectricity occurs only in crystal classes containing no center of symmetry. Among 32 crystal classes, 21 are non-centrosymmetric and 20 exhibits direct piezoelectric effect. It is as well forbidden in crystal class 432 which is globally symmetric although lacking center of inversion inside a single unit cell. 10 among these non-centrosymmetric crystal classes manifest a spontaneous polarization (P) without any external mechanical stress, owing to the existence of a permanent dipole moment originating from their unit cell. These are termed as polar crystal classes and all piezoelectric materials which are used in thin film form belongs to them. The direction of this polar axis is conventionally assigned as coordinate index 3. In polar materials the piezoelectric effect manifests itself by changing either or both the magnitude and direction of P in response to an external mechanical stress. In ferroelectrics this unit-cell polarization can be spontaneously reversed by the application of an external electric field. Often the ferroelectric materials have stronger piezoresponse in compared to non-ferroelectrics offering efficient way for electromechanical transformation of signals and energy [42, 43]. They are capable of displaying ferro and pyroelectric effects together with piezoelectricity. Moreover, most of the applied piezoelectric films are in polycrystalline form where the piezoelectric property is averaged over the constituent grains [8, 44]. Non-ferroelectric materials do not allow electric control on the orientation of the polar axis. Therefore in order to achieve higher piezoelectric effect in such materials one typically depends on the material grown process, to obtain a textured micro structure inducing alignment of the polar directions. Whereas, in ferroelectric materials the possibility of reorienting the polar axis by application of large electric field gives the freedom of alignment of individual dipoles to the desired direction for suitable application. This external field mediated polarization reorientation procedure is called as *poling*. Although in epitaxial thin films crystal polarization is unidirectional and pulsed laser deposition fabricated films are found to be self-poled.

Ferroelectric materials specially those with perovskite crystal structure have long been employed for piezoelectric applications with simultaneous possibility of being utilized for broad range of interest such as capacitors and giant positive thermal coefficient (PTC) resistors [45–48]. Therefore they are also advantageous in terms of existing knowledge on process and reliability. Lead zirconate titanate ($PbZr_xTi_{(1-x)}O_3$, PZT), specifically the composition with x= 0.52 has been extensively applied because of its very large electro-mechanical coupling and stable polarization response on external perturbations [46]. In this chapter we have utilized this stable ferroelectric oxide as the key piezoelectric material for MEMS devices. Compared to binary piezoelectric material like ZnO or AlN, PZT offers advantages in larger actuation amplitude, faster response time and lower power consumption. But, PZT is a complex solid solution oxide material and is very stable with respect

to different physical and chemical structuring processes [44]. Hence major challenges are faced when incorporating heteroepitaxial PZT in VLSI technology with Si for micro-fabrication of piezo-electromechanical components [8, 44].

5.1.3 Free-standing Epitaxial MEMS

Although PZT MEMS devices are promising for several applications, most of them incorporates polycrystalline PZT as the functional piezo material, often derived from sol-gel process [49–51]. Polycrystalline PZT suffers several key disadvantages over epitaxial PZT, including higher leakage current, lower piezoelectric coefficients and inferior ferroelectric properties [52–55]. Moreover thicker PZT films need very high electrical voltages for piezoelectric actuation which is a major problem in their integration with electronic read-out circuits [53, 56]. Hence in order to be compatible with Si-based very large scale integration (VLSI) technology, thinner PZT films (requiring moderate actuation voltages) are essential while maintaining superior piezo and ferroelectric properties and epitaxial films are ideal candidate to serve this purpose. Although epitaxial growth of piezoelectric perovskite oxides on Si is challenging, recent advances on thin film deposition technology and employment of suitable intermediate oxide layers had made it possible [57]. It was also shown that by tuning these transitional oxide layers between perovskite and Si-crystal it is even possible to control the crystal orientation of epitaxial PZT [54]. But to harvest functional properties of PZT optimally, it is necessary to employ appropriate electrode materials [58]. These suitable electrode materials are mostly high temperature grown perovskites and together with PZT they needs to be precisely structured as well in the final MEMS devices.

Conventional epitaxial piezo-MEMS devices fabricated using silicon on insulator (SOI) as substrate material contains relatively thicker (typically 3-50 μm) top Si layer from the substrate on the bottom side of the device [59]. This residual Si layer makes the MEMS devices heavier, often reducing their functional performances, for example the limit of detection (LOD) when used as mass sensors [60]. Moreover the functional properties of the perovskite layers are heavily dominated in these devices owing to the clamping by the thicker substrate base. In free standing cantilever it would be possible to employ and investigate properties intrinsic to the functional material itself. It was recently experimentally shown by Griggio et. al. that the dielectric non-linearity and underlying ferroelectric domain microstructure of the mechanically substrate-released $PbZr_{0.52}Ti_{0.48}O_3$ films are remarkably different than their substrate-clamped counterparts. Thee observed effects were ascribed to the enhancement of the mobility of the ferroelectric domain walls, influenced by the collective strain interactions from the local/global mechanical boundary conditions imparted by the substrate, which is as well expected to affect the piezoelectric properties. Hence free-standing piezo-MEMS devices are interesting

from fundamental understanding of the rich underlying material physics as well as important from the applicative perspective to achieve novel/enhanced material properties.

5.1.4 Lift-off fabrication of free-standing epitaxial PZT MEMS devices

Traditional epitaxial piezo-MEMS devices are fabricated utilizing silicon on insulator (SOI) as a substrates. These substrates are comprised of two Si crystal (with varying thickness, often the thicker one at bottom) sandwiching an intermediate SiO_2 layer, termed as buried oxide layer (BOX). Figure 5.1 shows a typical fabrication scheme for fabrication of epitaxial PZT MEMS devices on SOI substrates [59]. The fabrication strategy requires back-side etching of the bottom Si layer prior to high temperature deposition of the oxide stack, mostly utilizing dry reactive ion etching. The bottom Si layer is generally the thickest one in SOI substrates with typical thickness in the rage of $\sim$ 300 - 500 μm and needs longer etching time. The removal of this layer also makes the substrate fragile and susceptible to mechanical and thermal damage. After deposition of oxide one needs to etch the individual layer and the substrate Si-layer at the bottom (top Si layer of the SOI) in order to release the devices. Baek et. al. have demonstrated realization of very high piezoelectric coefficient and figure of merit for energy harvesting in clamping-free PMN-PT cantilevers utilizing metallic electrodes [61]. For all-oxide epitaxial devices the patterning is more intrigue, because the chemical and physical nature of individual constituent oxide layers (including the piezoelectric, top and bottom electrode layer and the buffer layers) are often very different from etch other. As a result they require individual etching procedures with precise photo-lithographic alignment at each steps. This makes the structuring procedure (for the entire epitaxial multilayer oxide stack) very tedious and time-consuming with simultaneously enhancing the chance of contamination from individual processing steps. Moreover, in order to grow epitaxial perovskites on Si, one needs to utilize buffer layers like yittria stabilized zirconia (YSZ) and/or cerium (IV) oxide (CeO_2) [54, 57] which are substantially stable with respect to traditional dry and wet etching requiring special procedures. Hence development of a combined etching strategy for the entire multilayer oxide stack would be of great ease to the patterning procedure.

In the previous chapter we have demonstrated that sacrificial mask associated epitaxial lift-off fabrication technique is capable of structuring heteroepitaxial multilayers (incorporating functional piezo-layer, electrodes and the buffer layer) without affecting their ferroelectric properties. The patterning techniques as well grants the direct access to the front-side substrate surface in uncovered areas which can be subjected to chemical etching for the release of functional devices like cantilevers. Hence in the current chapter we will demonstrate a novel fabrication

strategy for preparation of free-standing, all-oxide, hetero-epitaxial PZT cantilevers. The fabrication is facilitated by employment of the lift-off patterning approach in order to pattern multilayer epitaxial oxide stack, as described in the previous chapter. In stead of using SOI wafers and performing longer back-side etching, our fabrication pathway uses Si(001) crystals as substrates and addresses direct front-side etching for the device release. We have also investigated the influence of the in-plane orientation of cantilever devices with respect to {001} Si, on their release from the substrate by anisotropic basic-etching. Our results as described below can be useful to establish this novel fabrication pathway to prepare free-standing, all-oxide epitaxial piezo-MEMS devices directly on Si substrates without using any backside dry reactive-ion etching.

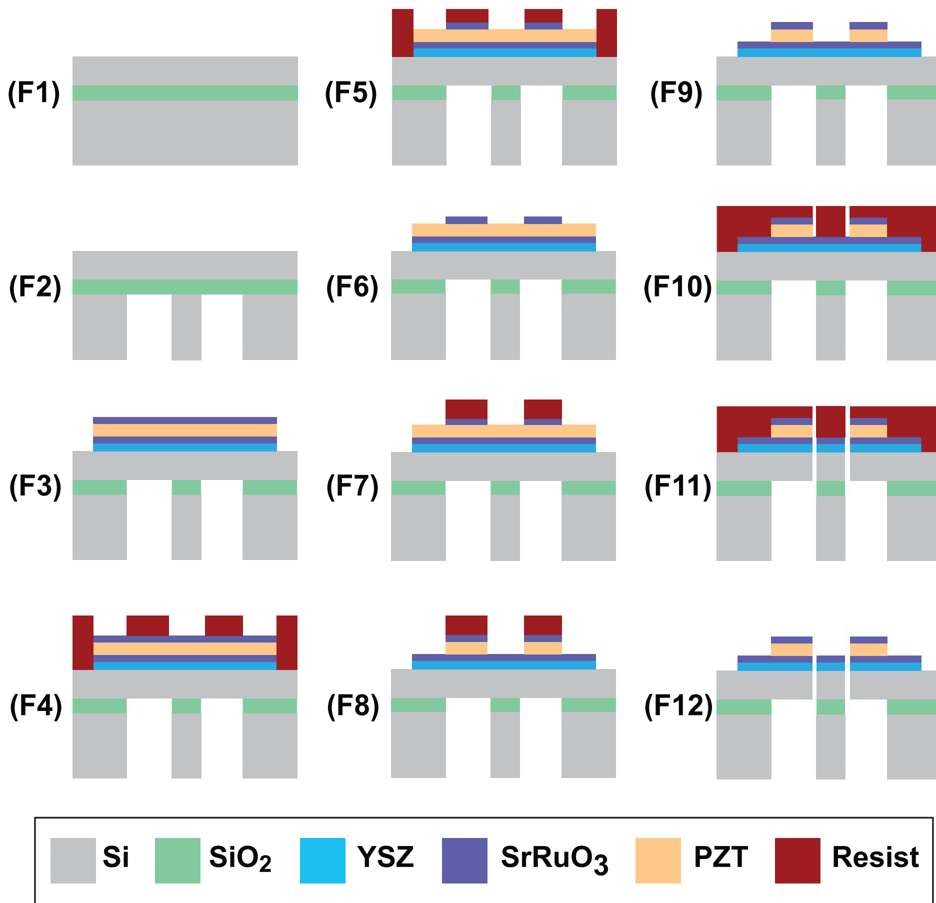

Figure 5.1: Typical fabrication strategy of free-standing MEMS devices using silicon on insulator (SOI) as substrate material.

5.2 Experimental Method

5.2.1 Fabrication of free standing PZT MEMS devices

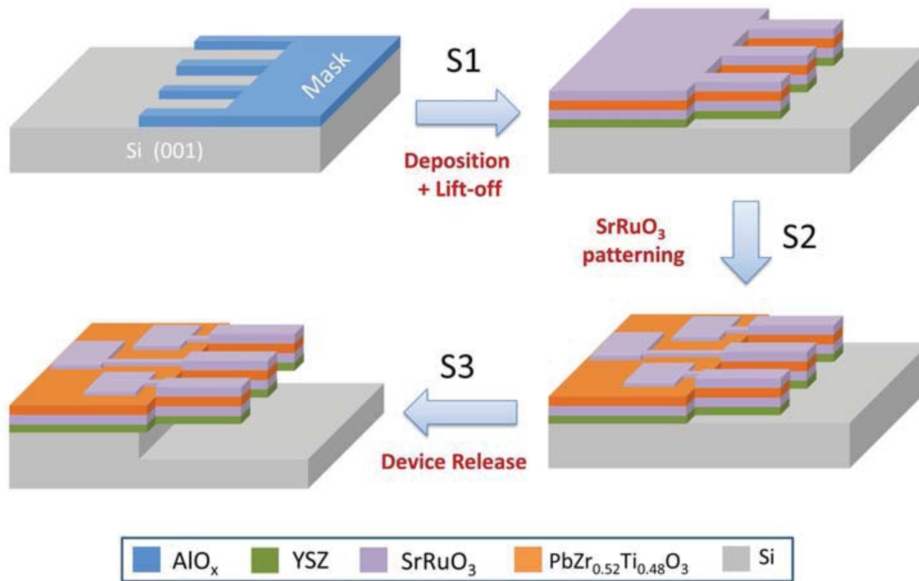

Figure 5.2: Schematic representation of the fabrication process shown in steps S1-S3. Step S1: Deposition of heteroepitaxial oxides followed by annealing of the oxide stack and AlO_x lift-off. Step S2: Patterning of the epitaxial top electrode. Step S3: Anisotropic chemical etching of Si to achieve free-standing piezo MEMS devices.

The all-oxide heteroepitaxial free-standing devices were fabricated using an oxide lift-off patterning technique for the epitaxial multilayer heterostructure followed by anisotropic substrate etching. We have structured the high temperature grown oxide multilayer stack, incorporating the buffer layer, the bottom and top oxide electrode layers and the functional PZT layer, via a single step epitaxial lift-off process as described in the previous chapter [62]. The process is schematically represented in Fig 5.2. In this process a layer of amorphous aluminum oxide (AlO_x) was used as a high temperature stable sacrificial resist mask. The amorphous, sacrificial AlO_x mask layer was grown initially on a standard-cleaned Si (001) substrate via pulsed laser deposition (PLD) at room temperature. The AlO_x mask layer was structured via conventional photo-lithography where an alkaline photo-

resist developer solution also acts as the etchant for the AlO_x layer, dissolving it in the exposed area as water soluble aluminates. This yields a positive mimic of the photo-resist pattern on the AlO_x mask layer with selective openings to the substrate for high temperature functional multilayer deposition. Details of the procedure can be found elsewhere [62].

In the next step the functional oxide layers were deposited at high temperatures by PLD. Since the functional properties of PZT are highly influenced by the crystal orientation [54] it is important to utilize a suitable buffer layer to ensure epitaxial growth. Yttria stabilized zirconia (YSZ) was employed as buffer layer (here $\sim$ 100 nm) on Si which facilitated epitaxial perovskite growth scavenging the native oxide on the substrate surface [63]. In the final device, the YSZ layer also enhances bi-morph actuation of the piezo layer creating an asymmetry of the heterostructure. A heteroepitaxial multilayer of PZT ($\sim$ 150 nm) sandwiched between $SrRuO_3$ (SRO) electrodes ($\sim$ 25 nm) was PLD grown at high (600°C) temperature on the templated substrate under optimized growth conditions [64]. The oxides grow

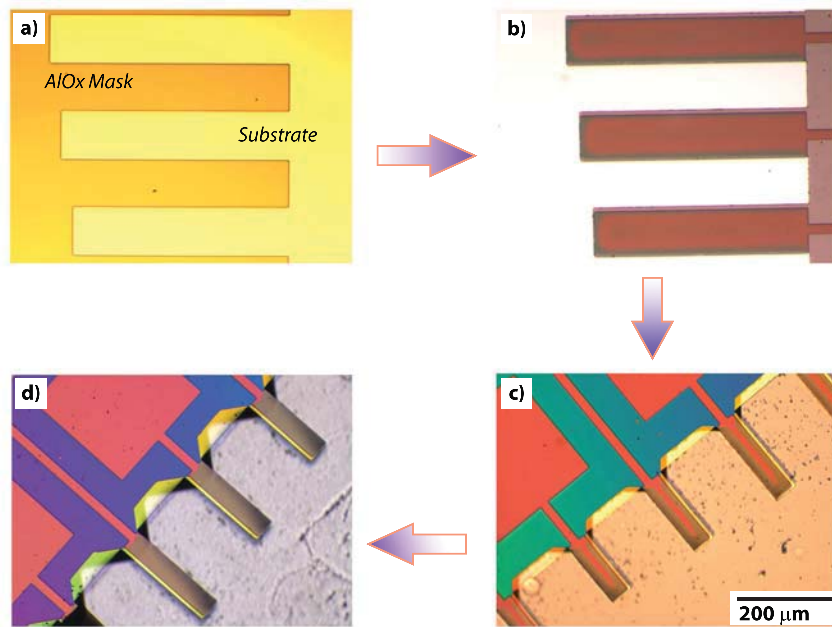

Figure 5.3: Optical microscopic image from different stages of the fabrication process, (a) AlO_x mask after development, (b) structured perovskite multilayer after deposition and lift-off, (c) partially etched cantilevers with backside Si-residues (d) free-standing cantilever arrays completely released from the substrate. The cantilevers shown at different sages of the fabrication procedure are not the identical throughout the steps.

epitaxially on the exposed buffered substrate, but on top of the AlO_x mask layer the growth is polycrystalline. After controlled annealing under high oxygen pressure, the sacrificial template AlO_x mask, together with the amorphous oxide layers were lifted-off using a 2M NaOH solution, patterning the entire heteroepitaxial multilayered oxide assembly. In order to apply an electric field at selective areas, the top SRO electrode layer was patterned via photolithography and dry Ar-ion etching. Lift-off removal of the sacrificial AlO_x mask gives direct access to the Si substrate. Anisotropic hot KOH-etching was employed in the next step to etch selectively the Si(100) substrate, releasing the all-oxide, free-standing epitaxial cantilevers.

5.3 Results and Discussions

5.3.1 Influence of device orientation on rate of their release from substrate

Strong basic solutions (like KOH, NaOH, TMAH) reacts with crystalline Si as follows - $Si + 2OH^- + 2H_2O \rightarrow SiO_2(OH)_2^{2-} + 2H_2$. This basic etching is highly anisotropic in nature and the etching rate of any particular Si crystal plane depends on the number of exposed dangling bonds for the chemical reaction. The rate also depends on the temperature and the concentration of the basic solution as well as on doping level of Si crystal. We have employed 50 wt% aqueous solution of KOH at 75°C and the obtained rate of (100) plane was ~ 1 μm/minute.

Fig. 5.4(a) and 5.4(b) show the optical microscopic images of the multilayer pattern aligned perpendicular (90°) and 45° to the [100] substrate crystal axis respectively, after partial etching of the substrate. The KOH solution etches the (001) crystal plane of Si much faster than the (111) plane [65]. Because of the anisotropic nature of the etching, the in-plane orientation of the cantilevers strongly effects the rate of release of the cantilever from the substrate. We have investigated two different orientations : (i) cantilevers which were oriented perpendicular to the Si [100] in plane crystal axis (90° cantilevers), and (ii) cantilevers which were oriented 45° with respect to that axis (45° cantilevers). Because of the anisotropic etching of Si, the 45° cantilevers displayed a much faster release than 90° cantilevers. The differential etching behavior also affects the geometry of the substrate residue at the base of the cantilever (the anchor) after partial etching. The 45° cantilevers had minimal undercut in the cantilever anchor and were used for all experiments described henceforth.The triangular anchor consists of slowly etched {111} and $\{1\bar{1}1\}$ planes as shown in Fig. 5.5 (a) and (b). It can be noticed from Fig. 5.5(b) that cantilevers are slightly twisted, which was caused by the misalignment between the devices and the substrate crystal axis.

Fig.5.6 shows microscopic images of hetero-epitaxial PZT cantilever devices

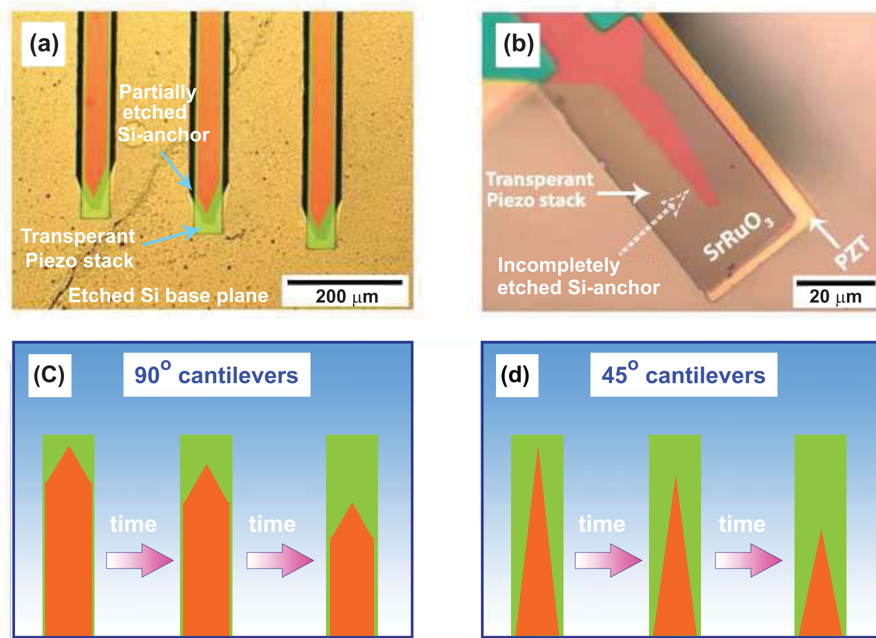

Figure 5.4: Optical Microscopic images (top view) of partially etched cantilevers aligned (a) perpendicular and (b) 45° to the substrate (001) crystal axis. While most of the substrate under the cantilever is etched a small Si residue can be visualized in (b) along the middle of the cantilever via contrast/color difference. The gradual retraction of the anchor during anisotropic KOH etching for perpendicular (90°) and 45° oriented cantilevers is schematically represented in (c) and (d) respectively.

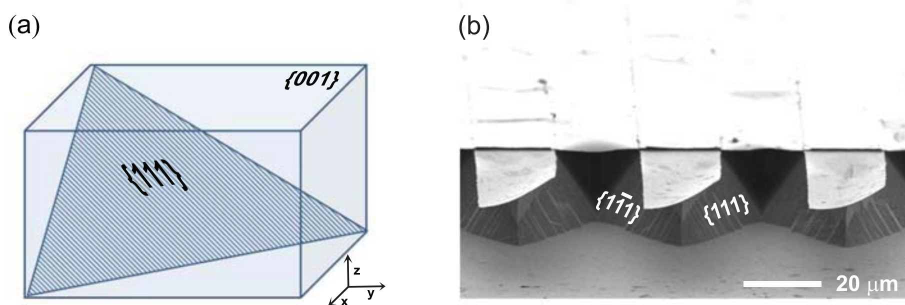

Figure 5.5: (a) Schematic representation of the etching planes and (b) SEM picture of the cantilevers from front-view showing the residual {111} planes.

after complete release from the underlying Si-substrate. Fig. 5.6(a) provides an overview SEM image of a series of devices with different cantilever lengths. Contact pads connected to the patterned $SrRuO_3$ top-electrode of the cantilever are also visible. Fig. 5.6(b) and (c) show a top-view optical microscopic image of an array and a single cantilever device respectively. Since the thin (300 nm) oxide stack is transparent, the different functional oxide layers (see Fig. 5.4(b)) and the triangular Si substrate anchor can be clearly identified in these images. Fig. 5.6(d) gives a side-view SEM image of a representative cantilever, proving that the fabricated device has no noticeable curvature (without application of an actuation voltage) as one may expect for a completely free-standing all-oxide cantilever. For a Si-based cantilever generally a significant curvature is present due to the thermal expansion mismatch between the perovskite layers and the Si support layer. In the nearly symmetric, all-perovskite cantilever there is little effect of the much smaller thermal expansion mismatch between the YSZ layer and SRO/PZT/SRO capacitor stack.

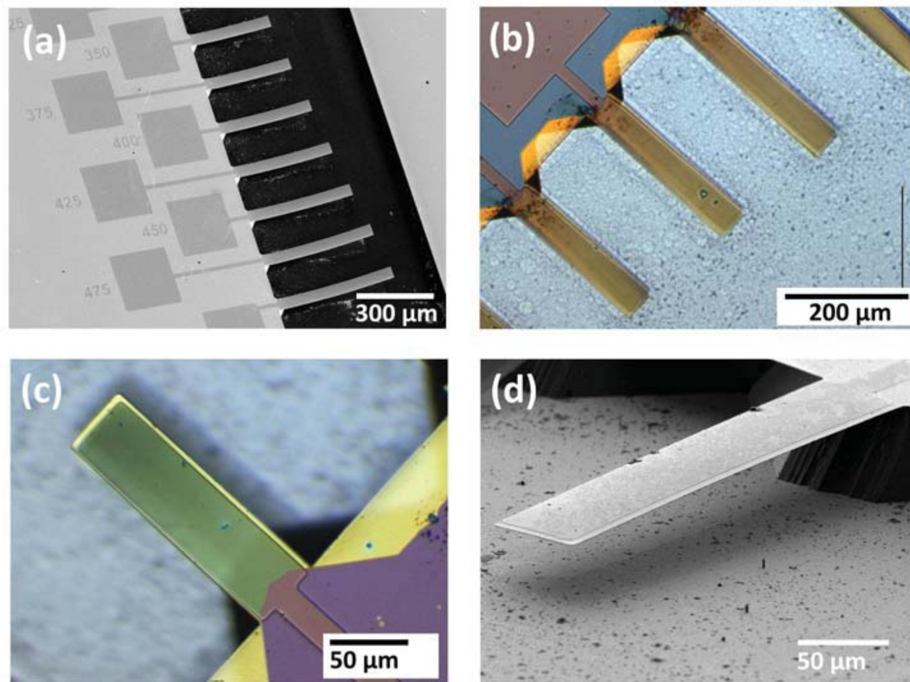

Figure 5.6: (a) SEM overview of a series of cantilevers with different lengths. (b) and (c) top-view optical microscopic images of a series of and a single cantilever device respectively, showing the triangular substrate anchor. (d) Side-view SEM image of a single cantilever proving that the post-etched devices were free-standing and flat.

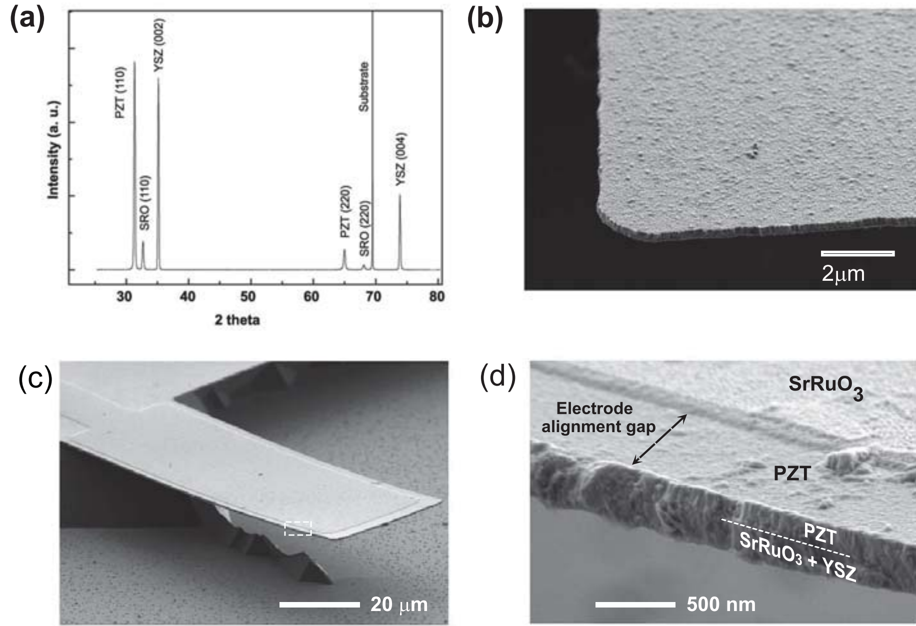

Figure 5.7: (a) XRD spectrum of the multilayer oxide stack after lift-off. (b) SEM image of the surface. (c) and (d) SEM image of a single cantilever device with ∼ 400 nm total thickness and zoomed-in view at the sides.

5.3.2 Structural Characterizations

Figure 5.7 (a) shows XRD spectrum of patterned epitaxial multilayers after the lift-off patterning of the oxide layers, thus proving that all patterned oxides layers are epitaxial and crystalline. As was shown in previous chapter for $SrTiO_3$(001) and Pt/Si substrates, the growth of the epitaxial perovskite multilayers on YSZ-buffered Si(001) via the amorphous mask also resembles well with unmasked substrates [54]. No signal from the mask in the XRD spectrum indicates its complete removal on lift-off. Figure 5.7 (b) presents magnified scanning electron microscopic (SEM) image of the surface of a free standing cantilever with total thickness of ∼ 400 nm. Existence of columnar grains can be noticed as the constituent microstructure which was also confirmed from AFM and cross sectional SEM studies. The average grain size was ∼ 40 nm. Figure 5.7 (c) and (d) shows SEM image of a single free-standing cantilever and magnified view on its side respectively. The electrode alignment gap of ∼ 1.5 μm as can be seen in (d) was kept in order to prevent contact between top and bottom $SrRuO_3$ electrodes in the final device.

5.3.3 Initial bending of the cantilevers

As fabricated cantilevers were found to be bend upwards. The radius of curvature (R) of this initial static bending was dependent on the individual thickness of oxide layers and total thickness of the cantilever beam. The observed initial bending is presumably originating from the combined effect of epitaxial and thermal strains, developed due to mismatch in lattice parameters and thermal expansion coefficients (TEC) between the substrate and the individual oxides layers. Figure 5.8 (a) and (b) presents front side view SEM images of relatively straight and bend cantilevers with total thickness of $\sim$ 300 nm and 500 nm respectively. SEM image of a single cantilever from the back side view is shown as the inset. Careful observation of Fig. 5.8 (a) also reveals that the cantilever is slightly U-shaped owing to triangular shape of the base. To compensate the in-plane lattice-mismatch, PZT(110)||YSZ grows 45° in-plane rotated cube on cube relationship on Si(001) [54, 66].

The static initial bending of the tip was quantitatively measured employing white light interferometry. Top and 3D views of a 100 μm long cantilever showing $\sim$ 1 μm initial tip-deflection is given in Figure 5.9 (a) and (b). The initial tip deflection (D) increases approximately with the cantilever length L, for constant device thickness t_s (300 nm), as is shown by the least-square fit in Figure 5.9 (c) to the data points. The initial curvature is due to build-in stress in the cantilever. There are multiple possible causes for the build-in stress: in the initial growth layer of the YSZ layer on the Si substrate the lattice mismatch causes the incorporation of defects and therefore compressive stress during deposition. After removal of the Si this stress is released and the initial growth layer expands, causing tensile stress in a thin surface layer. Its thickness is estimated to be $\sim$ 10 nm. This build-in stress would be independent of the device thickness and would cause upward curvature of the released cantilever. Secondly thermal expansion differences between the different layers cause build in stress. After removal of the Si the stress distribution is changed again. In this case the build-in stress will depend on the layer thicknesses. It can be shown that in this case D is approximately inversely proportional to the device thickness. Depending on the thermal expansion coefficients, Young's moduli and layer thicknesses the curvature can be upward or downward or change from downwards to upwards or vice versa with changing thicknesses.

A simple way to model beam curvature is by Stoney's equation, describing the radius of curvature R of a beam with a thin surface layer under stress -

$$R = \frac{L^2}{2D} = \frac{1}{6}\frac{E_s t_s^2}{(1-\nu_s)\sigma_f t_f} \tag{5.1}$$

E_s and ν_s are the (average) Young's modulus and (average) Poisson's ratio of the cantilever and σ_f and t_f are the stress in and thickness of the thin stressed layer. In Fig. 5.9 (c) also the values of the product $\sigma_f t_f$ for each cantilever, calculated from the deflection, are shown. With t_f = 10 nm the surface stress is of the order

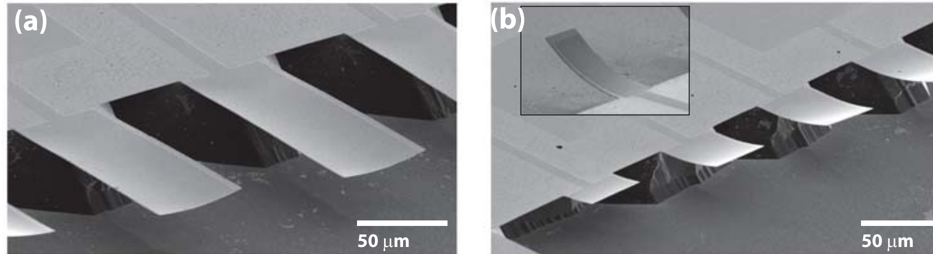

Figure 5.8: SEM image of the free-standing cantilevers with total thickness of (a) 300 nm and (b) 500 nm. SEM image of a single cantilever from back side is shown in the inset in (b)

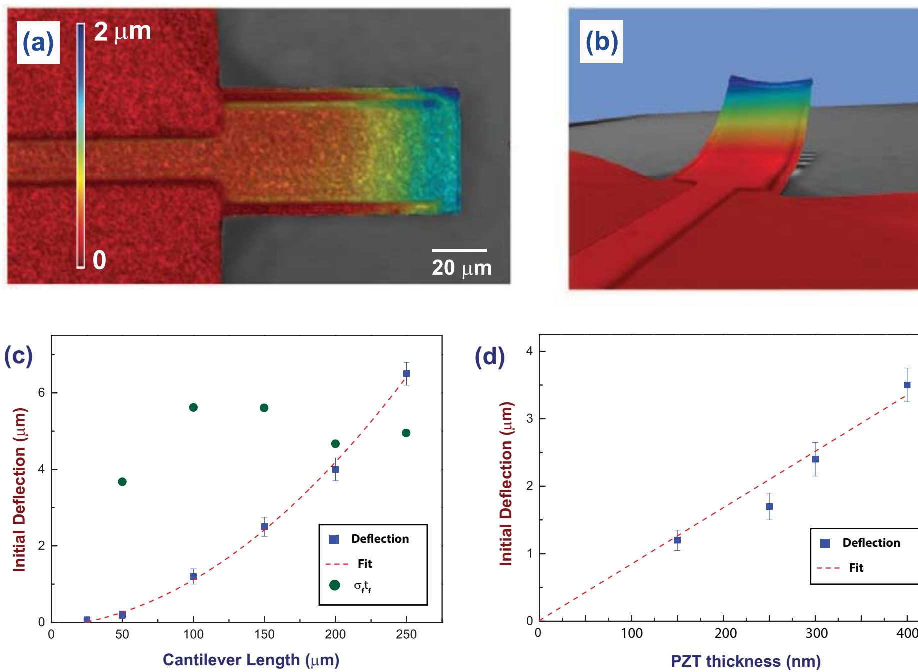

Figure 5.9: Top (a) and in-plane (b) view of the initial bending measured using white light interferometry on a 100 μm long free-standing cantilever. The initial deflection of the tip of the cantilever is shown, (c) as the function of the cantilever length (for devices with total thickness of 300 nm) and (d) thickness (with a cantilever of 100 μm length). All the cantilevers were of 50 μm width.

of $9 \times 10^7 N/m^2$, using the average $\sigma_f t_f$ value of the four longest cantilevers. The reduced deflection of the shortest cantilevers is ascribed to the increased stiffness, caused by the triangular silicon base.

Fig. 5.9 (d) shows the tip deflection as function of cantilever thickness t_s (the PZT thickness is equal to $t_s \sim 150$ nm), for 100 μm long and 50 μm wide cantilevers. The linear fit through the origin suggests that $D = L^2/2R$ is linearly proportional to the cantilever thickness. Assuming that Stoney's formula can also be applied in this case, this implies that $\sigma_f t_f \sim tCL^3$. This contradicts the predictions of the initial growth layer as well as of thermal expansion differences. At the moment it is unclear what the cause is of the increasing deflection of the cantilever with increasing PZT thickness.

5.4 Conclusion

In conclusion, free-standing hetero-epitaxial all-oxide piezo-MEMS cantilever devices, with PZT as active layer, were fabricated directly on Si(001) substrates without the use of a SOI wafer and backside etching. A sacrificial oxide mask was used in epitaxial liftoff structuring process to achieve simultaneous *in situ* patterning of the heteroepitaxial oxide layer stack deposited at high temperatures. Selective area, anisotropic front side etching of the substrates was employed for device-release. The structured devices show well-behaved ferro and piezo electric response. The resonant behavior of the cantilevers with length L = 25 - 325 μm, width W = 50 μm and thickness t = 300 nm was investigated using Doppler vibrometry when a single dominant bending resonant mode was observed for devices with L = 50 - 125 μm. For the other lengths different or multiple modes were excited. Conventional fabrication schemes for multilayered heteroepitaxial systems require multiple etching steps to structure the individual perovskite layers, increasing the chance of contamination and damage of the functional material. Hence the development of a combined patterning strategy as described above, for the entire oxide multilayer stack down to the substrate would pave the way for integrating functional perovskite oxide heteroepitaxial multilayers in VLSI technology. The fabrication of free-standing cantilevers without any residual Si layer on the bottom, opens up the possibility to achieve very high mass sensitivity by further reduction in cantilever surface area. This lift-off mediated fabrication of free standing cantilevers also enables the direct investigation of the influence of different material properties (like micro-structure) on the performance of the cantilever devices.

Bibliography

[1] M. Gad-el Hak, *MEMS: introduction and fundamentals*. CRC press, 2010.

[2] W. A. de Groot, J. R. Webster, D. Felnhofer, and E. P. Gusev, "Review of device and reliability physics of dielectrics in electrostatically driven MEMS devices," *IEEE Transactions on Device and Materials Reliability*, vol. 9, no. 2, pp. 190–202, 2009.

[3] T. L. Sounart, T. A. Michalske, and K. R. Zavadil, "Frequency-dependent electrostatic actuation in microfluidic MEMS," *Journal of Microelectromechanical Systems*, vol. 14, no. 1, pp. 125–133, 2005.

[4] D. Girbau, A. Lazaro, and L. Pradell, "Extended tuning range RF MEMS variable capacitors using electrostatic and electrothermal actuators," *Proceedings of SPIE Micromachining and Microfabrication 2004*, vol. 5344, pp. 59–70, 2004.

[5] W.-C. Chuang, H.-L. Lee, P.-Z. Chang, and Y.-C. Hu, "Review on the modeling of electrostatic MEMS," *Sensors*, vol. 10, no. 6, pp. 6149–6171, 2010.

[6] S. K. De and N. Aluru, "Theory of thermoelastic damping in electrostatically actuated microstructures," *Physical Review B*, vol. 74, no. 14, p. 144305, 2006.

[7] S. H. Goodwin-Johansson, "Arc resistant high voltage micromachined electrostatic switch," May 2 2000. US Patent 6,057,520.

[8] S. Trolier-McKinstry and P. Muralt, "Thin film piezoelectrics for MEMS," *Journal of Electroceramics*, vol. 12, no. 1-2, pp. 7–17, 2004.

[9] B. Borovic, A. Liu, D. Popa, H. Cai, and F. Lewis, "Open-loop versus closed-loop control of MEMS devices: choices and issues," *Journal of Micromechanics and Microengineering*, vol. 15, no. 10, p. 1917, 2005.

[10] S. Gorthi, A. Mohanty, and A. Chatterjee, "Cantilever beam electrostatic MEMS actuators beyond pull-in," *Journal of Micromechanics and Microengineering*, vol. 16, no. 9, p. 1800, 2006.

[11] G. lR Gilbert and S. Senturia, "3D modeling of contact problems and hysteresis in coupled electro-mechanics," 1996.

[12] Y. He, J. Marchetti, and C. Gallegus, "General contact and hysteresis analysis of multidielectric MEMS devices under thermal and electrostatic actuation," in *Design, Test, and Microfabrication of MEMS/MOEMS*, pp. 179–186, International Society for Optics and Photonics, 1999.

[13] M. I. Younis, H. M. Ouakad, F. M. Alsaleem, R. Miles, and W. Cui, "Nonlinear dynamics of MEMS arches under harmonic electrostatic actuation," *Journal of Microelectromechanical Systems*, vol. 19, no. 3, pp. 647–656, 2010.

[14] S. Muratet, S. Lavu, J.-Y. Fourniols, G. Bell, and M. P. Desmulliez, "Reliability modelling and analysis of thermal MEMS," in *Journal of Physics: Conference Series*, vol. 34, p. 235, IOP Publishing, 2006.

[15] M. Umeda, K. Nakamura, and S. Ueha, "Analysis of the transformation of mechanical impact energy to electric energy using piezoelectric vibrator," *Japanese Journal of Applied Physics*, vol. 35, no. 5, pp. 3267–3273, 1996.

[16] D. Shen, J.-H. Park, J. Ajitsaria, S.-Y. Choe, H. C. Wikle III, and D.-J. Kim, "The design, fabrication and evaluation of a MEMS PZT cantilever with an integrated Si proof mass for vibration energy harvesting," *Journal of Micromechanics and Microengineering*, vol. 18, no. 5, p. 055017, 2008.

[17] X. Chen, S. Xu, N. Yao, and Y. Shi, "1.6 V nanogenerator for mechanical energy harvesting using PZT nanofibers," *Nano Letters*, vol. 10, no. 6, pp. 2133–2137, 2010.

[18] W. Choi, Y. Jeon, J.-H. Jeong, R. Sood, and S.-G. Kim, "Energy harvesting MEMS device based on thin film piezoelectric cantilevers," *Journal of Electroceramics*, vol. 17, no. 2-4, pp. 543–548, 2006.

[19] R. Yang, Y. Qin, L. Dai, and Z. L. Wang, "Power generation with laterally packaged piezoelectric fine wires," *Nature Nanotechnology*, vol. 4, no. 1, pp. 34–39, 2009.

[20] L. Lin, R. T. Howe, and A. P. Pisano, "Microelectromechanical filters for signal processing," *Journal of Microelectromechanical Systems*, vol. 7, no. 3, pp. 286–294, 1998.

[21] F. D. Bannon, J. R. Clark, and C.-C. Nguyen, "High-Q HF microelectromechanical filters," *Solid-State Circuits, IEEE Journal of*, vol. 35, no. 4, pp. 512–526, 2000.

[22] L. Pescini, H. Lorenz, and R. H. Blick, "Mechanical gating of coupled nanoelectromechanical resonators operating at radio frequency," *Applied Physics Letters*, vol. 82, no. 3, pp. 352–354, 2003.

[23] A. Husain, J. Hone, H. W. C. Postma, X. Huang, T. Drake, M. Barbic, A. Scherer, and M. Roukes, "Nanowire-based very-high-frequency electromechanical resonator," *Applied Physics Letters*, vol. 83, no. 6, pp. 1240–1242, 2003.

[24] I. Bargatin, I. Kozinsky, and M. Roukes, "Efficient electrothermal actuation of multiple modes of high-frequency nanoelectromechanical resonators," *Applied Physics Letters*, vol. 90, no. 9, p. 093116, 2007.

[25] R. Lothar, "Piezoelectric crystal filter," Nov. 18 1941. US Patent 2,262,966.

[26] H.-P. Lobl, M. Klee, C. Metzmacher, W. Brand, R. Milsom, P. Lok, and R. Van Straten, "Piezoelectric materials for BAW resonators and filters," in *Ultrasonics Symposium, 2001 IEEE*, vol. 1, pp. 807–811, IEEE, 2001.

[27] K. Liu, W. Jing, G. Peng, J. Zhang, D. Jia, H. Zhang, and Y. Zhang, "Investigation of PZT driven tunable optical filter nonlinearity using FBG optical fiber sensing system," *Optics Communications*, vol. 281, no. 12, pp. 3286–3290, 2008.

[28] J. Zheng, G. Guo, Y. Wang, and W. E. Wong, "Optimal narrow-band disturbance filter for PZT-actuated head positioning control on a spinstand," *Magnetics, IEEE Transactions on*, vol. 42, no. 11, pp. 3745–3751, 2006.

[29] D. L. DeVoe and A. P. Pisano, "Surface micromachined piezoelectric accelerometers (PiXLs)," *Journal of Microelectromechanical Systems*, vol. 10, no. 2, pp. 180–186, 2001.

[30] K. Kunz, P. Enoksson, and G. Stemme, "Highly sensitive triaxial silicon accelerometer with integrated PZT thin film detectors," *Sensors and Actuators A: Physical*, vol. 92, no. 1, pp. 156–160, 2001.

[31] L.-P. Wang, R. A. Wolf Jr, Y. Wang, K. K. Deng, L. Zou, R. J. Davis, and S. Trolier-McKinstry, "Design, fabrication, and measurement of high-sensitivity piezoelectric microelectromechanical systems accelerometers," *Journal of Microelectromechanical Systems*, vol. 12, no. 4, pp. 433–439, 2003.

[32] Y. Nemirovsky, A. Nemirovsky, P. Muralt, and N. Setter, "Design of novel thin-film piezoelectric accelerometer," *Sensors and Actuators A: Physical*, vol. 56, no. 3, pp. 239–249, 1996.

[33] H. Van Lintel, F. Van de Pol, and S. Bouwstra, "A piezoelectric micropump based on micromachining of silicon," *Sensors and Actuators*, vol. 15, no. 2, pp. 153–167, 1988.

[34] J. G. Smits, "Piezoelectric micropump with three valves working peristaltically," *Sensors and Actuators A : Physical*, vol. 21, no. 1, pp. 203–206, 1990.

[35] R. Linnemann, P. Woias, C.-D. Senfft, and J. Ditterich, "A self-priming and bubble-tolerant piezoelectric silicon micropump for liquids and gases," in *Proceedings, The Eleventh Annual International Workshop on Micro Electro Mechanical Systems,*, pp. 532–537, IEEE, 1998.

[36] D. Laser and J. Santiago, "A review of micropumps," *Journal of Micromechanics and Microengineering*, vol. 14, no. 6, p. R35, 2004.

[37] G. Binnig, C. F. Quate, and C. Gerber, "Atomic force microscope," *Physical Review Letters*, vol. 56, no. 9, p. 930, 1986.

[38] H. G. Craighead, "Nanoelectromechanical systems," *Science*, vol. 290, no. 5496, pp. 1532–1535, 2000.

[39] J. J. Bernstein, S. L. Finberg, K. Houston, L. C. Niles, H. D. Chen, L. Eric Cross, K. Li, and K. Udayakumar, "Micromachined high frequency ferroelectric sonar transducers," *Ultrasonics, Ferroelectrics and Frequency Control, IEEE Transactions on*, vol. 44, no. 5, pp. 960–969, 1997.

[40] K. Yamashita, L. Chansomphou, H. Murakami, and M. Okuyama, "Ultrasonic micro array sensors using piezoelectric thin films and resonant frequency tuning," *Sensors and Actuators A: Physical*, vol. 114, no. 2, pp. 147–153, 2004.

[41] Z. Wang, W. Zhu, J. Miao, H. Zhu, C. Chao, and O. K. Tan, "Micromachined thick film piezoelectric ultrasonic transducer array," *Sensors and Actuators A: Physical*, vol. 130, pp. 485–490, 2006.

[42] W. Wersing, W. Heywang, H. Beige, and H. Thomann, "The role of ferroelectricity for piezoelectric materials," in *Piezoelectricity*, pp. 37–87, Springer, 2008.

[43] D. Damjanovic, "Ferroelectric, dielectric and piezoelectric properties of ferroelectric thin films and ceramics," *Reports on Progress in Physics*, vol. 61, no. 9, p. 1267, 1998.

[44] P. Muralt, "PZT thin films for microsensors and actuators: Where do we stand?," *Ultrasonics, Ferroelectrics and Frequency Control, IEEE Transactions on*, vol. 47, no. 4, pp. 903–915, 2000.

[45] W. Wersing and B. Steele, "Electronic ceramics," *Elsevier Science, New York, 1991) ch*, vol. 4, p. 69, 1991.

[46] E. Cross, "Materials science: lead-free at last," *Nature*, vol. 432, no. 7013, pp. 24–25, 2004.

[47] J. Scott, "Applications of modern ferroelectrics," *Science*, vol. 315, no. 5814, pp. 954–959, 2007.

[48] M. E. Lines and A. M. Glass, *Principles and applications of ferroelectrics and related materials*. Oxford University Press, 1977.

[49] N. Ledermann, P. Muralt, J. Baborowski, S. Gentil, K. Mukati, M. Cantoni, A. Seifert, and N. Setter, "{1 0 0}-textured, piezoelectric Pb(Zr_x, $Ti_{(1-x)}$)O_3 thin films for MEMS: integration, deposition and properties," *Sensors and Actuators A: Physical*, vol. 105, no. 2, pp. 162–170, 2003.

[50] Y. Jeon, R. Sood, J.-h. Jeong, and S.-G. Kim, "MEMS power generator with transverse mode thin film PZT," *Sensors and Actuators A: Physical*, vol. 122, no. 1, pp. 16–22, 2005.

[51] S. Xiong, H. Kawada, H. Yamanaka, and T. Matsushima, "Piezoelectric properties of PZT films prepared by the sol–gel method and their application in mems," *Thin Solid Films*, vol. 516, no. 16, pp. 5309–5312, 2008.

[52] R. Ramesh and D. Schlom, "Orienting ferroelectric films," *Science*, vol. 296, no. 5575, pp. 1975–1976, 2002.

[53] D. Isarakorn, D. Briand, A. Sambri, S. Gariglio, J.-M. Triscone, F. Guy, J. Reiner, C. Ahn, and N. de Rooij, "Finite element analysis and experiments on a silicon membrane actuated by an epitaxial PZT thin film for localized-mass sensing applications," *Sensors and Actuators B: Chemical*, vol. 153, no. 1, pp. 54–63, 2011.

[54] M. Dekkers, M. D. Nguyen, R. Steenwelle, P. M. te Riele, D. H. Blank, and G. Rijnders, "Ferroelectric properties of epitaxial Pb(Zr,Ti)O_3 thin films on silicon by control of crystal orientation," *Applied Physics Letters*, vol. 95, no. 1, pp. 012902–012902, 2009.

[55] I. Vrejoiu, G. LeRhun, L. Pintilie, D. Hesse, M. Alexe, and U. Gösele, "Intrinsic ferroelectric properties of strained tetragonal $PbZr_{0.2}Ti_{0.8}O_3$ obtained on layer-by-layer grown, defect-free single-crystalline films," *Advanced Materials*, vol. 18, no. 13, pp. 1657–1661, 2006.

[56] J. H. Park, T. Y. Kwon, D. S. Yoon, H. Kim, and T. S. Kim, "Fabrication of microcantilever sensors actuated by piezoelectric $Pb(Zr_{0.52}Ti_{0.48})O_3$ thick films and determination of their electromechanical characteristics," *Advanced Functional Materials*, vol. 15, no. 12, pp. 2021–2028, 2005.

[57] R. Ramesh, H. Gilchrist, T. Sands, V. Keramidas, R. Haakenaasen, and D. Fork, "Ferroelectric La-Sr-Co-O/Pb-Zr-Ti-O/La-Sr-Co-O heterostructures on silicon via template growth," *Applied Physics Letters*, vol. 63, no. 26, pp. 3592–3594, 1993.

[58] C. Eom, R. Van Dover, J. M. Phillips, D. Werder, J. Marshall, C. Chen, R. Cava, R. Fleming, and D. Fork, "Fabrication and properties of epitaxial ferroelectric heterostructures with $SrRuO_3$ isotropic metallic oxide electrodes," *Applied Physics Letters*, vol. 63, no. 18, pp. 2570–2572, 1993.

[59] M. D. Nguyen, H. Nazeer, K. Karakaya, S. Pham, R. Steenwelle, M. Dekkers, L. Abelmann, D. Blank, and G. Rijnders, "Characterization of epitaxial Pb(Zr,Ti)O_3 thin films deposited by pulsed laser deposition on silicon cantilevers," *Journal of Micromechanics and Microengineering*, vol. 20, no. 8, p. 085022, 2010.

[60] D. Isarakorn, A. Sambri, P. Janphuang, D. Briand, S. Gariglio, J. Triscone, F. Guy, J. Reiner, C. Ahn, and N. de Rooij, "Epitaxial piezoelectric MEMS on silicon," *Journal of Micromechanics and Microengineering*, vol. 20, no. 5, p. 055008, 2010.

[61] S. Baek, J. Park, D. Kim, V. Aksyuk, R. Das, S. Bu, D. Felker, J. Lettieri, V. Vaithyanathan, S. Bharadwaja, *et al.*, "Giant piezoelectricity on Si for hyperactive MEMS," *Science*, vol. 334, no. 6058, pp. 958–961, 2011.

[62] N. Banerjee, G. Koster, and G. Rijnders, "Submicron patterning of epitaxial $PbZr_{0.52}Ti_{0.48}O_3$ heterostructures," *Applied Physics Letters*, vol. 102, no. 14, pp. 142909–142909, 2013.

[63] S. Wang, C. Ong, L. You, and S. Xu, "Epitaxial growth of yittria-stabilized zirconia oxide thin film on natively oxidized silicon wafer without an amorphous layer," *Semiconductor Science and Technology*, vol. 15, no. 8, p. 836, 2000.

[64] P. M. Te Riele, G. Rijnders, and D. H. Blank, "Ferroelectric devices created by pressure modulated stencil deposition," *Applied Physics Letters*, vol. 93, no. 23, pp. 233109–233109, 2008.

[65] M. Elwenspoek and H. V. Jansen, *Silicon Micromachining.* Cambridge University Press, Cambridge, UK, 2004.

[66] S. Hou, J. Kwo, R. Watts, J.-Y. Cheng, and D. Fork, "Structure and properties of epitaxial $Ba_{0.5}Sr_{0.5}TiO_3/SrRuO_3/ZrO_2$ heterostructure on Si grown by off-axis sputtering," *Applied Physics Letters*, vol. 67, no. 10, pp. 1387–1389, 1995.

Chapter 6

Electromechanical Properties and Vibrational Damping in Freestanding Epitaxial PZT Cantilevers

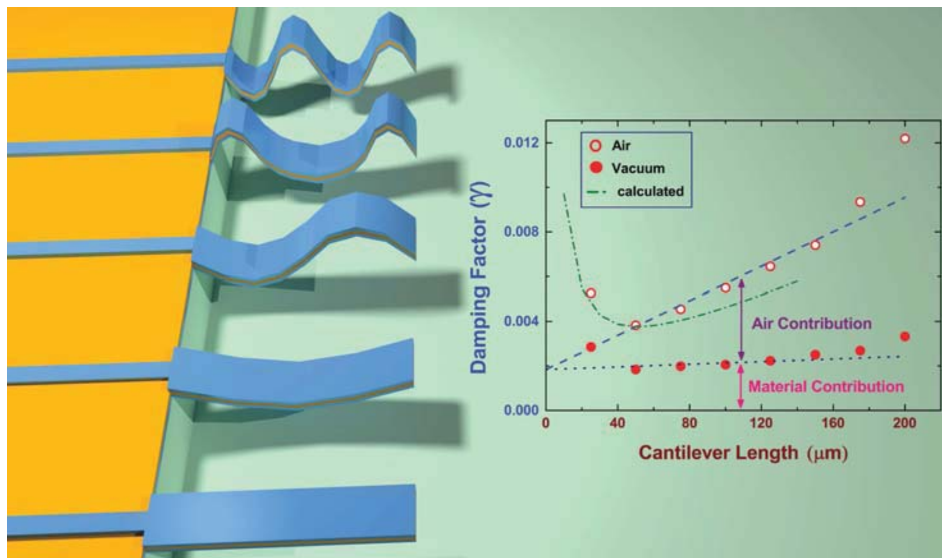

Part of the work discussed in this chapter is under preparation as a manuscript for publication in an international peer-reviewed scientific journal as : **N. Banerjee, E. P. Houwman, G. Koster, G. Rijnders, "*Intrinsic Damping in Freestanding Epitaxial PZT Cantilevers*"**

ABSTRACT

In this chapter we have investigated the electromechanical properties of all-oxide, free standing, heteroepitaxial $PbZr_{0.52}Ti_{0.48}O_3$ *(PZT) cantilever devices fabricated directly on Si(001) as described in the previous chapter. These MEMS devices were devoid of any silicon crystal on the backside, unlike traditional silicon on insulator (SOI) based cantilevers. Cantilevers, with length (L) in the range 25 - 325 μm, constant width (W) of 50 μm and total thickness of 300 nm, were actuated by an external AC drive bias of varying frequency. All devices displayed resonant vibration. We have employed Doppler vibrometry to investigate the quality factor of such resonant excitations. The second order bending mode was found to form the dominant resonance mode for cantilevers with a functional length in the range of 50 - 125 μm. For longer free-standing cantilevers other or multiple resonating modes were found to be present. We have identified the contribution of the operational medium (air, extrinsic contribution) and the contribution of the constituent material (intrinsic contribution) to the vibrational damping of the device by investigating the electromechanical response of a series of cantilevers in ambient and under vacuum conditions. For cantilevers with lengths in the range 50 - 125 μm, the damping increases linearly with the cantilever length, which is explained by the combined effect of air damping and intrinsic friction in the cantilever material. The developed model for the damping gives guidelines for optimizing the quality factor and dependent properties of resonating cantilevers.*

6.1 Introduction

6.1.1 Mass sensors with resonating cantilevers

Many of the piezoelectric MEMS devices have a cantilever configuration, operating in bending mode. They generate an open circuit voltage when deformed, as well as manifest mechanical actuation in response to an external voltage and hence can be conveniently employed for both sensing and actuation purposes. Such devices typically consist of an active piezoelectric film fabricated on a thin Si beam which is capable of free vertical movement. An external bias induces a lateral extension or contraction in the piezo-layer, causing a bimorph actuation due to the clamping with the substrate and/or asymmetries between the electrode layers. Very accurate sensing can also be realized by bringing the cantilever into a resonant state by applying an alternating bias voltage with appropriate frequency. For example in the mass sensor, any change in the cantilever mass alters the resonance frequency (f_n) and measurement of the frequency shift ($\triangle f_n$) offers the possibility to measure the mass change very accurately. This label-free mass sensing and measurement principle is utilized for a wide range of applications from bio-chemical [1], biological [2] to even atomic physics [3].

6.1.2 Damping in electromechanical cantilevers

Most applied cantilever MEMS devices operate in either frequency-output or amplitude output mode while in self-resonating condition, and are utilized for sensing purposes [4]. Traditionally such sensor devices have been made using Si beams [5–8], mainly because of the advantages in their integration with existing semiconductor electronics. The good mechanical properties of Si crystal wafers and the remarkable advances in the Si-based fabrication technology are added benefits to this cause. Although relatively less explored, piezo-driven MEMS cantilever devices are interesting over their electrostatic analogues specifically for targeted applications. They offer advantages like higher actuation amplitude, low power requirement, faster response time and hence piezo-driven MEMS devices have been conventionally utilized for a wide variety of applications [9–15]. Among different piezoelectric materials, perovskite PZT has found enormous pragmatic importance because of its very high electromechanical coupling coefficients [16], as described in the previous chapter.

One of the key parameters determining the resolution of a cantilever based resonant frequency-output sensor is its mechanical quality factor (Q) [8, 17–20]. It defines the sharpness of the resonance-peak, thus a higher quality factor implies a sharper peak, with consequent enhancement in the resolution of the frequency-output sensor. Theoretical understanding and evaluation of the mechanical quality factor needs several damping mechanism to be taken into account [8, 21–23].

It has been shown that when operating in ambient condition, air-pressure is the most important parameter to affect the cantilever quality factor [21, 24, 25]. Other different damping mechanisms were also observed as the pressure of the operating medium (air) was changed [8]. While most of the theories/experiments were designed/performed with Si-beams or piezo-driven cantilevers on silicon-on-insulator (SOI) substrates with backside residual Si-crystal as the major mechanical component [26], investigations with free-standing all-oxide devices are elusive in literature. One important difference between the two is that, unlike Si, oxide devices often constitutes of grains and grain-boundaries, which give rise to internal friction during vibrating. Thus internal-damping, existing inside the devices itself must be taken into consideration in addition to the damping introduced by the operational medium.

6.1.3 Free-standing piezo-driven cantilevers for high - sensitivity mass sensors

The bending resonance frequencies (f_n) of a cantilever of length L, width W, thickness t with (effective) Young's modulus E and beam mass per length m_L (density ρ_c), are given by (under the condition L≥W≫t) [19, 27, 28]

$$f_n = \frac{{\alpha_n}^2}{2\pi L^2}\sqrt{\frac{E(Wt^3)/12}{m_L}} = \frac{{\alpha_n}^2 t}{2\pi L^2}\sqrt{\frac{E}{12\rho_c}} = \frac{C_1 t}{L^2} \tag{6.1}$$

Here α_n are numerical factors, increasing with n (α_1=1.875 is the fundamental mode, α_2=4.69) and C_1 comprises parameters independent of the beam size. The mass sensitivity of such a cantilever for a particular resonant mode can be defined as the ratio between the shift of the resonance frequency ($\triangle f_n$) due to additional mass loading ($\triangle m_L$) and is equal to $S_m = \triangle f_n / \triangle m = -f_n/2m$ [29], where m is the sensor mass. The sensitivity can be written in terms of dimensional parameters as $S_m = -C_1/(\rho_c L^3 W)$, which is independent of the device thickness. To increase S_m, one has to decrease the lateral dimensions of the cantilever, but in order to maintain bending mode operation the cantilever should also be sufficiently thin. Hence, the first step towards miniaturizing a piezoelectric driven cantilever is the development of a technique capable of reducing the cantilever thickness, with the possibility of further reduction of the beam area.

In the previous chapter we have demonstrated a fabrication strategy for preparing freestanding cantilevers of all-oxide heteroepitaxial multilayer. The fabrication was enabled by the development of an epitaxial lift-off patterning strategy for simultaneous structuring of epitaxial multilayers. In order to employ such free-standing cantilever devices for high-sensitivity mass sensors it is necessary to investigate their electromechanical behavior triggered by external drive-bias voltages. In this chapter we have studied the electromechanical response and vibrational damp-

ing mechanisms of freestanding, all-oxide, hetero-epitaxial PZT cantilevers for high-sensitivity mass-sensor devices.

6.2 Methodes

All experimental measurement of electromechanical properties as described in the current chapter were performed with all-oxide, free-standing, heteroepitaxial PZT cantilevers, fabricated using the strategy as described in *Chapter 5*. Heteroepitaxial oxide stacks incorporating a functional piezo layer were deposited on Si(001) and patterned utilizing the epitaxial lift-off strategy. The patterning pathway allows simultaneous structurization of all functional oxide layers and promotes access to the underlying silicon substrate in the uncovered areas. This exposed Si(001) was etched using basic etching for the release of the devices.

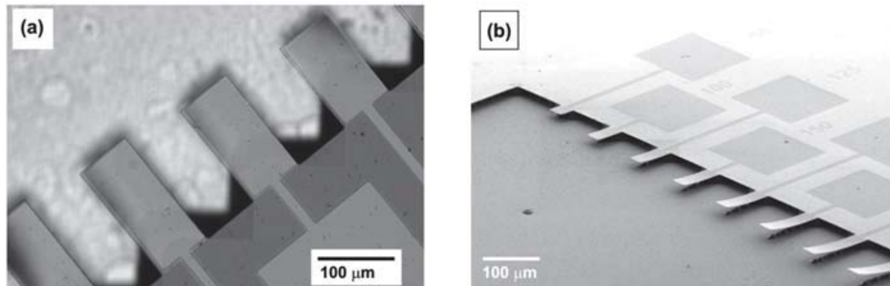

Figure 6.1: (a) Optical microscopic and (b) scanning electron microscopic images of arrays free-standing PZT cantilevers with different cantilever length, after complete release from the substrate. The series of cantilevers with identical deposition and fabrication history were electromechanically probed to investigate effect of cantilever length on vibrational response.

Figure 6.1 (a) and (b) shows optical and scanning electron microscopic images of an array of all-oxide heteroepitaxial free-standing cantilever devices after complete release from the substrate. As has been presented in the previous chapter, the obtained heteroepitaxial PZT cantilevers were free-standing after complete substrate etching, were well tunable in both length and width (in the photolithographic range) and had a triangular anchor-base originating from the slow etching rate of the Si (111) planes. Unlike traditional SOI-based devices, the fabricated cantilevers did not contain any residual Si crystal on the back-side. In order to probe the electromechanical vibrational properties of these free-standing PZT-devices, we have fabricated a series of heteroepitaxial cantilever devices with different functional length. The etching time of the underneath Si substrate to achieve the release of the cantilever devices depends crucially on the width of the cantilevers. Hence a wafer

sample with different cantilever-widths suffers form inhomogeneous undercuts. This has a substantial effect on their electromechanical properties, making the theoretical analysis complex. For this reason variation in the length of cantilever devices was preferred keeping all other functional parameters identical. We specifically emphasize that in a particular sample all the cantilevers with different lengths experience identical deposition and fabrication treatment, thus minimizing their influence on the electromechanical behavior.

The ferroelectric behavior of the lift-off fabricated devices in metal-insulator-metal (M-I-M) configuration was measured using a modified Sawyer-Tower circuit in aixACCT analyzer TF 2000. The room temperature electromechanical response of the post-etched piezo driven cantilevers was investigated employing laser Doppler vibrometry. The devices were biased with an AC-voltage of 0.1 V ($E_{tt} \approx 7$ kV/cm) at a DC bias voltage of 3 V ($E_{bias} = 200$ kV/cm).

6.3 Experimental

The room temperature ferroelectric response (current-voltage behavior and corresponding polarization-electric field hysteresis loop) of a representative lift-off fabricated PZT capacitor cantilever device (100×100 μm^2) before etching the Si, is shown in Figure 6.2. Note that these loops are dominated by the large area capacitor formed by the bonding path off the cantilever. The loop is very symmetric, with a coercive field of ~ 85 kV/cm. The remnant and saturation polarization are ~ 24 μC/cm^2 and ~ 35 μC/cm^2 respectively. The ferroelectric response was stable up to 10^8 switching cycles (because of the epitaxial electrodes used). In the bonding path area the film stack is clamped to the substrate after Si etching, whereas in the relatively small area freestanding beam this is not the case. After etching the device cannot be cycled anymore to high voltages, because of electromechanical damage to the cantilever, which we ascribe to the large piezoelectric stresses induced in the crystal structure. This well-behaved ferroelectric response obtained in lift-off patterned heteroepitaxial PZT capacitors shows that the patterning strategy does not affect the ferroelectric properties of perovskite heterostructures [30]. As noted above the devices could not be brought into saturation, hence one may expect non-optimal alignment of the ferroelectric domains, in the freestanding cantilever devices.

A representative frequency spectrum for a 125 μm $\times$ 50 μm free-standing cantilever is presented in Figure 6.3 as measured by a Doppler vibrometer. Sharp resonance excitations were obtained on excitation by an external AC bias, as can be noticed from the spectrum. To align the ferrroelectric domains a drive DC bias $\geq E_c$ was applied simultaneously. Resonant mode patterns corresponding to the different harmonic excitation peaks in the spectrum, as probed by scanning Doppler vibrometry, are shown schematically as insets in Figure 6.3. It can be noticed

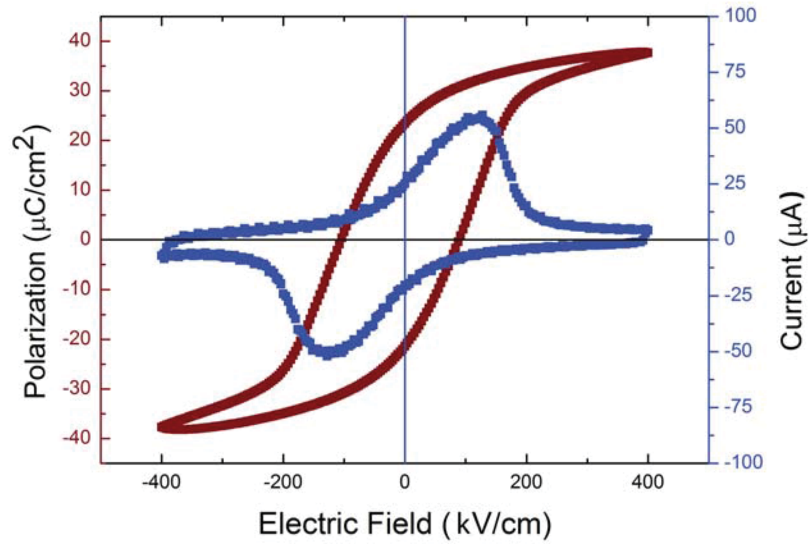

Figure 6.2: Current-electric field behavior (blue) and corresponding polarization-field loop (brown) at 1 kHz for ~ 150 nm ferroelectric $PbZr_{0.52}Ti_{0.48}O_3$ epitaxial film on $SrRuO_3$/YSZ/Si(001)

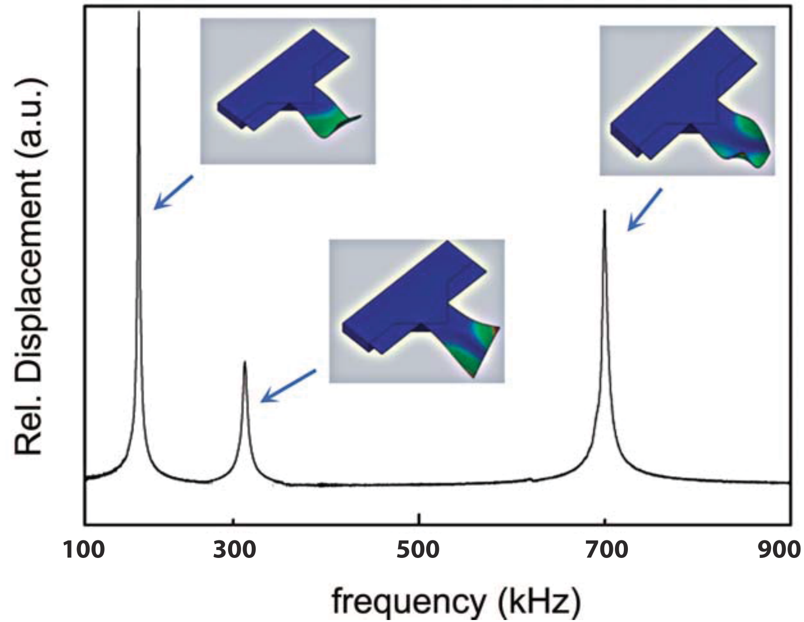

Figure 6.3: Frequency spectrum for a 125 μm long (50 μm wide) free-standing heteroepitaxial PZT cantilever device. Resonant modes corresponding to different harmonic excitation peaks on the spectrum is schematically shown as insets.

that the second harmonic bending mode appears as the dominant excitation as will be discussed in detail in the following sections. To gain insight in the energy loss mechanism during electromechanical vibration we have measured a series of cantilevers with functional length (L) in the range 25 - 325 μm, constant width (W) of 50 μm and total thickness of 300 nm. Utilizing laser Doppler vibrometry, we have investigated the dependence of the resonance frequency (f_{res}) and damping constant (γ) on the cantilever length.

6.4 Results and Discussion

6.4.1 Electromechanical response of the freestanding PZT cantilevers

Figure 6.4 shows the measured resonance frequency f_{res} of the mode with the highest resonance amplitude (in ambient conditions) versus beam length. The curve shown is calculated from eq.6.1 with C_1 = 4950 Hz.m using average E = 1.16×10^{11} N/m^2 and $\rho_c = 6.7 \times 10^3$ kg/m^3 for the oxide stack showing that f_{res} is fairly well described by the second order bending mode. A representative amplitude and phase response curve with 180° phase change is shown in the inset for a free-standing cantilever of 50μm × 50μm. According to eq.6.1 f_{res}L^2 is expected to have a constant value, independent of cantilever length. The dependence of f_{res}L^2 on the length of the cantilever is presented in Fig. 6.5 for devices with constant total thickness of 300 nm and width W = 50 μm. Four different regimes can be distinguished in this graph: L < 50 μm, 50 μm $\leq$ L $\geq$ 150 μm, a transition region 150 μm $\leq$ L $\geq$ 200 μm and the range with larger L. Constant value fitting was adopted to the range 50 μm $\leq$ L $\geq$ 150 μm to extract C_1 = 5240 Hz.m. This value is 6% larger than the calculated value.

The measured shape of the cantilevers in resonance, corresponding to the expected shape for a second order bending mode is presented in Fig. 6.6(a) and (b) with 50 μm and 300 μm functional lengths respectively. We ascribe the somewhat increased value of C_1 to the effect of the pyramid shape of the anchor of these cantilevers (Fig. 6.1(a)). It was observed that this causes a slight curvature over the width of the beam near the anchor, increasing the effective spring constant of the beam, which can be interpreted as an increased Young's modulus. The scatter of the value of $f_{res}L^2$ in this range may then be due to variation of the anchor shape, caused by local variations in the etching speed. We conclude that in this range the cantilevers oscillate in a pure bending mode. The appearance of the second order mode as the dominant resonance is presumably originating from the asymmetric clamping by the triangular substrate base. Since the cantilevers were very thin and flexible, higher order modes are easily excited and can absorb more of the energy supplied.

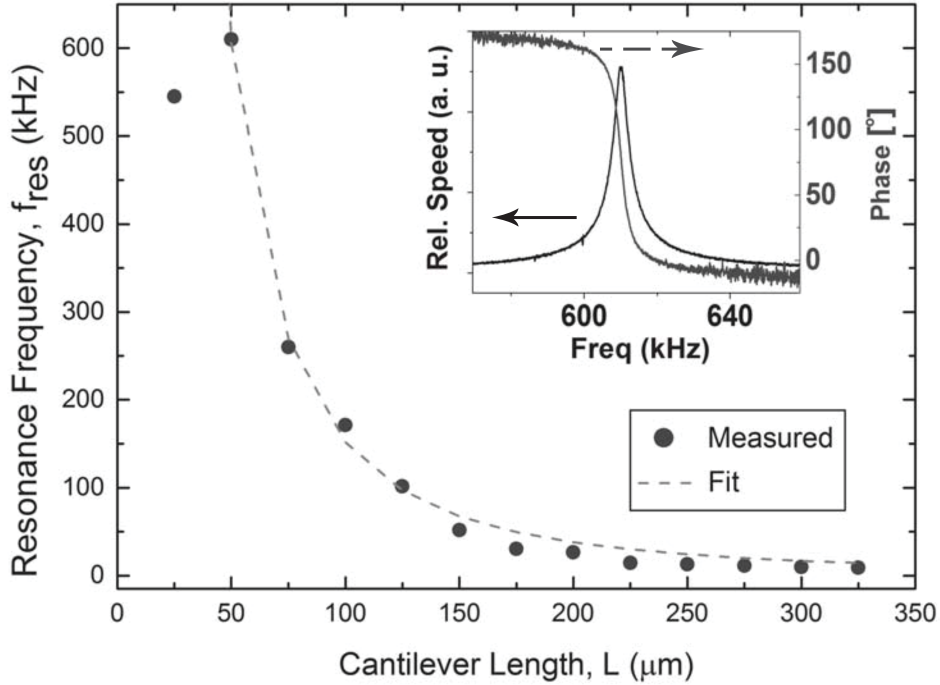

Figure 6.4: Measured dependence of the 2nd resonance frequency on the length of free-standing PZT-cantilevers with constant width of 50 μm , shown by symbols as measured using Doppler vibrometer. Broken line represent theoretical fitting to the measured data. The inset shows a representative relative speed and phase vs frequency spectrum obtained for a free standing epitaxial PZT cantilever (with both length and width of 50 μm).

For larger lengths the C_1 value drops significantly above 175 μm the cantilevers become progressively flexible and other resonances (which resemble torsional modes) were also observed. Fig. 6.6(b) shows the resonance profile of a 300 μm beam. This profile could not be fitted with a single bending mode and also not with a set of modes. This demonstrates the presence of mixed modes in longer freestanding cantilevers. For the shortest beam with aspect ratio L/W<1, the dominant mode was a vibrational mode over the width of the cantilever The influence of the beam length on the damping behavior of free standing cantilevers arising from intrinsic (material dependent) properties and from the operational medium is subject of further study.

6.4.2 Theoretical models to explain damping mechanisms

The damping factor (γ) of the resonance is equal to the inverse of the quality factor, determined by the ratio of the resonance frequency and its full width half maximum, Q=$\sqrt{3}f_{res}$/FWHM. The $\sqrt{3}$ factor arises when Q is determined from an amplitude-versus-frequency spectrum. The quality factor of the dominant second harmonic resonance-peak enhances with decreasing cantilever length as is seen in Fig. 6.7(a). γ, values of the dominant, second order bending mode determined in air, are shown in Fig. 6.7(b), as function of cantilever length. Fits to the two distinct linear regions with different slopes indicate a cross-over at about 175 μm length. The crossover corresponds also with the change in the value of f_{res}L^2, thus of the resonance frequency of the dominant mode As discussed above the cantilevers longer than about 175 μm become progressively flexible and higher order resonances are also observed, which absorb part of the available electrical energy and therefore apparently enhance the damping of the considered mode. Here we do not consider this regime any further. In Fig. 6.8 linear fits to the measured γ values in vacuum and in ambient conditions for the short cantilevers are shown.

At shorter lengths a linear dependence of damping on length is observed, both at low pressure as under ambient pressure. The damping is attributed to viscous damping by the air and due to internal friction within the cantilever body during vibration of the beam, hence the total damping is given by $\gamma = \gamma_{visc}+\gamma_{int}$. Following ref. [8] the viscous air damping of the cantilever can be expressed as, $\gamma_{visc.} = \beta_{visc.}/(\rho_c WLt\omega) = \beta_{visc.}/(m_c\omega)$. The friction coefficient $\beta_{visc.}$ is due to the frequency ($\omega = 2\pi f$) dependent frictional force $F_{visc}(w,x) = \beta_{visc.}(\omega)\nu(x)$, which is proportional to the velocity of the cantilever at length position x. At ambient pressure one can approximate the viscous force coefficient, due to air drag as -

$$\beta_{visc.} = 6\pi\mu_{air}(f_1W/2)(1+(\omega\tau_1)^{\frac{1}{2}}) \tag{6.2}$$

This formula was derived assuming that the moving beam can be approximated by a sphere (radius $f_1W/2$) oscillating in a viscous medium, where f_1 is a scaling parameter accounting for the difference between an oscillating beam and sphere. The frequency dependent part is due to a boundary layer perpendicular to the direction of motion, in which turbulent air motion takes place. From this follows (for the second order bending mode)

$$\gamma_{int} = \Big(\frac{2\sqrt{3}}{\alpha_2^2\sqrt{E\rho_c}}\Big)(3\pi\mu_{air}f_1)\frac{L}{t^2}\Big(1+(\frac{L_1}{L})\Big) = C_2\frac{\beta_1}{t^2}(L+L_1) \tag{6.3}$$

using eq.6.1 to rewrite frequency in terms of cantilever length. L_1 is a typical length related to the time constant τ_1, as $1/2\pi\tau_1 = C_1t/L_1^2$. Further, $C_2 = 2\sqrt{3}/\alpha_2^2\sqrt{E\rho_c} = 1/2\pi\rho_cC_1$ and $\beta_1 = 3\pi\mu_{air}f_1$.

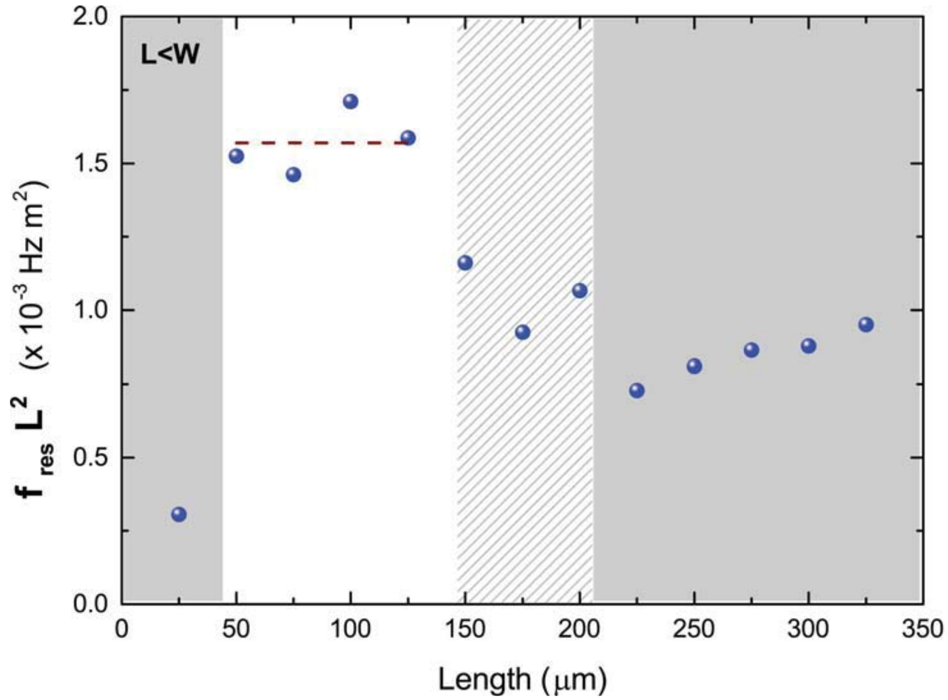

Figure 6.5: Measured variation of $f_{res}L^2$ as function of the length (L) for cantilevers with constant width W = 50μm and thickness t = 300 nm.. Different regions of the obtained values are shaded in the graph. Constant value (C_1t) fitting was applied to the data in the range L = 50 - 125μm (broken lines).

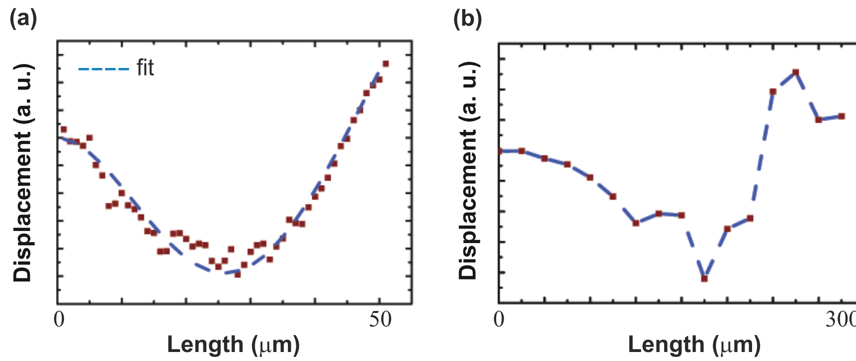

Figure 6.6: Displacement vs. length profile at resonance for representative cantilevers with L = 50 μm and L = 300 μm. While the broken line corresponding to the experimentally measured data points for 50 μm long cantilever in (a) represents theoretical fit for a second harmonic vibration, the line for for 300 μm long cantilever in (b) is guide to eye as it could not be fitted to any harmonic vibrational modes.

One would expect that the internal damping is due to mechanical friction as well as dielectric losses, which are both frequency dependent. For a nearly elastic material described with a single fractional visco-elastic damping element (the so-called fractional Zener model) one finds a mechanical damping parameter of the form $\gamma_m = E''/E' \approx \beta_m^{'}(\omega\tau)^{-m}$, where m can vary in the range $0 < m < 1$ and τ a material viscoelastic relaxation time [31]. Here E' and E'' are the real and imaginary parts of the complex Young's modulus. $\beta_m^{'}$ and m are parameters that are specific for the material. Dielectric loss is modeled by $\gamma_e = \beta_e^{'}\omega^{(n-1)}$, with n in the range $0 < n < 1$. n is generally much lower than 1 for frequencies lesser than the microwave range, which is the case for the mechanical vibrations considered here [32]. Summing these damping terms and rewriting as function of beam length, the total internal damping is obtained as -

$$\gamma_{int} = \gamma_m + \gamma_e = \beta_m^{'}\omega^{(-m)} + \beta_e^{'}\omega^{(n-1)} = \beta_m L^{2m} + \beta_e L^{-2(n-1)} \tag{6.4}$$

For m≪0 and $\omega\tau \gg 1$, which corresponds to materials with very large relaxation times (very high viscosity), i.e. with approximately linear elastic response, the mechanical losses become frequency independent and one can approximate eq.6.4 as

$$\gamma_{int} \approx \beta_m \Big(1 + (\beta_e/\beta_m)L^{2(1-n)}\Big) \tag{6.5}$$

Hence γ_{int} can also be written as

$$\gamma_{int} = \beta_m \Big(\Big(\frac{L}{L_0}\Big)^{(2-2n)} + 1\Big) = \beta_0(L + L_0) \tag{6.6}$$

where $L_0 = (\beta_m/\beta_e)^{1/(2-2n)}$. In vacuum the damping is due to internal damping only, thus from the experimental data suggesting a linear fit, one obtains $n \approx 1/2$, resulting in the last equality. The slope of the linear fit is set by the friction coefficient $\beta_0 = 2.96$ m^{-1} and from the offset $L_0 = 621$ μm, from which follows that the mechanical damping is $\gamma_m = \beta_m = \beta_0 m_0 = 0.00184$ and that the dielectric losses $\gamma_e = \beta_0 L = \beta_m(L/L_0)$ are much less than the mechanical losses for $L << L_0$.

The total damping in air is now given by -

$$\gamma = \gamma_{int.} + \gamma_{visc.} = \beta_0(L + L_0) + C_2\frac{\beta_1}{t^2}(L + L_1) \tag{6.7}$$

Fitting the data gives, $f_1 \approx 0.12$ (for $\mu_{air} = 1.81 \times 10^{-5}$ kg/(m.s)) and $L_1 \approx 0\mu$m when used as free fitting parameters. This indicates that the frequency dependent friction due to turbulent air motion at the edges of the cantilever is negligible compared to the viscous motion through the air. However we expect that with miniaturization of the cantilever (smaller width) the effect of the edges

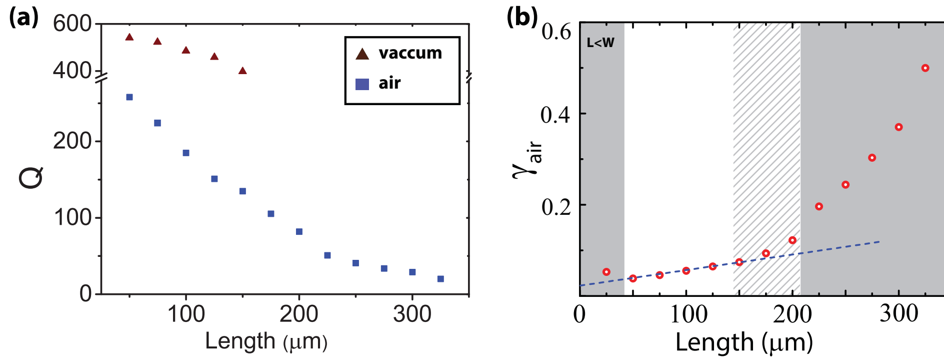

Figure 6.7: (a) Variation of Q-factor with cantilever length in air and in vacuum (10^{-4} mbar). (b) Ambient damping factor (γ_{air}) of free-standing heteroepitaxial cantilevers as function of length. Different regions of the cantilever length are shaded. The dotted line represents fit for measured γ values corresponding to cantilever lengths L = 50 - 125μm.

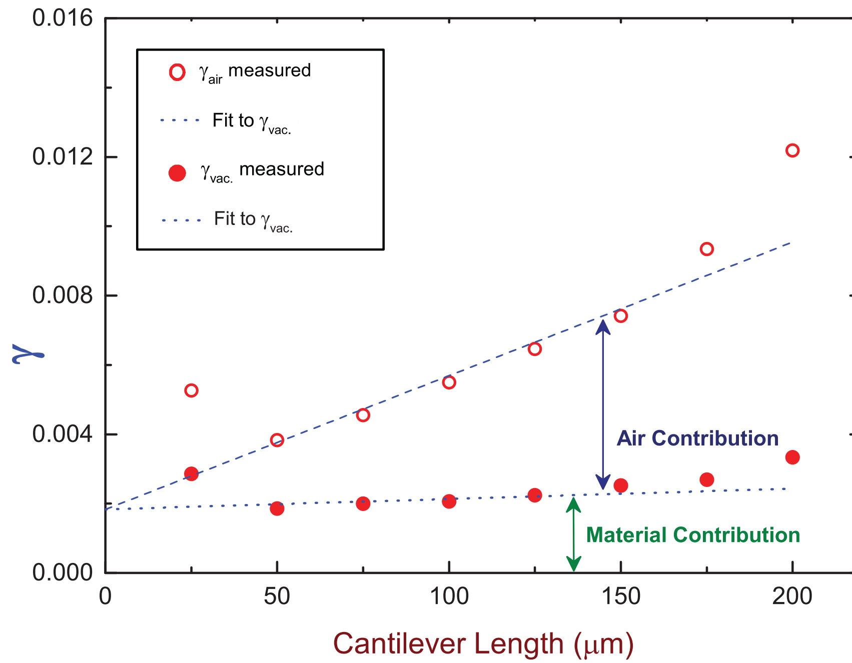

Figure 6.8: Variation of damping factor (γ) with cantilever length for free-standing PZT-cantilevers in air and in vacuum, 10^{-4} mbar. Broken lines represent linear fitting to the experimentally measured data(symbols). The inset shows variation of corresponding Q-factors.

may increase. The low value of the fitting parameter f_1 indicates that the flat cantilever experiences less viscous friction than a sphere with diameter W.

We conclude that the damping behavior of the freestanding cantilever can be described by the combined viscous damping of air and internal losses, which we have attributed to mechanical losses and dielectric losses. The internal damping is dominated by the frequency independent mechanical damping, whereas the air damping is dominated by frequency independent viscous flow, giving rise to a frequency dependent damping coefficient.

Taking the damping terms together one arrives at -

$$\gamma = (\beta_0 + \frac{C_2}{t^2}\beta_1)L + (\beta_0 L_0 + \frac{C_2}{t^2}\beta_1 L_1) \approx (\beta_0 + \frac{C_2}{t^2}\beta_1)L + \beta_0 L_0 \tag{6.8}$$

Minimization of the damping can be achieved by optimizing the cantilever dimensions under the restriction $L \geq W >> t$, thus increasing the cantilever thickness and decreasing its length (and width). This model does not pose any restrictions on the cantilever width.

The model does not describe the measured damping for the shortest cantilever with L = 25 μm and width W = 50 μm, for which γ increases above the model curves for the measurement in vacuum as well as in air. This is attributed to the violation of the condition $L \geq W$, so that also torsional modes can be excited, which absorb part of the input energy, thus increasing the damping of the bending mode.

Next to reduction of the lateral cantilever dimensions we expect that by improving the crystalline quality of the cantilever material one can reduce the total damping, thus reducing γ_m. It is likely that with increased crystalline quality also the dielectric losses will be reduced, since it is expected that these are largely related to the defects in the material (grain boundaries). The dependence of the damping on beam width, thickness and crystalline quality is subject of further study.

6.5 Conclusion

In conclusion, electromechanical properties of free-standing heteroepitaxial all-oxide piezo-MEMS cantilever devices, with PZT as active piezo layer was investigated. Devices with different functional lengths in the range of 25 - 325 μm, together with constant width of 50 μm and a total thinckness of 300 nm were fabricated. It was found that second order bending mode constituted the dominant resonance mode for devices with functional length in the range 50 - 125 μm with corresponding higher quality factor values. For longer free-standing cantilevers in the range of 150 - 325 μm other or multiple resonating modes were observed. In order to gain insight on energy loss mechanism, we have identified the contribution of the operation medium (air, extrinsic contribution) and the contribution of the constituent material (intrinsic contribution) on the cantilever damping. This was concluded by investigating the electromechanical response of the series of cantilevers in ambient and under vacuum conditions. An air-initiated viscous damping model together with consideration of internal friction inside the cantilever oxides was adopted in order to explain their electromechanical behavior. For cantilevers with length in the range 50 - 125 μm, the damping increases linearly with cantilever length, which is explained by the combined effect of air damping and intrinsic friction in the cantilever material. It is shown that for a given cantilever width, minimum damping is obtained for a cantilever with equal length. The developed model for the damping gives guidelines for optimizing the quality factor dependent properties of resonating cantilevers. Unlike traditional SOI - based cantilevers, freestanding cantilevers were without any Si-crystal at the backside which is an important step to achieve high mass sensitivities. This as well makes it possible to investigate the direct influence of the material parameters (like microstructure, crystalline quality and effect of epitaxial strain) on the electromechanical behavior of the cantilever systems, which is subject to future research.

Bibliography

[1] T. Y. Kwon, K. Eom, J. H. Park, D. S. Yoon, T. S. Kim, and H. L. Lee, "In situ real-time monitoring of biomolecular interactions based on resonating microcantilevers immersed in a viscous fluid," *Applied Physics Letters*, vol. 90, no. 22, pp. 223903–223903, 2007.

[2] A. Janshoff, H.-J. Galla, and C. Steinem, "Piezoelectric mass-sensing devices as biosensors - an alternative to optical biosensors?," *Angew. Chem. Int. Ed*, vol. 39, pp. 4004–4032, 2000.

[3] Y. Yang, C. Callegari, X. Feng, K. Ekinci, and M. Roukes, "Zeptogram-scale nanomechanical mass sensing," *Nano Letters*, vol. 6, no. 4, pp. 583–586, 2006.

[4] H. P. Lang, M. Hegner, and C. Gerber, "Cantilever array sensors," *Materials Today*, vol. 8, no. 4, pp. 30–36, 2005.

[5] G. Stemme, "Resonant silicon sensors," *Journal of Micromechanics and Microengineering*, vol. 1, no. 2, p. 113, 1991.

[6] M. Elwenspoek and H. V. Jansen, *Silicon Micromachining.* Cambridge University Press, Cambridge, UK, 2004.

[7] T. Thundat, P. Oden, and R. Warmack, "Microcantilever sensors," *Microscale Thermophysical Engineering*, vol. 1, no. 3, pp. 185–199, 1997.

[8] F. Blom, S. Bouwstra, M. Elwenspoek, and J. Fluitman, "Dependence of the quality factor of micromachined silicon beam resonators on pressure and geometry," *Journal of Vacuum Science and Technology B*, vol. 10, no. 1, pp. 19–26, 1992.

[9] P. Muralt, "PZT thin films for microsensors and actuators: Where do we stand?," *Ultrasonics, Ferroelectrics and Frequency Control, IEEE Transactions on*, vol. 47, no. 4, pp. 903–915, 2000.

[10] S. Trolier-McKinstry and P. Muralt, "Thin film piezoelectrics for MEMS," *Journal of Electroceramics*, vol. 12, no. 1-2, pp. 7–17, 2004.

[11] C. W. Wong, Y. Jeon, G. Barbastathis, and S.-G. Kim, "Analog tunable gratings driven by thin-film piezoelectric microelectromechanical actuators," *Applied Optics*, vol. 42, no. 4, pp. 621–626, 2003.

[12] W. Choi, Y. Jeon, J.-H. Jeong, R. Sood, and S.-G. Kim, "Energy harvesting MEMS device based on thin film piezoelectric cantilevers," *Journal of Electroceramics*, vol. 17, no. 2-4, pp. 543–548, 2006.

[13] Y. Lee, G. Lim, and W. Moon, “A self-excited micro cantilever biosensor actuated by PZT using the mass micro balancing technique,” *Sensors and Actuators A: Physical*, vol. 130, pp. 105–110, 2006.

[14] C. Niezrecki, D. Brei, S. Balakrishnan, and A. Moskalik, “Piezoelectric actuation: State of the art,” *The shock and vibration digest*, vol. 33, no. 4, pp. 269–280, 2001.

[15] S. Tadigadapa and K. Mateti, “Piezoelectric MEMS sensors: state-of-the-art and perspectives,” *Measurement Science and Technology*, vol. 20, no. 9, p. 092001, 2009.

[16] E. Cross, “Materials science: lead-free at last,” *Nature*, vol. 432, no. 7013, pp. 24–25, 2004.

[17] J. Lu, T. Ikehara, T. Kobayashi, R. Maeda, and T. Mihara, “Quality factor of micro cantilevers transduced by piezoelectric lead zirconate titanate film,” *Microsystem Technologies*, vol. 13, no. 11-12, pp. 1517–1522, 2007.

[18] B. Kim, M. A. Hopcroft, R. N. Candler, C. M. Jha, M. Agarwal, R. Melamud, S. A. Chandorkar, G. Yama, and T. W. Kenny, “Temperature dependence of quality factor in MEMS resonators,” *Microelectromechanical Systems, Journal of*, vol. 17, no. 3, pp. 755–766, 2008.

[19] A. W. McFarland, M. A. Poggi, L. A. Bottomley, and J. S. Colton, “Characterization of microcantilevers solely by frequency response acquisition,” *Journal of Micromechanics and Microengineering*, vol. 15, no. 4, p. 785, 2005.

[20] A. K. Huttel, G. A. Steele, B. Witkamp, M. Poot, L. P. Kouwenhoven, and H. S. van der Zant, “Carbon nanotubes as ultrahigh quality factor mechanical resonators,” *Nano Letters*, vol. 9, no. 7, pp. 2547–2552, 2009.

[21] W. E. Newell, “Miniaturization of tuning forks,” *Science*, vol. 161, no. 3848, pp. 1320–1326, 1968.

[22] J. Lu, T. Ikehara, Y. Zhang, R. Maeda, and T. Mihara, “Energy dissipation mechanisms in lead zirconate titanate thin film transduced micro cantilevers,” *Japanese Journal of Applied Physics*, vol. 45, no. 11R, p. 8795, 2006.

[23] S. Schmid, K. Jensen, K. Nielsen, and A. Boisen, “Damping mechanisms in high-q micro and nanomechanical string resonators,” *Physical Review B*, vol. 84, no. 16, p. 165307, 2011.

[24] J. Lu, T. Ikehara, Y. Zhang, T. Mihara, T. Itoh, and R. Maeda, “High quality factor silicon cantilever transduced by piezoelectric lead zirconate titanate film for mass sensing applications,” *Japanese Journal of Applied Physics*, vol. 46, no. 12R, p. 7643, 2007.

[25] J. Yang, T. Ono, and M. Esashi, "Energy dissipation in submicrometer thick single-crystal silicon cantilevers," *Microelectromechanical Systems, Journal of*, vol. 11, no. 6, pp. 775–783, 2002.

[26] M. D. Nguyen, H. Nazeer, K. Karakaya, S. Pham, R. Steenwelle, M. Dekkers, L. Abelmann, D. Blank, and G. Rijnders, "Characterization of epitaxial $Pb(Zr,Ti)O_3$ thin films deposited by pulsed laser deposition on silicon cantilevers," *Journal of Micromechanics and Microengineering*, vol. 20, no. 8, p. 085022, 2010.

[27] W. Weaver Jr, S. P. Timoshenko, and D. H. Young, *Vibration problems in engineering.* John Wiley & Sons, 1990.

[28] C. Lee, T. Itoh, and T. Suga, "Micromachined piezoelectric force sensors based on PZT thin films," *Ultrasonics, Ferroelectrics and Frequency Control, IEEE Transactions on*, vol. 43, no. 4, pp. 553–559, 1996.

[29] K. Ekinci, Y. Yang, and M. Roukes, "Ultimate limits to inertial mass sensing based upon nanoelectromechanical systems," *Journal of Applied Physics*, vol. 95, no. 5, pp. 2682–2689, 2004.

[30] N. Banerjee, G. Koster, and G. Rijnders, "Submicron patterning of epitaxial $PbZr_{0.52}Ti_{0.48}O_3$ heterostructures," *Applied Physics Letters*, vol. 102, no. 14, pp. 142909–142909, 2013.

[31] J. Bartkowska and J. Ilczuk, "The internal friction and the relaxation time spectrum of ferroelectric ceramic PZT type," *Acta Phys. Pol.*, vol. 114, no. 6-A, pp. A–7 – A–13, 2008.

[32] A. Tagantsev, *Encyclopedia of Materials: Science and Technology, Chapter: Degradation and Dielectric Loss mechanisms in Dielectric Films.* Elsevier Science Ltd., 2001.

CHAPTER 7

Future Possibilities of Lift-off Patterning for Oxide-Electronics

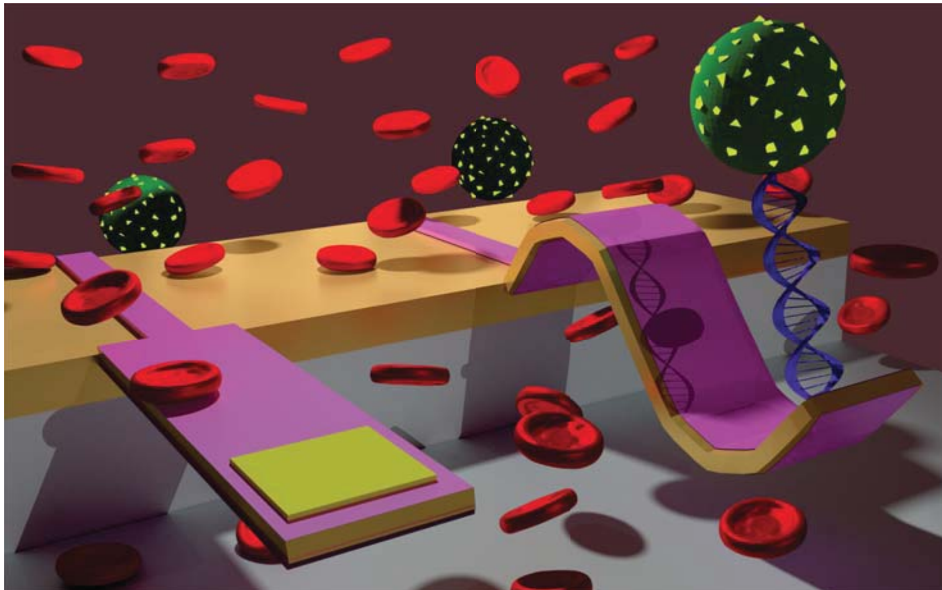

ABSTRACT

In the previous chapters we have described the development of the lift-off fabrication pathway, suitable for patterning thin films of high temperature grown materials, specially epitaxial complex perovskite oxides. In contrast to the traditional top-down structuring, the epitaxial lift-off patterning approach utilizes a structured sacrificial mask of a high temperature stable amorphous oxide and the perovskite films are patterned directly during their growth. Since the fabrication process does not require any physical ion-etching step, it was shown to be able of structuring the conducting $LaAlO_3$*-*$SrTiO_3$*(001) interface without inducing any substrate conductivity, while preserving the high quality interfacial transport properties. Heteroepitaxial multilayer perovskite oxide devices, with sizes both in micro and nano-dimension were fabricated utilizing the epitaxial lift-off patterning pathway, without the need of separately structuring the individual perovskite layers.*

In the final chapter of this thesis, we highlight some future directions that are enabled by the epitaxial lift-off patterning strategy. We show some preliminary results achieved utilizing the fabrication technique such as the patterning of the $SrCuO_2$*-*$LaAlO_3$*-*$SrTiO_3$*(001) interface containing high mobility carriers. Interestingly, some novel properties were observed in these structured interface-devices, including carrier mobilities up to* $\sim$ *70,000* $cm^2 V^{-1} s^{-1}$ *and positive magnetoresistance values up to* $\sim$ *800 % at 2 K, possibly originating from the structural confinement.*

Here we also demonstrate the opportunities of the lift-off patterning pathway from the application perspective by showing that the epitaxial freestanding piezo-MEMS cantilever devices, as described in Chapter 5, are capable of functioning as very high-sensitivity mass sensors. A patterned top-layer of gold was added to the cantilevers for estimating their mass sensitivity. They also can be utilized for quantitative sensing of biological molecules and microbes via gold-thiol binder coordina-

tion. Further research work is recommended to investigate the effect of dimensional confinement on magnetotransport properties and on quantum phenomena (like Shubnikov-deHaas oscillations) in high-mobility oxide devices as well as to implement the high sensitive freestanding piezo-MEMS devices for faster bio-sensing.

7.1 Introduction

This thesis demonstrates the development of a lift-off fabrication technology for micro and nano-scale patterning of high temperature grown complex perovskite oxides. While the traditional patterning processes require selective area etching (physical or chemical) of unstructured oxide films, the developed lift-off fabrication strategy utilizes a high temperature stable sacrificial oxide mask and thus is capable of structuring heteroepitaxial multiple layers simultaneously in a single lift-off process. We have demonstrated that unlike the high energetic ion mediated dry etching technology, which can potentially damage the single crystal $SrTiO_3$(001) substrate [1, 2], the lift-off patterning can precisely structure the conducting interface between $LaAlO_3$ and $SrTiO_3$(001) while preserving the high quality interfacial properties and without damaging the delicate substrate crystal [3]. The fabrication pathway is especially advantageous for patterning the entire heteroepitaxial perovskite multilayer assembly into the desired device configuration [4], as it is often found that the physical and chemical nature of the individual constituent oxide layers are very different from each other, hindering implementation of a combined etching pathway. In addition to the micro-scale patterning, we have extended the lift-off patterning strategy to the nano-fabrication by modifying the pathway to be integrated with traditional electron beam lithographic process. It is also shown that the underlying domain-configuration and domain-distribution of the epitaxial ferroelectric nano-structures, when fabricated by lift-off technology, can be quite different from analogous structures prepared by 'top-down' etching processes.

From developing a suitable structuring strategy for heteroepitaxial perovskite micro and nano-structures, we went on to fabricate all-oxide freestanding piezo-MEMS (micro electro mechanical systems) devices utilizing the developed lift-off patterning pathway. The key motivation for fabricating such freestanding cantilever piezo-MEMS devices is to achieve very high mass sensitivity, enabled by the reduction in the cantilever thickness. Another important parameter is the vibrational quality factor of the devices in order to achieve high sensitivity. In this respect we have investigated a series of all-oxide freestanding cantilever piezo-MEMS devices, with varying length and in different operational conditions, in order

to understand the influence of different intrinsic (material and microstructure) and extrinsic (operational medium) parameters in the vibrational damping mechanism.

Many functional micro and nano devices incorporate high temperature grown materials, especially complex perovskite oxides, as a key component. Some popular examples are ferroelectric-RAMs, piezoelectric sensor/actuator/transducers, oxide-photovoltaic devices, oxide-spintronic devices, etc. In the majority of these devices, the single/multilayer perovskite film should be precisely patterned, both for functional operation and for integration with other device-parts. In the final chapter of this thesis we extend our work towards the fabrication of more complex device systems, utilizing the lift-off pathway, for the investigation of fundamental physics and the application purposes. Our results prove that the lift-off patterning is a suitable choice to fabricate devices incorporating delicate epitaxial oxide interface with unprecedented carrier mobility and very high magnetoresistance values as well as to generate piezodriven all-oxide MEMS devices with high mass-sensitivity, which can be utilized for bio-detection, as is described below.

7.2 Patterned High Mobility $SrCuO_2$-$LaAlO_3$ -$SrTiO_3$(001) Hetero-Interfaces

Recently it has been shown that by incorporating a nano-layer of strontium copper oxide ($SrCuO_2$, SCO) it is possible to reduce the impurity scattering at the conducting interfaces in $LaAlO_3$-$SrTiO_3$(001) heterostructures [5], and hence to promote higher carrier mobilities. The proposed mechanism suggests that the cuprate layer reduces the kinetic barrier for the oxygen exchange in the heteroepitaxial system, and thus suppresses the creation of oxygen vacancies. This phenomenon of enhanced surface oxygen exchange promoted by the incorporation of the SCO layer in the LAO-STO system is schematically represented in Fig. 7.1. Studies of the transport properties of $SrTiO_3$ capped SCO-LAO-STO(001) heteroepitaxial system have shown that mobility values as high as $\sim$ 50,000 $cm^2V^{-1}s^{-2}$ can be attained in unstructured films [5]. High mobility systems are especially interesting from the perspective of fundamental physics as they can exhibit quantum phenomena such as Shubnikov-deHaas (SdH) oscillations. Further research work has proved that the SCO-LAO-STO(001) heterointerface shows signatures of SdH oscillations when subjected to high magnetic fields [6]. In order to utilize this exciting high mobility interface into working devices, precise patterning without damaging the substrate $SrTiO_3$ crystal is an essential step. Moreover the dimensional restriction as induced by the patterns can lead to interesting novel functional behaviors.

In *Chapter 2* of this thesis we have shown that the epitaxial lift-off patterning strategy can fabricate precise devices incorporating heteroepitaxial $LaAlO_3$-$SrTiO_3$(001) interfaces while preserving the interfacial properties. The fabrication process utilizes a patterned sacrificial AlO_x layer as the high temperature resistant lift-off mask and does not require any physical ion-etching, thus minimizes the risk of inducing substrate conductivity or magnetism [1, 2]. Here we demonstrate that the patterning pathway can be extended to fabricate devices incorporating SCO-LAO-STO(001) heterointerfaces with higher carrier mobilities while preserving the high quality interfacial properties. The Hall-bar devices were prepared following a fabrication process which was similar to that described in the *Chapter 2*. Atomically smooth vicinal steps were observed by AFM in the substrate areas not covered by the mask layer (see *Chapter 2*, Fig. 2.2). This enabled the monitoring of the layer by layer perovskite growth utilizing the RHEED technique. Laser ablation parameters and the individual perovskite layer thicknesses were kept identical to that of unstructured films as reported by Huijben et. al [5].

The temperature dependent magnetotransport properties of the patterned Hall-bar devices, incorporating a heteroepitaxial $SrTiO_3$ capped $SrCuO_2$-$LaAlO_3$-$SrTiO_3$(001) interface, are shown in Fig. 7.2 (a)-(d). (a) Shows the temperature dependence of the sheet resistance without and in presence (9 Tesla) of external

magnetic fields for two different devices having different Hall-bar lengths (represented by Device1 with length 50 μm and Device2 with length 100 μm). Although small variation in the electrotransport behavior can be noticed between the measured devices, located at different regions of the substrate (dimension $\sim 5 \times 5$ mm^2), the overall transport characteristics are comparable. The initial higher resistance values, which disappear upon cooling, are presumably due to the presence of atmospheric water in the measurement set-up. As can be seen in Fig. 7.2(a), a positive magnetoresistance is observed in structured SCO-LAO-STO interface devices in contrast to generally observed negative magnetoresistance in LAO-$SrTiO_3$ interfaces [3].

The dependence of the hall resistance on the applied magnetic field, measured from a structured Hall-bar device at 2K is presented in the inset of Fig. 7.2(b). Although the Hall-characteristic is mostly linear, an anomalous region with higher slope can be noticed in the magnetic field range $\pm$ 1 T, suggesting a deviation from the single band model. However, the Hall-mobility (μ_H) is calculated with the single band model in the region $\geq$ 1 T and the variation of μ_H with the temperature is shown in Fig. 7.2(b). A carrier mobility (μ_H) of $\sim$ 70,000 cm^{2}V^{-1}s^{-1} was achieved at 2 K with a corresponding room-temperature value of $\sim$ 40 cm^{2}V^{-1}s^{-1}. The associated sheet carrier density [n_S] was found to exhibit a constant value of $\sim 4 \times 10^{13}$ cm^{-2}, in the measured temperature range. Fig. 7.2(c) presents the normalized magnetoresistance [$R_s(H) = R_s(H)/R_s(0) \times 100$] as a function of the applied magnetic field, measured at different temperatures. A highest value of $\sim$ 800% was obtained at 2 K with a magnetic field of 8 T which is considerably higher as compared to conventional $LaAlO_3$-$SrTiO_3$(001) heteroepitaxial devices [3]. The observation of enhanced carrier mobility values as compared to the unstructured films and very high positive magnetoresistance is presumably originating from the structural confinement of the heterostructures in the patterned devices. The signature of a SdH oscillation is also measured at 2 K, as presented in Fig. 7.2(d). It may be required to perform the measurements at even lower temperatures and with application of higher magnetic fields in order to measure more prominent SdH oscillations.

These results demonstrate that the heteroepitaxial $SrCuO_2$-$LaAlO_3$-$SrTiO_3$(001) interface with higher carrier mobilities enabled by enhanced surface oxygen exchange can be patterned in a suitable device geometry, while preserving their high quality interfacial electro and magneto transport properties. Since the patterning procedure does not involve any physical ion etching, it possesses minimal chance of damaging the underlying single crystal $SrTiO_3$ substrate. These initial results open up future possibilities for investigating low-dimensional quantum confinement effects facilitated by patterned devices incorporating the high mobility heteroepitaxial perovskite interfaces.

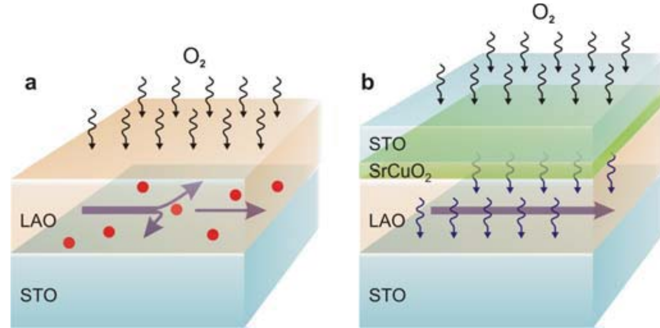

Figure 7.1: A schematic representation of enhanced oxygen incorporation in $SrCuO_2$-$LaAlO_3$-$SrTiO_3$(001) heterostructures(b) in comparison to conventional LAO-STO interface(a) (reprinted with permission from [5]), copyright 2013, WILEY-VCH.

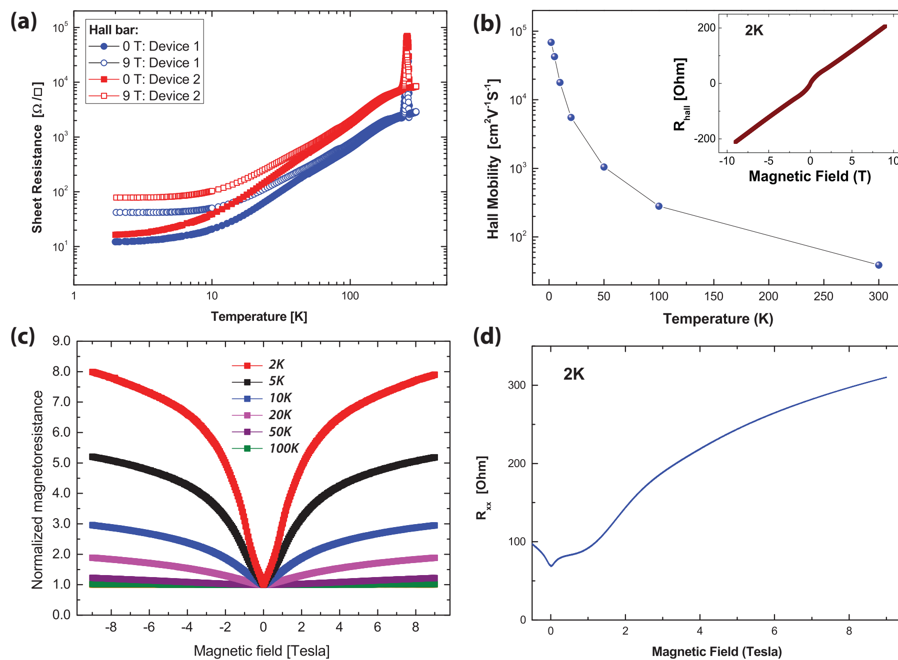

Figure 7.2: Transport properties of structured $SrCuO_2$-$LaAlO_3$-$SrTiO_3$(001) hetero-interfaces. (a) Temperature dependence of the sheet resistance at different magnetic fields (0 and 9 Tesla) for two different devices (shown as Device1 and Device2).(b) Temperature dependence of the Hall-mobility. The variation of the Hall-resistance with magnetic field at 2 K is shown in the inset. (c) Magnetoresistance (normalized) as a function of the magnetic field, measured at different temperatures. (d) Variation of the linear resistance (R_{xx}) as functional of the magnetic field at 2 K showing signature of the SdH oscillations.

7.3 Epitaxial freestanding Piezo-MEMS Devices as quantitative Mass-sensor and Bio-detectors

High sensitivity sensors are an essential part of modern technology and are employed for a wide range of purposes. Piezoelectric materials posses many promising advantages like faster response time and low power consumption which can be utilized in traditional sensor devices to make them faster and more efficient. In *Chapter 5* we have described a novel fabrication pathway to prepare all-oxide, epitaxial, freestanding piezo-MEMS with $PbZr_{0.52}Ti_{0.48}O_3$as the key functional material. A detailed account of their resonating characteristics and damping behavior is also presented in *Chapter 6*. Here we take our fabrication pathway one step forward by incorporating an area of gold (Au) on the freestanding cantilevers and demonstrate their sensing capabilities via measuring the resonance behavior.

The freestanding cantilevers are prepared following a fabrication pathway similar to that described in *Chapter 5*. The patterned Au top-layer was incorporated after patterning of the top-$SrRuO_3$ layer on PZT. This required a second lithographic alignment step followed by deposition of Au, utilizing electron beam evaporation. The precise thickness of the Au-layer was measured and monitored utilizing a quartz-crystal oscillator. To estimate the precise mass sensitivity, cantilevers with and without (reference cantilevers) Au-layer are fabricated side by side as can be seen in Fig. 7.3(a), in order to minimize any effect originating from the processing conditions.

The vibrational resonance characteristics triggered by the external actuating voltages of two adjacent cantilevers with and without the Au top layer are presented in Fig. 7.3(b). As expected, the resonance peak corresponding to the 2nd harmonic resonating excitation can be seen to be shifted to the lower frequency region. A resonance frequency (δf) difference of 6.1 kHz was measured between the cantilevers with and without 50 nm extra top Au-layer [Fig. 7.3(b)]. Considering the density of Au as $19.3 \times 10^3 kg/m^3$ the mass sensitivity ($S_m = \delta f/\delta m$) of the free-standing PZT cantilever is obtained as 4 Hz/fg. The sensitivity is considerably higher than that reported for traditional SOI-mediated cantilevers $\sim$ Hz/pg [7], which is presumably originating from the low sensor mass and/or the second order bending mode as the dominant resonance with higher quality factor values.

Incorporating the gold layer on the top of the freestanding cantilevers gives the possibility to attach organic thiols to the gold layer. These organic thiol molecules can be designed to contain binding groups on the other side, which can co-ordinate to biological molecules like proteins, nucleotides and antibodies [8]. Hence the next step towards utilizing the fabricated high-sensitivity, freestanding, all-oxide, epitaxial cantilevers would be their implementation to detect chemical and biological entities in ambient conditions and under liquid environment.

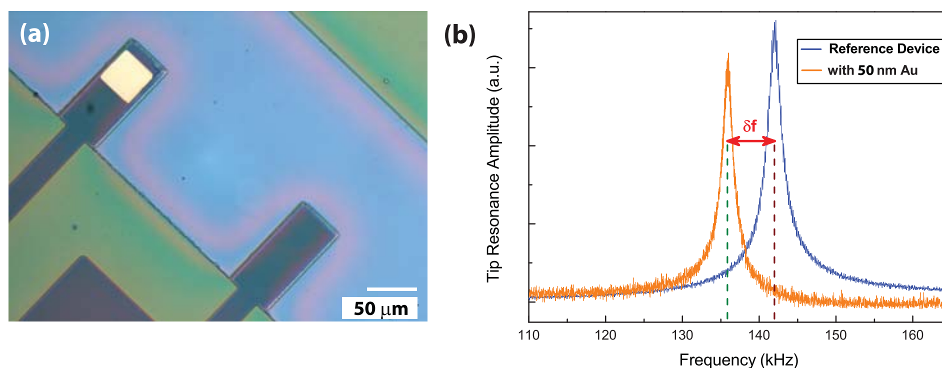

Figure 7.3: (a) Optical microscopic images of two adjacent cantilever devices with and without gold layer (before substrate-etching). (b) Frequency spectrum showing the frequency shift for the second harmonic resonance vibration, measured from the devices in (a) with and without the Au-layer, after their release from the substrate.

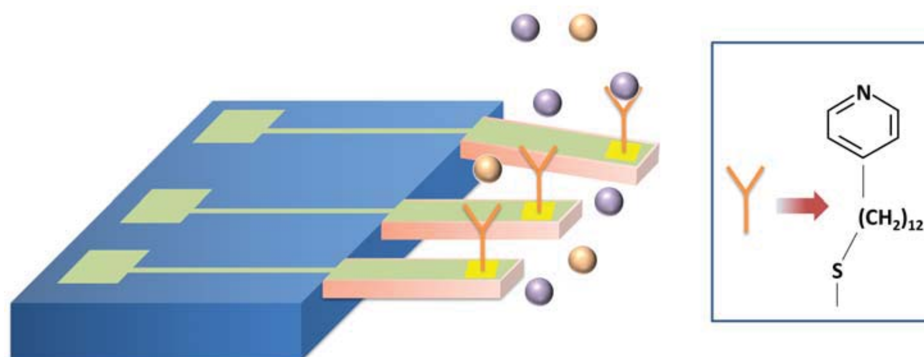

Figure 7.4: Artistic representation of the resonating cantilver sensors capable of detecting with the help of gold-thiol layers on top.

A piezo-MEMS device capable of such sensing behavior can be termed as 'electronic nose' and is artistically shown in figure 7.4.

7.4 Conclusion

To conclude, we have demonstrated that the epitaxial lift-off patterning strategy for high temperature grown complex perovskite oxide patterns is of suitable choice to fabricate micro and nano devices, even when incorporating delicate epitaxial interface such as $SrCuO_2$-$LaAlO_3$-$SrTiO_3$(001), in order study for example the effect of structural confinement on magnetotransport properties. In the initial studies involving the structured SCO-LAO-STO interface devices few interesting phenomena such as very high carrier mobilities upto $\sim$ 70,000 $cm^2V^{-1}s^{-1}$ and positive magnetoresistance values upto $\sim$ 800 % at 2 K were measured which was not observed in case of unstructured full-films. The patterning pathway opens up new possibilities to investigate the occurrence of fundamental quantum phenomena in such high carrier mobility systems as well as to integrate these hetero-interfacial devices with other functional components. From the view-point of functional application of oxide devices, we also establish in this chapter that the freestanding piezo-MEMS devices which are fabricated via a lift-off patterning mediated pathway are capable of working as a very high sensitive mass sensor. The demonstrated fabrication involving the patterned gold top layer facilitates the oppertunities to utilize these devices for biosensing purposes. Although the epitaxial lift-off structuring pathway can be utilized to fabricate wide range of devices involving complex perovskite oxides, these two investigated specific research directions establish the patterning procedure suitable and effective for complex fabrication processes.

Bibliography

[1] D. W. Reagor and V. Y. Butko, “Highly conductive nanolayers on strontium titanate produced by preferential ion-beam etching,” *Nature Materials*, vol. 4, no. 8, pp. 593–596, 2005.

[2] W. Rice, P. Ambwani, M. Bombeck, J. Thompson, G. Haugstad, C. Leighton, and S. Crooker, “Persistent optically induced magnetism in oxygen-deficient strontium titanate,” *Nature Materials*, 2014.

[3] N. Banerjee, M. Huijben, G. Koster, and G. Rijnders, “Direct patterning of functional interfaces in oxide heterostructures,” *Applied Physics Letters*, vol. 100, no. 4, p. 041601, 2012.

[4] N. Banerjee, G. Koster, and G. Rijnders, “Submicron patterning of epitaxial $PbZr_{0.52}Ti_{0.48}O_3$ heterostructures,” *Applied Physics Letters*, vol. 102, no. 14, pp. 142909–142909, 2013.

[5] M. Huijben, G. Koster, M. K. Kruize, S. Wenderich, J. Verbeeck, S. Bals, E. Slooten, B. Shi, H. J. Molegraaf, J. E. Kleibeuker, *et al.*, “Defect engineering in oxide heterostructures by enhanced oxygen surface exchange,” *Advanced Functional Materials*, vol. 23, no. 42, pp. 5240–5248, 2013.

[6] A. McCollam, S. Wenderich, M. Kruize, V. Guduru, H. Molegraaf, M. Huijben, G. Koster, D. Blank, G. Rijnders, A. Brinkman, *et al.*, “Quantum oscillations and subband properties of the two-dimensional electron gas at the $LaAlO_3/SrTiO_3$ interface,” *APL Materials*, vol. 2, no. 2, p. 022102, 2014.

[7] D. Isarakorn, D. Briand, A. Sambri, S. Gariglio, J.-M. Triscone, F. Guy, J. Reiner, C. Ahn, and N. De Rooij, “Finite element analysis and experiments on a silicon membrane actuated by an epitaxial PZT thin film for localized-mass sensing applications,” *Sensors and Actuators B: Chemical*, vol. 153, no. 1, pp. 54–63, 2011.

[8] J. Tamayo, P. M. Kosaka, J. J. Ruz, Á. San Paulo, and M. Calleja, “Biosensors based on nanomechanical systems,” *Chemical Society Reviews*, vol. 42, no. 3, pp. 1287–1311, 2013.

Summary

Perovskite oxides constitute a fascinating class of materials owing to their diverse functional properties, while retaining similar inherent crystal structures. The wide range of functionalities manifested by different perovskite oxides extend from insulating to superconducting, from non-magnetic to ferromagnetic, and from dielectric to ferroelectric - making them an extremely interesting and promising class of functional materials, both for fundamental understanding and for commercial applications. Also, the well-defined crystal structure of the perovskites gives the opportunity to understand and manipulate their functional behavior by tuning lattice, orbital and/or spin degrees of freedom. This is experimentally realized by artificially creating different well-ordered atomic stacks, termed *perovskite epitaxial heterostructures*, which often display remarkable functional properties different from any of its individual constituents. In previous research on perovskite materials, much attention has been devoted to achieve novel and/or enhanced functional properties by engineering the constituents and their strain state in such systems. But in order to utilize these fascinating functional properties in commercial devices, precise patterning of these stable oxide materials into the desired geometry and their integration with traditional Si-based electronics and fabrication technology is essential. In general perovskite oxides are very stable materials with respect to different physical and/or chemical etching processes. Therefore the fabrication of their highly precise structures is a challenging task, especially when fabricating epitaxial oxide mutlilayer devices. Moreover, in accordance with the current era of electronic miniaturization, the size of these devices also needs to be in the nano-scale, requiring suitable nano-patterning approaches. In this thesis a novel, lift-off mediated fabrication pathway has been developed to fabricate precise micro and nano-structures of these high temperature grown complex oxide materials.

The fabrication process utilizes a layer of high temperature stable amorphous oxide (AlO_x) as the sacrificial template mask. The mask layer is deposited on the substrate using pulsed laser ablation and structured utilizing conventional photolithographic process.The advantage of this sacrificial mask is that it can be developed in precise structures employing mild basic solutions like a standard photolithographic developer solution, and can also be lifted off after the high

temperature deposition, using a basic solution, without affecting the perovskite properties. In order to demonstrate that this epitaxial lift-off fabrication strategy can structure delicate hetero-structures, we have chosen $LaAlO_3$-$SrTiO_3$ hetero-interface as model system. It was shown in recent times that the interface between $LaAlO_3$ and $SrTiO_3$ (001), both being wide band-gap insulators individually, can posses a 2-dimensional electron gas (2DEG) when deposited under appropriate conditions. In addition to the conductivity, the interface was found to display magnetism and superconductivity giving rise to the promise of its utilization in future multifunctional electronic devices like a high mobility electron transistor (HMET). The traditional fabrication pathways utilizing physical ion-etching processes are not suitable for incorporating such functional interfaces into device structures as they damage the substrate (STO) crystal inducing conductivity and even magnetism. We have employed the epitaxial lift-off patterning approach to fabricate $LaAlO_3$-$SrTiO_3$ heteroepitaxial devices without using any physical etching process. We have performed detailed studies of the temperature dependent magnetotransport properties on the patterned heterostructures with variable thickness of the $LaAlO_3$ layer and compared to analogous unstructured thin film samples. The results obtained from temperature dependent magnetotransport measurements demonstrate the conservation of the high-quality interface properties in the patterned structures, very similar to their unstructured analogues. The development of this lift-off patterning strategy for the preparation of high-quality interfacial devices, will help enable future studies of the effect of low-dimensional confinement on high mobility interface conductivity, as well as on interface magnetism.

As next step in our studies we have shown that the lift-off fabrication strategy is not only suitable for structuring a single epitaxial perovskite oxide thin film into the desired device geometry, but is also capable of simultaneously patterning multilayer heterostructures while preserving their functional behavior. As discussed above, epitaxial multilayer and superlattices are highly valued as electronic materials because of their often exhibited superior functional properties in comparison to the individual constituents, but are difficult to pattern due to their different physical and chemical nature. We have demonstrated that the high temperature grown multilayer stack of $SrRuO_3/PbZr_{0.52}Ti_{0.48}O_3/SrRuO_3$ can be patterned utilizing the epitaxial lift-off pathway, without the need of structuring each perovskite layer individually. The ferroelectric properties of the lift-off patterned epitaxial PZT heterostructures, grown on $SrTiO_3$(001) as well as on commercial platinized Si substrates, were investigated and compared with analogous structures fabricated by traditional multiple etching steps (comprising both dry and wet-etching processes) and established that the lift-off patterning approach preserves the functional behaviors of perovskite heterostructures.

Along with the micro-scale structures fabricated by conventional photolithographic processing, the lift-off patterning technique was extended to the nano-scale by integrating the fabrication strategy with an electron-beam lithographic (eBL) process. The advantage of using eBL as the primary lithographic technique to structure the template AlO_x mask is it's design flexibility and very high resolution. The fabrication pathway was modified by inserting a thin metallic layer to prevent the charging-effect arising from the insulating sacrificial mask layer. An improvement of this modified patterning strategy is also demonstrated here without utilizing any physical-ion etching process to pattern the metallic layer. PZT nano-structures, with dimensions down to 100 nm were fabricated using this pathway. Piezoresponse force microscopic (PFM) investigations revealed that the fabricated structures were individually addressable, preserved ferroelectric response and were separately switchable without any noticeable cross-talk. Reciprocal space maps (RSM) of the fabricated structures revealed the existence of extended c-domains below dimension of 200 nm, which can potentially give hints for the understanding of the ferroelectric size effect. The extension of the lift-off patterning approach to fabricate the epitaxial nano-structures can enable achieving very high device density to realize compact, faster and multifunctional electronics.

In addition to the development of the lift-off approach for micro and nano-patterning of the epitaxial perovskite heterostructures, we have also demonstrated the fabrication of practical devices in this thesis. The coupling between mechanical and electrical properties in piezoelectric materials has been traditionally employed for both sensing and actuation purposes. One such vital application is the piezo-mass sensor, with a piezoelectric driven cantilever as the most popular device configuration. Although free-standing epitaxial piezo-cantilever devices are promising to achieve very high sensitivity, experimental realization of such device-systems have been hampered because of difficulties in their fabrication, specially when epitaxial oxides are the key functional materials. Employing the developed lift-off patterning technique, piezodriven all-oxide epitaxial free-standing micro electro mechanical systems (MEMS) were fabricated on Si-substrates. The special advantage of the lift-off approach is that it offers an one-step patterning of the entire oxide multilayer heterostructure with simultaneous access to the underlying Si(001) substrate, which can be etched to release the cantilever devices. Hence, the employment of the lift-off patterning approach enables the fabrication of freestanding epitaxial piezo-MEMS devices in fewer processing steps. As Si wafers were utilized as the substrate, the fabricated MEMS devices were devoid of any silicon crystal on the backside of the cantilever, unlike traditional silicon on insulator (SOI) based cantilevers. In order to investigate the electromechanical response of such freestanding devices Doppler vibrometry was employed. All devices were found to exhibit resonant vibration when actuated by an external AC drive bias. The second order bending mode was found to form the dominant resonance mode for cantilevers with

a functional length in the range of 50 - 125 μm. For longer free-standing cantilevers other or multiple resonating modes were found to be present. We have identified the contribution of the operational medium (air, extrinsic contribution) and the contribution of the constituent material (intrinsic contribution) to the vibrational damping of the device by investigating the electromechanical response of a series of cantilevers in ambient and under vacuum conditions. A model has been proposed to explain the variation of the damping on the length of the cantilever by taking in account the combined effect of air damping and intrinsic friction in the cantilever material.

In the final part of the thesis, we highlight some future directions that are enabled by the epitaxial lift-off patterning strategy, and present some preliminary results achieved utilizing this fabrication technique. As an example, the patterning of the heteroepitaxial $SrCuO_2$-$LaAlO_3$-$SrTiO_3$(001) interface, containing high mobility carriers, is demonstrated. The structured device incorporating the delicate interface was found to preserve the high quality transport properties previously observed only in unstructured films. Interestingly, some novel properties were also observed in these structured interface-devices, including carrier mobilities up to $\sim$ 70,000 $cm^2V^{-1}s^{-1}$ and positive magnetoresistance values upto $\sim$ 800 % at 2K, possibly originating from the structural confinement. As another example of the possibilities of the lift-off patterning pathway, more from an application perspective, we demonstrated that the epitaxial freestanding piezo-MEMS cantilevers are capable of functioning as very high-sensitivity mass sensors. A patterned top-layer of gold was added to the device for estimating its mass sensitivity. This layer also makes it possible of utilizing them for quantitative sensing of biological molecules and microbes via gold-thiol-binder coordination. These initial results open the doorway for further future investigations on the effect of dimensional confinement on magnetotransport properties and on quantum phenomena (like Shubnikov-deHaas oscillations) in high-mobility oxide devices as well as to implement the high sensitive freestanding piezo-MEMS devices for faster bio-sensing.

Samenvatting

Perovskieten vormen binnen de oxides een fascinerende materiaalklasse vanwege hun verscheidenheid aan functionele eigenschappen en behoud van vergelijkbare kristalstructuren. Deze verscheidenheid aan functionaliteiten van de verschillende perovskieten varieert van isolerend tot supergeleidend, van niet-magnetisch tot ferromagnetisch en van diëlektrisch tot ferro-elektrisch. Dit maakt deze materiaalklasse erg interessant en veelbelovend, zowel voor fundamenteel onderzoek als voor commerciële toepassingen. Vanwege hun goed gedefinieerde kristalstructuur kunnen de functionele eigenschappen van deze perovskieten bovendien beïnvloedt worden door manipulatie van het rooster, de orbitalen en/of de spin toestanden. Dit is experimenteel gerealiseerd door het maken van verschillende geordende atomaire stapelingen, die epitaxiale perovskiet heterostructuren worden genoemd. Vaak leidt dit tot opmerkelijke functionele eigenschappen die verschillen van elk van de individuele materialen. In voorgaand onderzoek naar perovskieten is veel aandacht gegaan naar het bereiken van nieuwe en/of verbeterde eigenschappen door het manipuleren van de vervormingen in deze materialen. Om deze fascinerende eigenschappen in commerciële toepassingen te kunnen gebruiken is het echter nodig om deze stabiele oxides in een gewenste geometrie te kunnen structureren. Integratie met op silicium gebaseerde elektronica en aanverwante fabricage technologieën is ook van wezenlijk belang. In het algemeen zijn perovskieten erg stabiele materialen wanneer deze worden blootgesteld aan verschillende fysische en chemische etsprocessen. Hierdoor is het fabriceren van nauwkeurige structuren een uitdaging, in het bijzonder in het geval van epitaxiale multilagen van oxides. Bovendien zijn afmetingen op de nanoschaal benodigd, vanwege het huidige tijdperk van miniaturisatie van elektronica, waardoor geschikte nano-structurerings technieken vereist zijn. In dit proefschrift worden nieuwe fabricage strategieën ontwikkeld, gebaseerd op "lift-off" processen, om nauwkeurige micro- en nanostructuren van deze oxides, die op hoge temperatuur gegroeid zijn, te kunnen maken.

Het fabricage proces maakt gebruik van een laag van een amorfe oxide (AlO_x) met een goede stabiliteit op hoge temperatuur, welke gebruikt wordt als tijdelijke maskerlaag. Deze maskerlaag wordt gedeponeerd met behulp van gepulste laser ablatie en wordt gestructureerd door middel van conventionele fotolitografieprocessen.

Het voordeel van deze tijdelijke maskerlaag is dat deze ontwikkeld kan worden tot nauwkeurige structuren met behulp van fotolithografie en door gebruik te maken van een milde basische oplossing, zoals een standaard fotolithografie ontwikkelaar. Bovendien kan deze later ook verwijderd worden ("lift-off") na de depositie op hoge temperatuur, door gebruik te maken van een basische oplossing. Dit proces heeft geen effect op de eigenschappen van de perovskieten. Om te demonstreren dat deze epitaxiale "lift-off" fabricage strategie gebruikt kan worden voor delicate monsters, hebben we gekozen voor het $LaAlO_3$-$SrTiO_3$ grensvlak als model-systeem. Hiervoor is recentelijk aangetoond dat aan het grensvlak tussen $LaAlO_3$ en $SrTiO_3$ (001), beide isolatoren met een grote bandgap, een twee-dimensionaal elektronengas kan ontstaan, wanneer dit onder de juiste omstandigheden gedeponeerd wordt. Naast geleiding is ook magnetisme en supergeleiding gemeten aan het grensvlak, waarmee dit een veelbelovend systeem is voor toekomstige toepassingen in elektronica, zoals een hoge mobiliteit elektron transistor (HMET). Traditionele fabricage strategieën om structuren te maken aan dit grensvlak die gebruik maken van fysische ionen etsprocessen zijn niet geschikt omdat deze leiden tot schade aan het $SrTiO_3$ substraat. Deze schade veroorzaakt geleiding en zelfs magnetisme in het substraat. De epitaxiale "lift-off" strategie is gebruikt om $LaAlO_3$-$SrTiO_3$ heterostructuren te structureren zonder gebruik te maken van fysische etsprocessen. Gedetailleerde studies van de temperatuursafhankelijkheid van de magnetoweerstand zijn uitgevoerd op gestructureerde heterostructuren met een variabele dikte van de $LaAlO_3$ laag en deze zijn vergeleken met vergelijkbare ongestructureerde dunne film monsters. De resultaten van de temperatuursafhankelijke magenetoweerstand demonstreren het behoud van de hoge kwaliteit van de grensvlak eigenschappen van deze gestructureerde monsters, omdat de resultaten vergelijkbaar zijn met ongestructureerde monsters. De ontwikkeling van deze "lift-off" structureringsstrategie voor het fabriceren van heterostructuren met een hoge kwaliteit van het grensvlak helpt toekomstige onderzoeken naar het effect van beperking tot kleine structuren op hoge mobiliteit grensvlak geleiding en grensvlak magnetisme.

In een vervolgstap van dit onderzoek is aangetoond dat deze "lift-off" strategie niet alleen gebruikt kan worden voor het structureren van enkele epitaxiale lagen, maar ook gebruikt kan worden voor het gelijktijdig structureren van multilaags-heterostructuren met behoud van de functionele eigenschappen. Zoals hierboven aangegeven zijn epitaxiale (periodieke) multilagen interessant vanwege hun superieure eigenschappen, wanneer deze worden vergeleken met de afzonderlijke materialen. Deze monsters zijn echter vaak moeilijk te structureren vanwege hun verschil in gevoeligheid voor fysisch en chemisch etsen. Hier hebben we aangetoond dat de op hoge temperatuur gegroeide multilaag van $SrRuO_3/PbZr_{0.52}Ti_{0.48}O_3/SrRuO_3$ gestructureerd kan worden met deze epitaxiale "lift-off" strategie zonder de noodzaak om elke laag afzonderlijk te moeten structureren. De ferroelektrische eigenschappen van deze gestructureerde $PbZr_{0.52}Ti_{0.48}O_3$

multilagen, gegroeid op zowel $SrTiO_3(001)$ als op commercieel geplatineerd Si, zijn gemeten en vergeleken met traditioneel gestructureerde multilagen (door verschillende fysische en chemische etsstappen). Hieruit is gebleken dat de "lift-off" strategie leidt tot behoud van de functionele eigenschappen van deze perovskiet heterostructuren.

In toevoeging op structureren op de micro-schaal door conventionele fotolithografie, is deze "lift-off" strategie uitgebreid tot de nano-schaal door gebruik te maken van electron-beam lithografie (eBL). De voordelen van eBL als primaire lithografie techniek om het AlO_x masker te structureren zijn de ontwerp flexibiliteit en de hoge resolutie. De fabricage strategie is aangepast door een dunne metaallaag toe te voegen die oplading van het tijdelijke masker voorkomt. Een verbetering van deze aangepaste strategie wordt hier ook getoond waarbij geen fysische etsprocessen nodig zijn om de metaallaag te structureren. Met deze strategie zijn $PbZr_{0.52}Ti_{0.48}O_3$ nanostructuren gemaakt met een kleinste afmeting van ongeveer 100 nm. "Piezoresponse force microscopy" (PFM) onderzoek heeft aangetoond dat de gemaakte structuren afzonderlijk benaderd kunnen worden en dat de ferroelektrische eigenschappen behouden zijn. Bovendien kunnen ze afzonderlijk geschakeld worden zonder dat een significante hoeveelheid overspraak gemeten wordt. "Reciprocal space maps" (RSM) van de gemaakte structuren laten uitgebreide c-domeinen zien voor structuren kleiner dan 200 nm, wat inzicht kan geven voor het begrijpen van ferroelektrische schaaleffecten. De uitbreiding van deze "lift-off" techniek om epitaxiale nano-structuren te maken, maakt het mogelijk om een hele hoge dichtheid van componenten te maken. Dit kan gebruikt worden voor het fabriceren van snellere en multifunctionele elektronica.

In toevoeging op het ontwikkelen van de "lift-off" strategie for micro- en nanostructurering van epitaxiale perovskiet heterostructuren, demonstreren we in dit proefschrift ook het fabriceren van praktische functionele componenten. De koppeling tussen mechanische en elektrische eigenschappen in piëzoelektrische materialen wordt vaak gebruikt voor zowel detectie als actuatie doeleinden. Een belangrijke toepassing is piëzo massadetectie, met een piëzo-aangedreven "cantilever" als meest populaire component configuratie. Hoewel vrijstaande epitaxiale "piëzo-cantilevers" veelbelovend zijn om een hoge gevoeligheid te bereiken, het experimenteel realiseren van dergelijke componenten wordt bemoeilijkt vanwege problemen bij de fabricage, in het bijzonder wanneer epitaxiale oxides de functionele materialen vormen. Door gebruik te maken van de ontwikkelde "lift-off" structureringstechniek zijn vrijstaande piëzo-aangedreven micro-elektro-mechanische systemen (MEMS) uit epitaxiale oxides gemaakt op Si substraten. Het specifieke voordeel van deze "lift-off" strategie is dat in een enkele stap complete multilaags oxides gestructureerd kunnen worden. Bovendien kan ook toegang worden verkregen tot het onderliggende Si(001) substraat, wat vervolgens geëtst kan worden om de "cantilevers" vrij te maken. Hierdoor kunnen vrijstaande epitaxiale piëzo-MEMS

componenten in minder processtappen gefabriceerd worden met behulp van de "lift-off" structureringstechniek. Omdat Si wafers gebruikt worden als substraat, worden de MEMS componenten gemaakt zonder enige silicium aan de achterkant van de "cantilever", in tegenstelling tot traditionele MEMS componen waar "silicon on insulator" (SOI) als substraat wordt gebruikt. Doppler vibrometrie is gebruikt om de elektromechanische response van deze vrijstaande componenten te onderzoeken. Het is aangetoond dat alle componenten resonante vibraties hebben wanneer ze geactueerd worden door een externe wisselspanning. De tweede orde "buigmodus" is dominant gebleken voor "cantilevers" met een functionele lengte tussen 50 en 125 μm. Voor langere vrijstaande "cantilevers" zijn andere of meerdere resonantie modi gevonden. Door de elektromechanische response van een serie "cantilevers" in lucht en in vacuum te onderzoeken zijn verschillende bijdrages van het medium (lucht, extrinsieke bijdrage) en het gebruikte materiaal (intrinsieke bijdrage) op de demping van de vibratie bepaald. Een model wordt voorgesteld wat de variatie van de demping bij verschillende lengtes van de "cantilever" verklaart door gebruik te maken van gecombineerde effecten van lucht demping en intrinsieke frictie in het "cantilever" materiaal.

In het laatste deel van dit proefschrift worden een aantal toekomstige onderzoeken uitgelicht die mogelijk worden gemaakt door de epitaxiale "lift-off" techniek. Ook worden een aantal voorlopige resultaten getoond die gebruik maken van deze structureringstechniek. Als voorbeeld wordt het structureren van het heteroepitaxiale grensvlak van $SrCuO_2$-$LaAlO_3$-$SrTiO_3$(001) gedemonstreerd, wat ladingsdragers met een hoge mobiliteit bevat. Het delicate grensvlak is gestructureerd met behoud van de hoge kwaliteit transport eigenschappen, die voorheen alleen in volledige films gemeten zijn. Opmerkelijk is dat nieuwe eigenschappen gemeten zijn aan deze gestructureerde grensvlakken, waaronder een mobiliteit van de ladingsdragers tot $\sim$ 70,000 cm^{2}V^{-1}s^{-1} en positieve magnetoweerstandwaardes tot $\sim$ 800 % op 2K, wat mogelijk veroorzaakt wordt door de opgelegde structurele beperkingen. Als een ander voorbeeld van de mogelijkheden van deze "lift-off" structureringstechniek voor toekomstige toepassingen hebben we aangetoond dat epitaxiale vrijstaande piëzo-MEMS "cantilevers" gebruikt kunnen worden voor massadetectie met een zeer hoge gevoeligheid. Een gestructureerde toplaag van goud is toegevoegd om de massagevoeligheid van de componenten af te kunnen schatten. Deze laag maakt het ook mogelijk om dergelijke structuren te gebruiken voor kwantitatieve detectie van biologische moleculen en microbes via goud-thiol bindingen. Deze initiële resultaten leiden tot nieuwe mogelijkheden voor toekomstig onderzoek naar het effect van kleine structuren op magnetotransport eigenschappen en op quantumverschijnselen (zoals Shubnikov-deHaas oscillaties) in hoge mobiliteit oxide structuren. Deze resultaten leiden ook tot nieuwe mogelijkheden voor het implementeren van vrijstaande piëzo-MEMS componenten met een hoge massagevoeligheid voor snelle bio-detectie.

Acknowledgments

It is a pleasure for me to gratefully acknowledge and thank all the people who have helped, supported, accompanied and encouraged me during the past 4 years to reach this stage. I am very fortunate to meet and know many wonderful persons, also to experience several unforgettable events in this beautiful journey. Coming from a very different social, economic and cultural background, the support and encouragement that I received, especially in the initial days of my Ph.D., have helped me enormously to adopt to a new environment and to pursue my research work.

I would like to express my deep and sincere gratitude to my promotor, Prof. Dr. Guus Rijnders, for giving me the great opportunity to join the IMS group as a Ph.D. student. You have introduced me to the fascinating world of perovskite devices and have always been supporting me while working in the Piezo-NEMS project. Your guidance, constant encouragement and motivation at different stages of my Ph.D. has been a treasure for me to keep moving. I am ever thankful to you for your care and advices for my professional career and also beyond. I want to express my sincere appreciation and gratitude to my daily supervisor Dr. Gertjan Koster for his regular guidance, fruitful discussions and support throughout these four years. Your views and suggestions have been of great help towards performing my Ph.D. research work. Thank you for allowing me ample research freedom and encouraging me to learn new topics. I sincerely thank Dr. Mark Huijben for his very useful helps in many occasions of my research, especially regarding the investigation of the patterned LAO-STO devices (Chapter 2 of this thesis). I appreciate your friendly suggestions and practical advice whenever I needed. I express my heartfelt thanks to Prof. Dr. Dave Blank for encouraging me when we occasionally meet. I thank Prof. Jos Benschop for his help and the useful discussions regarding the lift-off patterning technology. Also, thanks to Prof. Dr. Andre Elshof for advices and very interesting discussions, often about history at Dave's corner, IMS. My sincere thanks to Dr. Evert Houwman for carefully analyzing my experimental data from theoretical perspective and helping me to understand them. I would like to thank the members of my doctoral graduation committee for arranging time to evaluate this work, carefully checking my concept thesis and providing me with very useful

comments and suggestions.

I would like to sincerely thank Prof. S. B. Krupanidhi, the supervisor of my Master's research project at Material's Research Center, Indian Institute of Science for his support towards me and encouragement to pursue the scientific research. I am also very thankful to Prof. N. Ravishankar, Prof. K. K. Nanda, Prof. K. B. R. Verma, Prof. S. Ramakrishnan and Prof. P. Maity of IISc for helping me and giving useful advice during my study there. My special thanks to Dr. Akhtar Hussian for being an excellent friend. I have always cherished our friendship and treasured your positive support for me.

The excellent collaborative atmosphere in IMS and the very friendly colleagues have made the work described in this thesis possible. I am very grateful to the present and past members of the piezo-team at IMS - Minh, Ruud, Evert, Matthijn, Xin, Muhammed, Kurt, Ben, who took part in the inspiring discussions on Wednesday morning PZT-meetings. I especially thank Minh and Ruud for helping me optimizing PZT growth parameters at the initial stage of my project. I am also thankful to the people working with the small PLD, the system for which I was in charge, for their assistance in maintaining the system up and running. Thanks to Brian for helping me with the PTO growth and with PFM measurements. You have been always very helpful and friendly to me. My special thanks to my present and past office mates - Bouwe, Brian, Josée, Alim, Werner and Bram. You all have made it possible to create a very beautiful office environment and your amicable nature has made my desk-time enjoyable. My heartfelt thanks to Marion for her overwhelming helps in all the official works. My sincere thanks to Maarten and Peter for being my paranymphs and for all your invaluable helps. I especially thank Ronald for introducing me to Guus. I would like to thank all my present and past colleagues of IMS - Bernard, Hajo, Ole, Jeroen, Hans, Debakanta, Matjaz, Frank, Anuj, Tjeerd, Lin, Zhaoliang, Ozlem, Peter D, Joska, Eddy, Antony, Tomasz, Nicolas, Wouter, Rogier, David, Anirban, Rik, Kenan, Tom, Sjoerd, Gerard, Pablo, Michelle, Petra, Huiyu, Suresh. Thanks to the bachelor students Sander and Daniel, whom I have supervised, for the cooperation. I also thank the Master's students of IMS with whom I have worked/interacted, especially Roy, Herman, Tülin, Thomas, Wouter V and Bahruz.

I gratefully acknowledge the support from the technical personnel who has helped me performing my Ph.D. research, Dominic, Henk, Arjen, Josée, Laura and Kees. Thanks to Frank and Dick of the ICE group for their help and support when working in the PLD lab. Also, I am very thankful to the technical staff members of MESA+ Nano-Lab for their co-operation while working in the cleanroom. I want to thank Pino (TST group) for his help regarding the measurements with the vibrometer and to Meint for the useful advices regarding Si-etching processes. Also, thanks to the present and past members of the ICE group with whom I have worked and interacted.

I am thankful to the personnel from FOM and M2i who did the formalities for my project. My thanks to Dr. Derk Bol and Prof. Mark Geers for their kind co-operations during my project. I am very thankful to Maria Teuwissen of FOM for all her helps regarding the VISA for the Netherlands.

During my Ph.D. I was involved in several fruitful scientific collaborations and would like to express my sincere thanks to the collaborators. I am thankful to Dr. L. Pellegrino and Dr. D. Marré of CNR-SPIN, Genoa, Italy for their efforts to fabricate epitaxial PZT-STO devices. My sincere thanks to Prof. D. Schlom and Dr. Zhe Wang of Cornell University for providing $SrTiO_3$-Si substrates in order to investigate epitaxial devices. I also thank Prof. J. Verbeeck for the TEM studies on PZT nano-structures.

I thank my friends here whose company, help, support and encouragement have made my stay in the Netherlands pleasurable. My thanks to Rajesh, Santosh and Tarun for helping me a lot in the initial days to get adjusted to the new life style. I am very thankful to Saurabh-da and Jaya-di for the nice tea breaks with good casual talks and for the very tasty Indian foods. It is difficult for me to express my thanks to Robin in right words. You have accompanied me a lot, have always been supportive and have helped me whenever I needed. The events and trips we organized together will always be unforgettable. I want to thank Ramen-da, Siddhartha-da, their spouses and Nupur-di for their support during my initial days here. My special thanks to my friends and colleagues from University of Groningen with whom I have had many memorable events. I want to express my sincere thanks to Prof. Tamalika Banerjee for her help, encouraging words and positive advices to me. Thank you for your invitation and celebration of my birthday which will remain as a beautiful memory. I am very thankful to Subir, Gaurav, Saurabh, Alok, and Milon for offering me a very good time in Groningen. Thanks to Subir for your nice friendship and support. Thank you Gaurav for the beautiful discussions and the great time. Thanks to Saurabh for your overwhelming hospitality.

Lastly, I want to thank my family for their unconditional love towards me and giving me support at every stage of my life. My family has been the most important strength for me while staying abroad. Apart from my parents, I am ever thankful to my elder brother, Anupam Banerjee, for being always by my side. It is impossible for me to express my deep respect and gratitude to my family in words. I also thank my relatives for their support to me and my family.

Nirupam Banerjee

Enschede, September, 2014